이학석사학위논문

Fluorescent Oligomers Built with Triazole-Based Turn-Motifs: Length- and Solvent-Dependent Photophysical Properties

트리아졸 기반 형광성 올리고머의 길이와 용매에 따른 광물리적 특성 연구

2016년 2월

서울대학교 대학원
화학부 유기화학전공
이 미 림

Fluorescent Oligomers Built with Triazole-Based Turn-Motifs: Length- and Solvent-Dependent Photophysical Properties

by

Milim Lee

Thesis Advisor: Prof. Dongwhan Lee

A Thesis for the Master Degree
in Organic Chemistry

Department of Chemistry
Graduate School
Seoul National University
February, 2016

Fluorescent Oligomers Built with Triazole-Based Turn-Motifs: Length- and Solvent-Dependent Photophysical Properties

지도교수 이 동 환

이 논문을 이학석사 학위논문으로 제출함
2016년 2월

서울대학교 대학원
화학부 유기화학전공
이 미 림

이미림의 이학석사 학위논문을 인준함
2016년 2월

위 원 장 Soon Hyeok Hong (인)

부위원장 이 동 환 (인)

위 원 홍 종 인 (인)

Fluorescent Oligomers Built with Triazole-Based Turn-Motifs: Length- and Solvent-Dependent Photophysical Properties

Abstract

Foldable oligomers can reversibly change their conformations under specific conditions. Among such molecules, fluorescent foldamers could potentially allow for the detection of the folding events by straightforward spectroscopic measurements. We have designed and synthesized foldable oligomers by using *N*-2-aryl substituted bis(triazolo)benzene motif as a conformationally well-defined and fluorescent repeating unit. These new π-conjugated oligomers were constructed by consecutive reduction, azo coupling, and oxidative cyclization reaction sequences, which facilitated access to a series of fluorescent (Φ_F = 81–83%) oligomers from pre-assembled building blocks. Our structure design and synthetic strategy allow for a precise control over both the chain length and interchromophore spatial relationship, which was also confirmed by X-ray crystallographic studies on select systems. In addition, solvent-dependent interchromophore interactions elicited significant changes in fluorescence intensity, which becomes more pronounced with increasing chain length.

Keywords: Foldable oligomers, triazolobenezene, fluorescence, azo coupling, solvent-dependent

Student Number: 2013–22930

Contents

B. Aryltriazole-Based Fluorogenic Oligomers

Introduction

In biological systems, proteins carry out sophisticated chemical reactions by specific binding and catalytic transformations. The important feature is that proteins adopt compact conformations as a result of precise three-dimensional arrangement of amino acid residues. In protein folding, local conformational preference of the protein backbone is determined by secondary structures including helices, sheets, and turns.[1]

As a previously underutilized synthetic motifs to mimic the protein turn motif, *N*-substituted triazoles and their ring-fused polyheteroaromatic derivatives could be considered. As nitrogen-rich aromatic systems, 1,2,3-triazoles and their derivatives have been used primarily as ultraviolet absorbers to prevent photo degradation of materials,[2] and corrosion inhibitors for copper and copper alloys.[3] In addition, these compounds are finding applications in biological sciences,[4] materials chemistry,[5] and medicinal chemistry.[6] In Figure 1 are shown representative examples of *N*-2-aryl-1,2,3-triazolobenzene derivatives: dopamine receptor ligand (I), human PPAR-α activator (II), Tinuvin-P (III) as a UV light absorber, PCDTPBt as an electron acceptor in organic solar cell, UV-stabilizer (V), and antiviral agent (VI).[7] For 1,2,3-traizole derivatives, substitution at the *N*-2 position usually leads to enhanced light-emitting properties when comparison is made with the *N*-1 substituted isomer (Figure 2).[8] Compared with the *N*-1-aryl triazolobenzene, showed little distortion between the triazole ring and aryl group at the *N*-2 position (Figure 2).[9] Recently, Padalkar et al. reported photophysical properties of *N*-2-aryl-1,2,3-triazolobenzene derivatives as a new class of blue emitting fluorophores.[10]

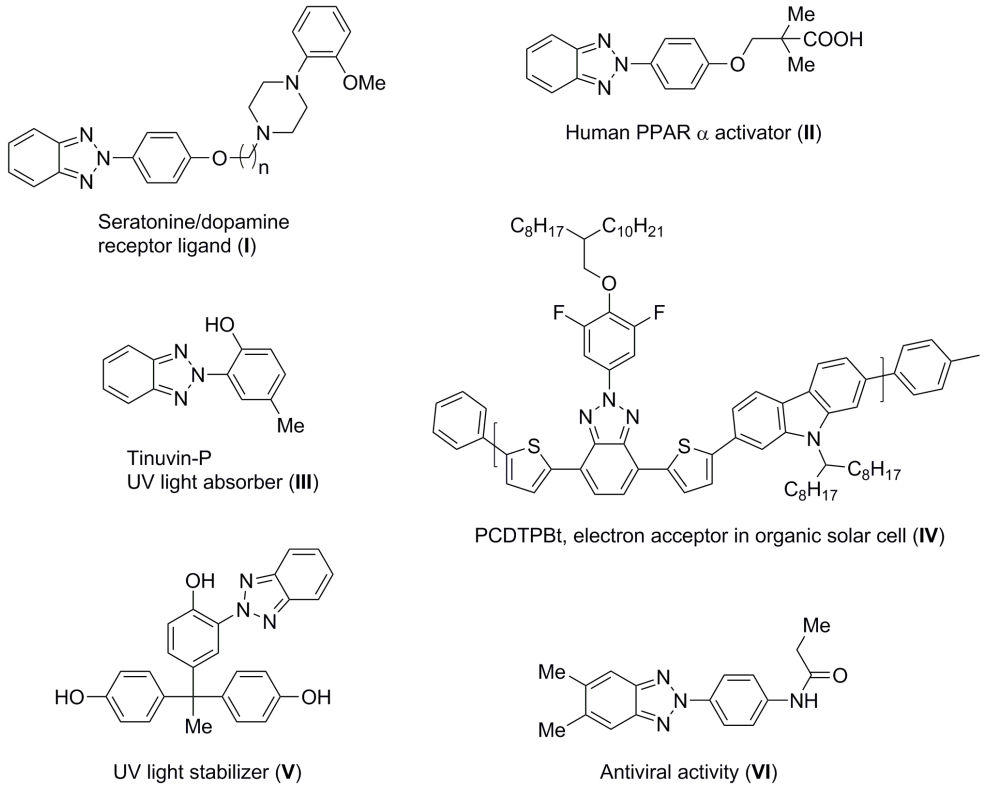

Figure 1. Representative molecules having *N*-2-aryl-benzotriazole motifs.

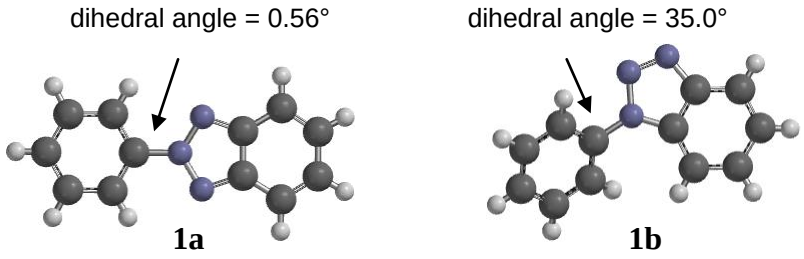

Figure 2. X–ray crystal structures of **1a** (CCDC code: 659842) and **1b** (CCDC code: 99300).[9]

In recent a few decades, a considerable amount of effort has been devoted to the design and construction of artificial molecules that spontaneously fold. Such foldable oligomers are called '*foldamers*', a term

coined by Gellman to describe "*any polymer with a strong tendency to adopt a specific compact conformation*".[1] The folding event is usually accompanied by hypochromism in UV–vis spectrum,[11] but rarely involves change in fluorescence.

In order to design foldamers that change fluorescence properties upon folding, fluorescent dyes can be introduced at the ends of the foldable molecules.[12] Alternatively, foldamer backbone could be constructed with fluorescent residues. In 2008, Jeong et al. reported that a series of oligoindole molecules undergo structural folding upon binding of an anion, and such molecular recognition event can be monitored by change in fluorescence intensity.[13] Except for these few examples, foldable oligomers comprised of fluorogenic repeating units are still rare. In this thesis are described the design and implementation of modular synthetic strategies to construct foldable oligomers that are comprised of *N*-2-aryl-1,2,3-triazolobenzene repeats.

1. *N*-2-Aryl-1,2,3-triazolobenzene as a Fluorophore

Many strategies are currently available to synthesize 1,2,3-triazoles. However, most of the efforts have been devoted to unsubstituted 1,2,3-triazoles or *N*-1 substituted 1,2,3-triazoles. This is in part due to the discovery and wide applications of copper-catalyzed azide–alkyne cycloaddition reaction.[14]

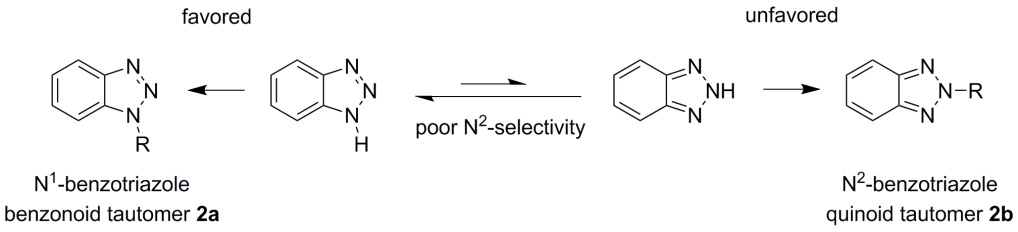

Scheme 1. *N*-1-Selective substitution of benzotriazoles.

While *N*-2-aryl-1,2,3-triazoles display intense fluorescence (vide supra),

the equilibrium between *N*-1 (or *N*-3) and *N*-2 tautomers makes it difficult to prepare *N*-2-aryl-1,2,3-triazole and *N*-2 substituted benzotriazole as major products by simple nucleophilic substitution reactions (Scheme 1).[15] In terms of thermodynamic preference, the benzonoid tautomer **2a** is 9.5 kcal mol^{-1} more stable than quinoid tautomer **2b**.

In spite of the difficulties in synthesis, significant efforts have recently been devoted to the preparation and utilization of fluorescent *N*-2-aryl-benzotriazoles. In this following sections are described representative synthetic routes to *N*-2-arylbenzotriazole and their applications as fluorescent sensors.

1.1. Synthetic Approach

1.1.1. Tandem Synthesis of *N*-2-Aryl-1,2,3-triazoles from α-Arylhydrazonoketones

A traditional approach for synthesizing *N*-2 substituted 1,2,3-triazole is intramolecular cyclization of 1,2-diketone bis(arylhydrazones) or α-hydroxyimino hydrazones as shown in Scheme 2a.[16] In 1963, Hiesch et al. reported that *N*-2-aryl-1,2,3-triazoles can be prepared by the reactions of 1,2-diketone imine hydrazones with NH_3 in the presence of stoichiometric amount of $CuSO_4$ (Scheme 2b).[17] Recently, Punniyamurthy et al. converted bisarylhydrazones to *N*-2-substituted 1,2,3-triazoles by copper(II)-catalyzed aerobic oxidation (Scheme 2c).[18] A tandem process from α-arylhydrazonoketones to *N*-2-aryl-1,2,3-triazoles under copper-catalyzed oxidative condition was also reported (Scheme 2d).[19]

(a) cyclization of bishydrazones or α-hydroxyimino hydrazones

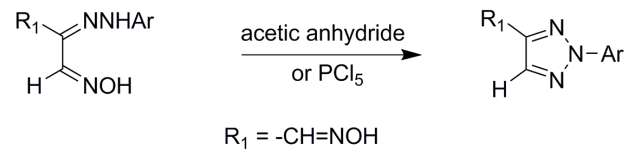

R_1 = -CH=NOH

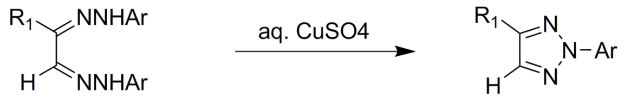

R_1 = -(CHOH)$_3$CH$_2$OH

(b) cyclization of 1,2-diketone imine hydrazones

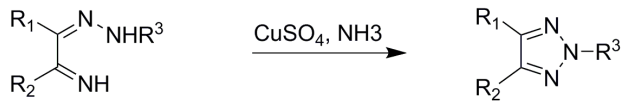

R_1 = R_3 = alkyl, aryl; R^2 = Ac, aroyl, CO_2Et, CN

(c) cyclization of bisarylhydrazones

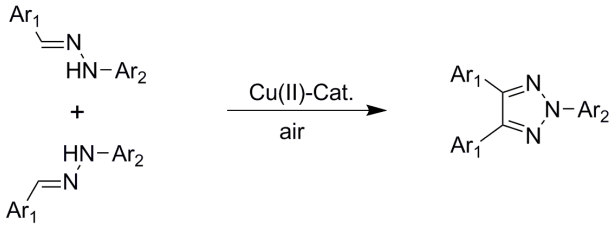

(d) cyclization of α-arylhydrazonoketones

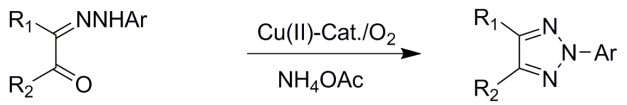

Scheme 2. Different routes for *N*-2-aryl-1,2,3-triazole synthesis.

1.1.2. C-N Coupling for *N*-2-Selective Pd–Catalyzed Arylation of 1,2,3-Triazoles

Buchwald et al. synthesized *N*-2 substituted 1,2,3-triazoles by highly (> 90%) *N*-2-selective C–N coupling.[20] This *N*-arylation reaction is generally applicable to aryl bromides, chlorides, and triflates substrates, and tolerates a wide range of functional groups including ester, ketone, aldehyde, acetal, nitro, and cyano.

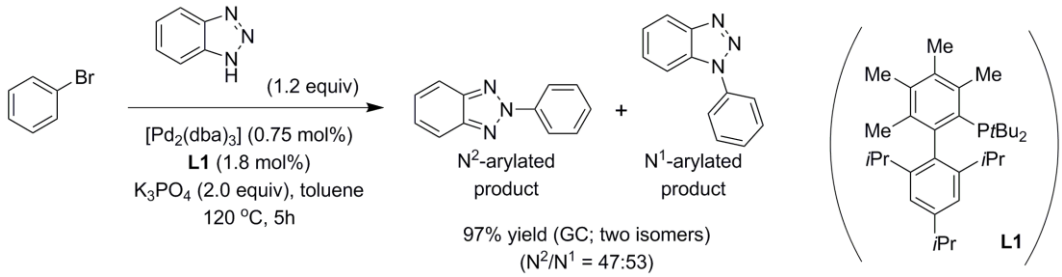

Scheme 3. Palladium–catalyzed *N*-2-arylation of benzotriazole.

Although 4,5-unsubstituted and 4-substituted 1,2,3-triazoles showed high *N*-2-selectivity, an essentially equimolar mixture of *N*-1 and *N*-2-aryl isomer was obtained in the C–N coupling reaction between benzotriazole and bromobenzene (Scheme 3). This low *N*-2-selectivity was investigated by DFT calculations of the presumed intermediates. After transmetallation, the difference in the relative energy is only 1.6 kcal mol^{-1} between the *N*-2-benzotriazolate complex and the *N*-1-benzotriazolate complex. Moreover, the relative energy gap of each transition state is very small ($\Delta\Delta G^{\circ}$= 0.1 kcal mol^{-1}), which accounts for the experimentally observed poor regioselectivity.

1.2. *N*2-Aryltriazolobenzene as a Fluorescent Sensor

The chemistry of *N*-2-aryl-1,2,3-benzotriazole can be traced back to the initial report on the synthesis of the simple *N*-phenyl derivative, which was reported in 1887.[21] As shown in Scheme 4, thermal decomposition of *o*-azidoazobenzene furnishes *N*-2-aryl-1,2,3-benzotriazole. The other synthetic route was reported in 1921, which employed synthetically more accessible azoaniline as the precursor. After oxidative cyclization, *N*-2-aryl-1,2,3-benzotriazoles were obtained.[22]

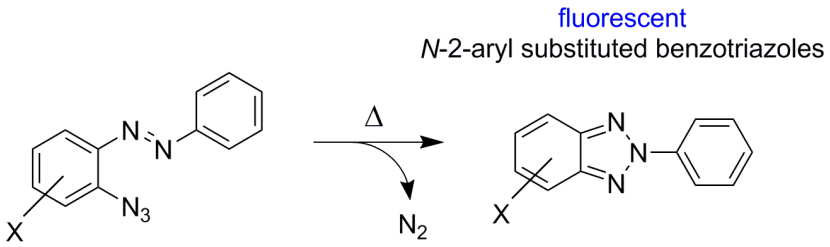

Scheme 4. Synthetic routes to benzotriazoles by thermal decomposition method.

In 2012, Lee et al. reported that oxidative cyclization reaction could be exploited for fluorescence turn-on detection of copper(II) ions. In the optimized system, shown in Figure 3, nonemissive azoaniline is converted to highly fluorescent benzotriazole under ambient aqueous conditions in the presence of copper(II) ions.[23]

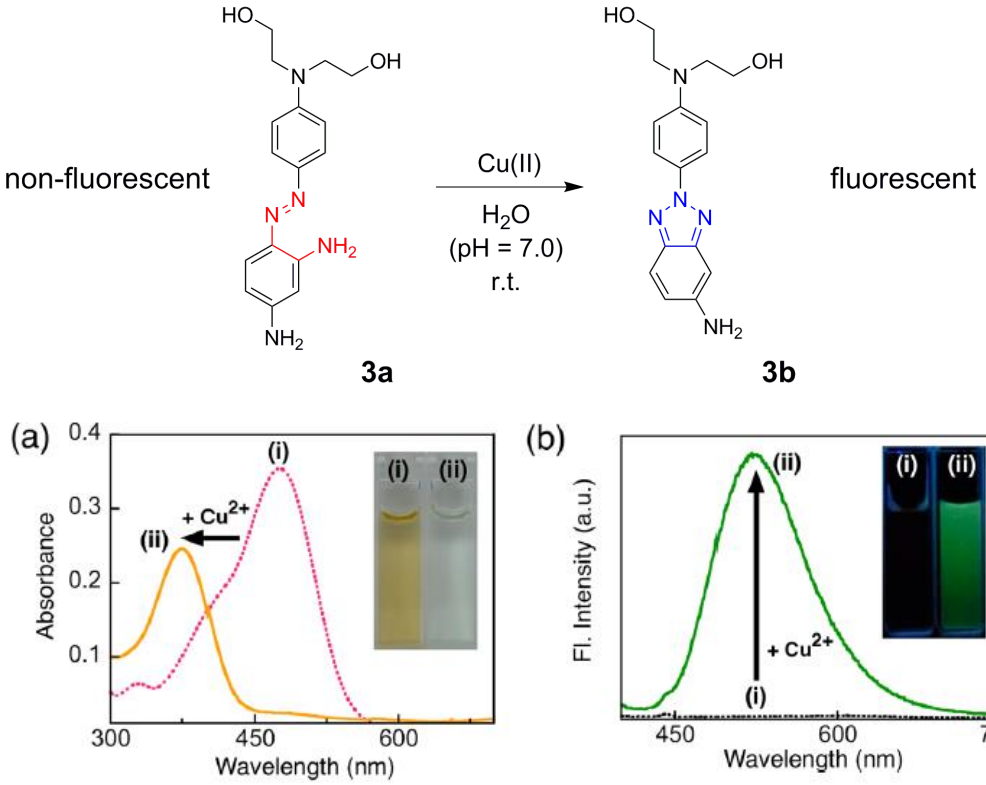

Figure 3. Oxidative cyclization of **3a** (10 μM) to **3b**, triggered by copper(II) ions (100 equiv) in water (pH = 7.0; HEPES, 50 mM) and monitored by (a) UV−vis and (b) fluorescence spectroscopy after 10 min. Digital images in the insets were obtained (with ambient light for (a), and a hand-held UV lamp (λ_{ex} = 365 nm) for (b)) for the samples prepared using the same experimental conditions. Reprinted with permission from ref 24. Copyright 2012 American Chemical Society.

2. Biomimetic Approaches to Spontaneously-Folding Molecules

Synthetic molecules that mimic molecular recognition events in biological systems continue to remain an area of active research. In the design of such

molecules, the most important considerations are implementing noncovalent interactions to produce well-defined secondary structures.

2.1. Noncovalent Approach

Noncovalent interactions are important for maintaining compact three-dimensional structures of large molecules, such as proteins and nucleic acids. Among various noncovalent interactions, hydrogen bonding is key to the sequence-dependent folding and assembly. Since anions behave as hydrogen bonding acceptors, synthetic molecules presenting multiple hydrogen bonding donor groups on the concave side can function as anion receptors.

2.1.1. Utilizing Hydrogen Bond to Anion-Anion Proton Transfer

Gale et al. discovered that complexation of dihydrogen phosphate by a receptor molecule having six-hydrogen bond donor (HBD) groups reduces the pK_a value of the bound anionic species.[24] As a consequence, host bound $H_2PO_4^-$ was deprotonated by the free $H_2PO_4^-$ in solution, not by the receptor.

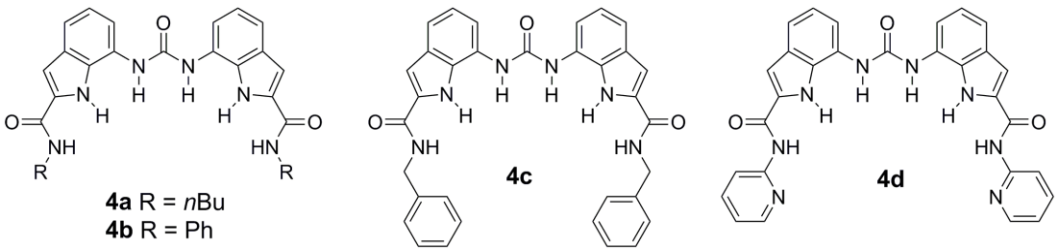

Figure 4. Chemical structures of diindolylurea-based anion receptors.

a) b)

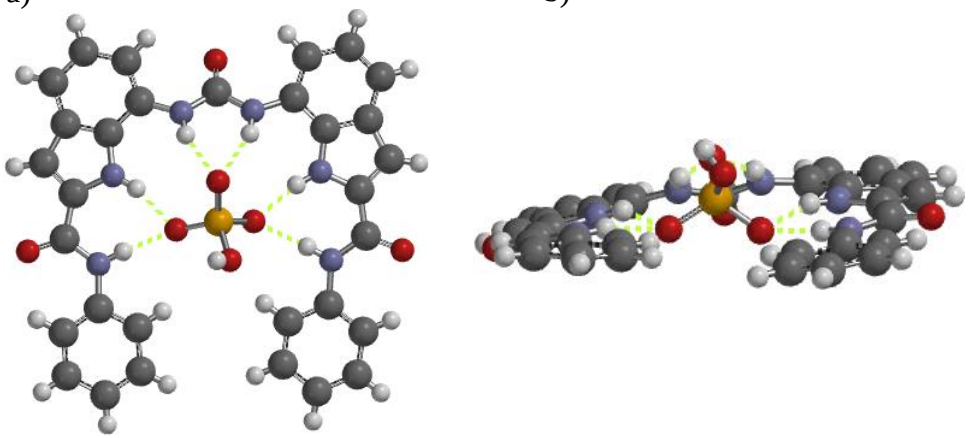

Figure 5. (a) Face-on and (b) edge-on view of the hydrogen phosphate complex of **4b** (CCDC code: 734479).[24] Solvent and counter cations have been omitted for clarity.

The same research group has also synthesized diindolylurea receptors having additional amide groups at both ends (Figure 4). Among BzO^-, AcO^-, HCO_3^-, and $H_2PO_4^-$, deprotonation of the bound $H_2PO_4^-$ was effected only by $H_2PO_4^-$. This finding was also supported by the crystal structure of **4b** obtained as a hydrogen phosphate complex (Figure 5).

2.2. Rigid Turn Motif Approach

2.2.1. Oligomers with Helix–Turn–Helix Supersecondary Structures

In the spontaneous folding of linear molecules to secondary structures, turn motifs can impart a twist sense. The helix–turn–helix(H–T–H) supersecondary structure is a simple but important motif in DNA–binding protein,[25] and comprised of a combination of helix and turn units. Chen et al. reported the first example of artificial aromatic oligoamide-based H–T–H supersecondary structure.[26] Here, binaphthyldiamine moieties were employed

to impart a bias in the twist sense of the H–T–H supersecondary structure (Figure 6).

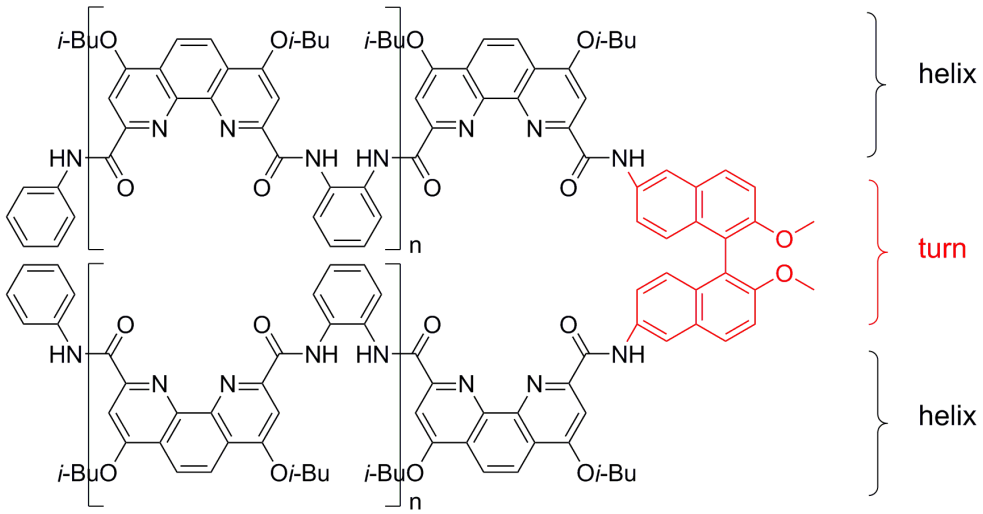

Figure 6. Chemical structures of HTH motif oligomers.

With increasing number of the phenanthroline rings, a hypochromic effect was observed in the UV–vis spectra. This is a typical spectroscopic signature of folding, which arises from helical ordering and π–π^* stacking. As shown in Figure7, the oligomer (±)**–2** has the two helix segments across a binaphthyldiamine turn moiety in the middle. This folded conformation is stabilized by intramolecular hydrogen bonds. Based on the crystal structure (Figure 7c), intermolecular hydrogen bonds with solvent molecules might also play a role in the conformational stability.

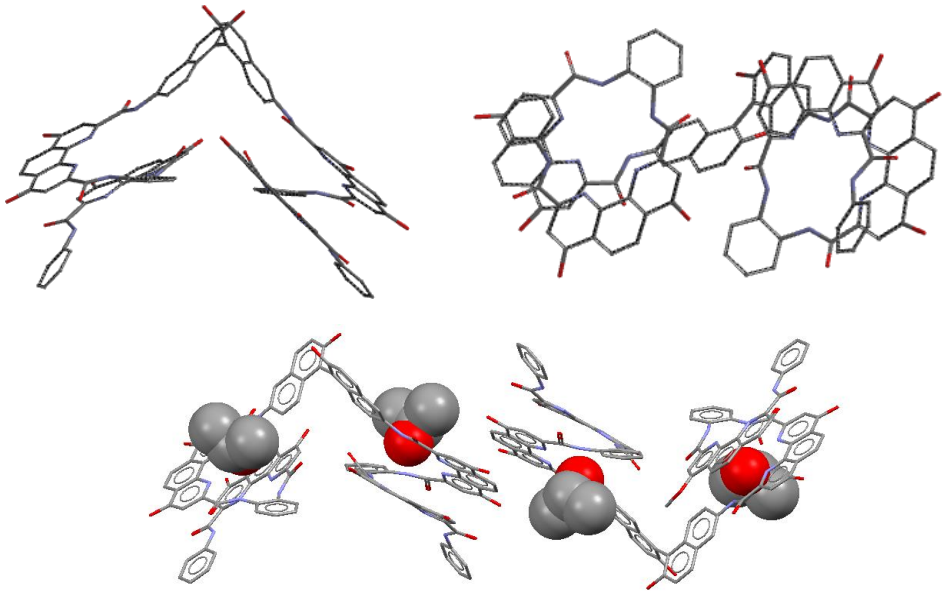

Figure 7. (a) Side view and (b) top view of crystal structure and (c) crystal packing of (±)–**2** (CCDC code: 676528).[26] Side chains and hydrogen atoms have been omitted for clarity.

3. Applications of Foldable Oligomers: Current State of the Art

Synthetic foldamers have been studied as receptors or catalysts. For example, Moore et al. utilized oligo(*m*-phenylene ethynylene)s (*m*PE-13mers) as receptors for single-walled carbon nanotubes (SWCNTs).[27] They have demonstrated that unfolded *m*PE-13mers in $CHCl_3$ associate with SWCNTs via intermolecular π–π interactions, thereby increasing dispersion stability of the nanotubes. The oligomer-wrapped SWCNTs are well-dispersed without aggregation. Addition of MeCN, however, elicits folding of *m*PE-13mers to release SWCNTs, which precipitate from the solution (Figure 8).

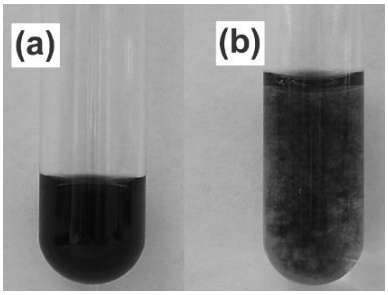

Figure 8. Photograph of (a) well dispersed SWCNTs/*m*PE-13mer in chloroform and (b) after addition of acetonitrile, resulting the precipitated nanotubes. Reprinted with permission from ref 26. Copyright 2010 American Chemical Society.

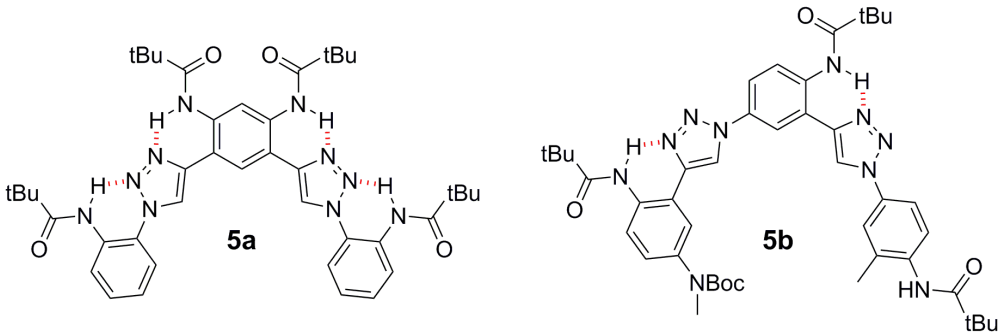

Figure 9. Structures of preorganized foldamers **5a** and **5b**.

Preorganized foldamers increase binding affinity toward anions. For example, Shang et al. synthesized preorganized aryltriazole foldamers as effective receptors and transmembrane transporters of chloride ion.[28] They compared the binding affinities of preorganized foldamer **5a** and partially organized foldamer **5b** to investigate the effect of structural pre-organization in anion binding (Figure 9). The fully pre-organized **5a** has anion binding affinity in order of $Cl^- > Br^- > I^-$. In contrast, the partially organized foldamer **6b** showed different anion binding affinity in order of $Br^- > Cl^- > I^-$. Notably, the binding constant of **5a** for Cl^- is 8-times larger than that of **5b**. In addition, **5a** also showed good Cl^- transport ability across a lipid bilayer.

In order to introduce asymmetric bias in the helical folding, chiral residues can be introduced at the chain end or as the side chains. Alternatively, chiral guests are added to racemic helical strands. Ousaka et al. introduced a salicylaldehyde group at the end of a chiral oligomer helix (Scheme 5)[29]. By

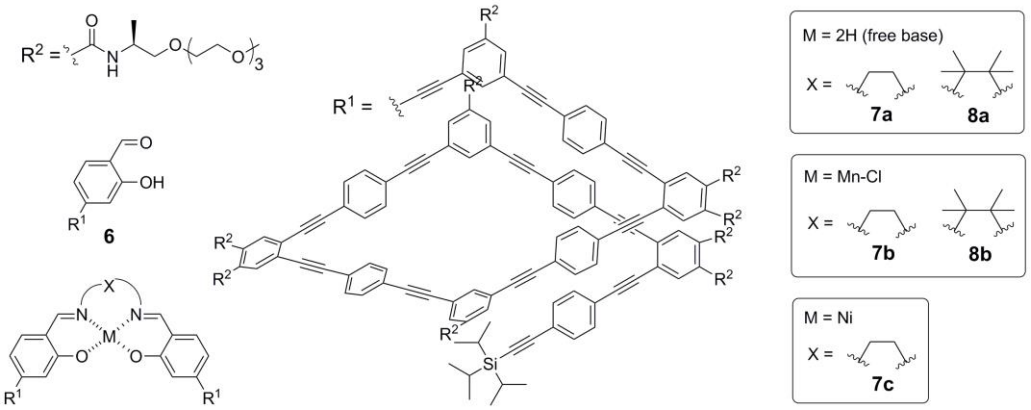

Scheme 5. Chemical structures of **6**, and salen and metallosalen foldamers.

Schiff base condensation reactions with flexible achiral diamines salen–linked dimeric foldamers were obtained, and studied by circular dichroism (CD) spectroscopy. Here, the helical bias, either (*P*)- or (*M*)-, was induced by intramolecular hydrogen-bonding network. The energy-minimized structures shown in Figure 10 suggest that the homochiral **7c** can have up to ten intramolecular hydrogen bonds. On the other hand, the heterochiral **7c** cannot support interstrand hydrogen bonds, and thus does not show any CD signal. This system was engineered further to introduce a manganese(III) salen complex for asymmetric catalysis of substrates that are placed inside the helical cavity. Although the manganese(III) salen–linked foldamers **7b** and **8b** show up to 5.6% e.e for asymmetric epoxidation, this finding suggests the possibility of foldamer-based asymmetric catalysis.

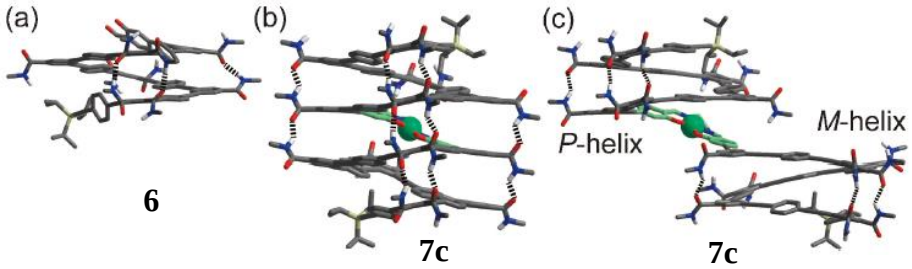

Figure 10. Energy-minimized right-handed helical structures of (a) **6**, (b) homochiral (*P–P*), and (c) heterochiral (*P–M*) helical structures of **7c**. Reprinted with permission from ref 29. Copyright 2014 The Chemical Society of Japan.

4. References

1. Gellman, S. H. *Acc. Chem. Res.* **1998**, *31*, 173–180.
2. Leaver, I. H.;Waters, P. J.;Evans, N. A. *J. Polym. Sci., Part A: Polym. Chem.* **1979**, *17*, 1531–1541.
3. Walker, R. *J. Chem. Educ.* **1980**, *57*, 789–791.
4. Costa, M. S.;Boechat, N.;Rangel, E. A.;da Silva Fde, C.;de Souza, A. M.;Rodrigues, C. R.;Castro, H. C.;Junior, I. N.;Lourenco, M. C.;Wardell, S. M.;Ferreira, V. F. *Bioorg. Med. Chem.* **2006**, *14*, 8644–8653.
5. Nandivada, H.;Jiang, X.;Lahann, J. *Adv. Mater.* **2007**, *19*, 2197–2208.
6. Tron, G. C.;Pirali, T.;Billington, R. A.;Canonico, P. L.;Sorba, G.;Genazzani, A. A. *Med. Res. Rev.* **2008**, *28*, 278–308.
7. Liu, Y.;Yan, W.;Chen, Y.;Petersen, J. L.;Shi, X. *Org. Lett.* **2008**, *10*, 5389–5392.
8. Yan, W.;Wang, Q.;Lin, Q.;Li, M.;Petersen, J. L.;Shi, X. *Chem. Eur. J.* **2011**, *17*, 5011–5018.
9. (a)Claramunt, R. M.;María, D. S.;Pinilla, E.;Torres, M. R.;Elguero, J. *Molecules* **2007**, *12*, 2201–2214; (b)Takagi, K.;Al-Amin, M.;Hoshiya, N.;Wouters, J.;Sugimoto, H.;Shiro, Y.;Fukuda, H.;Shuto, S.;Arisawa, M. *J. Org. Chem.* **2014**, *79*, 6366–6371.
10. Padalkar, V. S.;Lanke, S. K.;Chemate, S. B.;Sekar, N. *J. Fluoresc.* **2015**, *25*, 985–996.
11. Nelson, J. C. *Science* **1997**, *277*, 1793–1796.
12. (a)Arunkumar, E.;Ajayaghosh, A.;Daub, J. *J. Am. Chem. Soc.* **2005**, *127*, 3156–3164; (b)Zhong, Z.;Zhao, Y. *Org. Lett.* **2007**, *9*, 2891–2894; (c)Chou, C.;Wang, D.;Hsu, J. F.;Liu, Y.;Peng, Z. *Synthetic Met.* **2009**, *159*, 1657–1663; (d)Lu, Z.;Zhu, Y.;Lin, J.;Jiang, X.;Li, Z. *Chinese Sci. Bull.* **2010**, *55*, 2870–2878; (e)Dehm, V.;Büchner, M.;Seibt, J.;Engel, V.;Würthner, F. *Chem. Sci.* **2011**, *2*, 2094–2100; (f)Sakamoto, N.;Ikeda, C.;Yamamura, M.;Nabeshima, T. *Chem. Commun.* **2012**, *48*, 4818–4820.
13. Kim, U. I.;Suk, J. M.;Naidu, V. R.;Jeong, K. S. *Chem. Eur. J.* **2008**, *14*, 11406–11414.
14. Rostovtsev, V. V.;Green, L. G.;Fokin, V. V.;Sharpless, K. B. *Angew. Chem., Int. Ed.* **2002**, *41*, 2596–2599.
15. Xu, K.;Thieme, N.;Breit, B. *Angew. Chem., Int. Ed.* **2014**, *53*, 7268–7271.
16. Riebsomer, J. L.;Sumrell, G. *J. Org. Chem.* **1948**, *13*, 807–814.
17. Hirsch, B.;Ciupe, J. *Chimia* **1963**, *17*, 159.
18. Guru, M. M.;Punniyamurthy, T. *J. Org. Chem.* **2012**, *77*, 5063–5073.
19. Wu, L.;Guo, S.;Wang, X.;Guo, Z.;Yao, G.;Lin, Q.;Wu, M. *Tetrahedron Lett.* **2015**, *56*, 2145–2148.
20. Ueda, S.;Su, M.;Buchwald, S. L. *Angew. Chem., Int. Ed.* **2011**, *50*, 8944–8947.
21. Zincke, T.;Th. Lawson, A. *Chem. Ber.* **1887**, *20*, 1176–1183.
22. (a)Schmidt, M. P.;Hagenböcker, A. *Chem. Ber.* **1921**, *54*, 2191–2200; (b)Schmidt, M. P.;Hagenböcker, A. *Chem. Ber.* **1921**, *54*, 2201–2207.
23. Jo, J.;Lee, H. Y.;Liu, W.;Olasz, A.;Chen, C. H.;Lee, D. *J. Am. Chem. Soc.* **2012**, *134*, 16000–16007.
24. Gale, P. A.;Hiscock, J. R.;Moore, S. J.;Caltagirone, C.;Hursthouse, M.

B.;Light, M. E. *Chem. Asian J.* **2010**, *5*, 555–561.
25. (a)Huffman, J. L.;Brennan, R. G. *Curr. Opin. Struc. Biol.* **2002**, *12*, 98–106; (b)Rodionov, D. A. *Chem. Rev.* **2007**, *107*, 3467–3497.
26. Hu, H. Y.;Xiang, J. F.;Yang, Y.;Chen, C. F. *Org. Lett.* **2008**, *10*, 69–72.
27. Zhang, Z.;Che, Y.;Smaldone, R. A.;Xu, M.;Bunes, B. R.;Moore, J. S.;Zang, L. *J. Am. Chem. Soc.* **2010**, *132*, 14113–14117.
28. Shang, J.;Si, W.;Zhao, W.;Che, Y.;Hou, J. L.;Jiang, H. *Org. Lett.* **2014**, *16*, 4008–4011.
29. Ousaka, N.;Yamaguchi, T.;Yashima, E. *Chem. Lett.* **2014**, *43*, 512–514.

Fluorescent Oligomers Built with Triazole-Based Turn-Motifs: Length- and Solvent-Dependent Photophysical Properties

1. Introduction

As exemplified by protein folding, spontaneous structural collapse of linear biological molecules leads to compact three-dimensional structures for specific function. In this process, secondary structures such as helices, sheets, and turns contribute significantly to local structural ordering and stability.[1] A "turn" motif, as shown in Figure 1, connects two antiparallel strands, and has been mimicked by appropriately designed synthetic molecules.

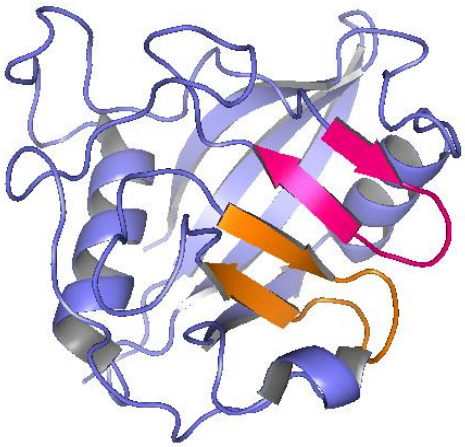

Figure 1. Ribbon diagram of cyclophilin-3 (PDB code: 1E3B) with β-sheets and turn structures highlighted in orange-red.

In Figure 2 and Table 1 are summarized representative π-conjugated molecular skeletons to support two linear strands that run in opposite directions.[2] By a judicious combination of five- and six-membered (hetero)aromatic motifs, both the (i) degree of conformational freedom, and (ii)

distance between the two antiparallel strands can be controlled.

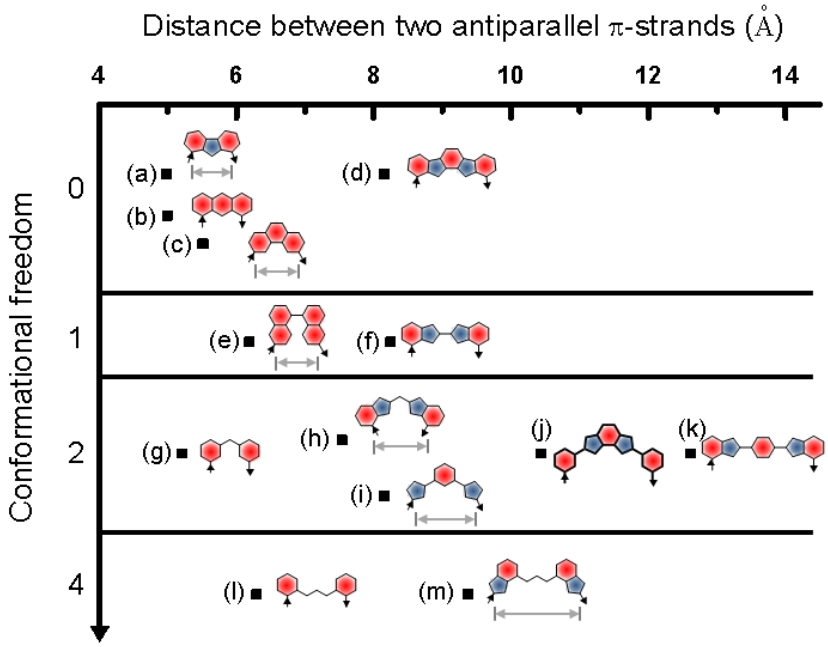

Figure 2. Selected turn motifs with increasing degree of conformational freedom (vertical direction) and the distance between two antiparallel strands (horizontal direction).

Synthetic turn motifs having hydrogen bond donor (HBD) groups can function as anion receptors. Gale and coworkers have shown that the anion binding affinity of diindolylurea moiety can be controlled by changing the number of HBD,[3] and demonstrated anion-to-anion proton transfer in hydrogen bonded complexes.[2g] In addition, rigid turn motifs can impart a bias in the twist sense of the entire structures. For example, Chen and coworkers reported that the structures of helix–turn–helix oligomers could be rearranged across the rigid turn motif as evidenced by CD spectroscopic studies.[2c]

Table 1. Examples of select turn motifs.

Compound	Reported structure	Reference
(a), (d)	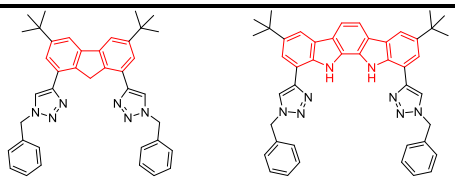	2k
(b), (c)	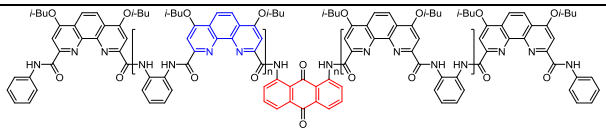	2b
(c), (e)	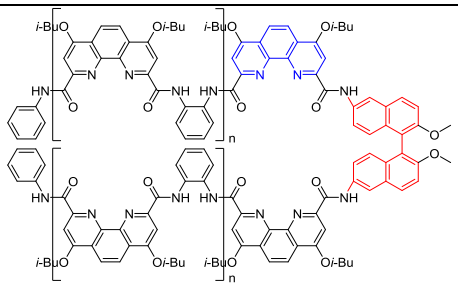	2c
(f)	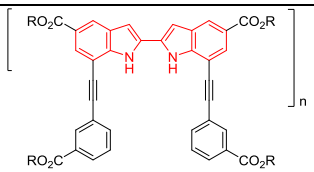	2d
(g)	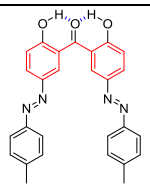	2a
(h)	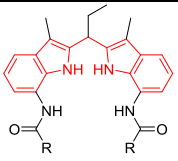	2e
(i)	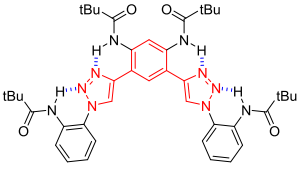	2j

(j)	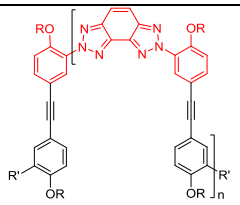	This work
(k)	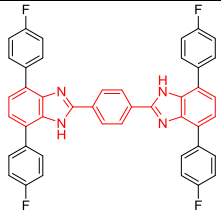	2i
(l)	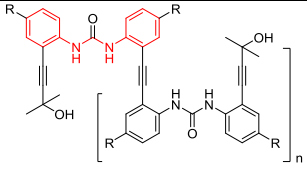	2h
(m)	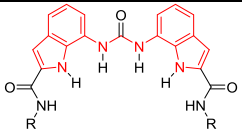	2g

Linear oligomers that fold to compact helical structures are called *foldamers*. Depending on specific conditions, such molecules can switch between folded and unfolded conformations. During the past decades, significant efforts have been made in foldamer research with primary focus on the design and synthesis of new "foldable" motifs.[4] Equally important is devising and implementing mechanisms to drive the folding–unfolding transition. Moreover, if foldamers are endowed with readily detectable photophysical properties that are already embedded within the repeat unit structures and reversibly controlled by structural folding and unfolding, such properties hold significant practical implications. However, the chemistry of fluorescent foldable oligomers is yet to be developed. Only a handful of systems are currently known.[2d, 5]

In this study, we have incorporated fluorescent *N*-2-aryl-1,2,3-

benzotriazole units as key building blocks for foldable oligomers. Our research group has previously shown that *N*-2-aryl-1,2,3-benzotriazole can serve as a reporter group in fluorescence turn-on detection of copper(II) ions.[6] Here, oxidative cyclization reaction transforms non-emissive azoanilines into highly fluorescent *N*-2-aryl-1,2,3-bezotriazole products. We reasoned that a formal "fusion" of two *N*-2-aryl-1,2,3-triazoles across a central benzene ring, as shown in Figure 2 should provide a rigid and fluorescent turn motif that can support two parallel π-strands. Modularity in the synthesis is an added bonus in this system, although we still had to devise a concise and high-yielding bond assembly strategies using a minimal number of building blocks. In the following sections are described the design, synthesis, and structure-dependent photophysical properties of this previously unknown class of fluorescent foldamers.

2. Results and Discussion

2.1. Design and Synthesis

We initially targeted bis(triazolo)benzene-based oligomers **II**–**V** (Scheme 1), in which a systematic variation is made in the number of the repeating units. As a "mono" triazolobenzene model system, compound **I** was also designed (Scheme 3). Here, the bis(triazolo)benzene units serves as turn motifs; hexyl groups were introduced to enhance solubility in organic solvents. In order to gain a precise control over the chain length, we devised a highly modular synthetic scheme involving five building blocks **5**–**9**. As outlined in Scheme 2, these molecules can readily be prepared from common precursors **1**–**4** by following straightforward functional group transformations.

R= -C_6H_{13}

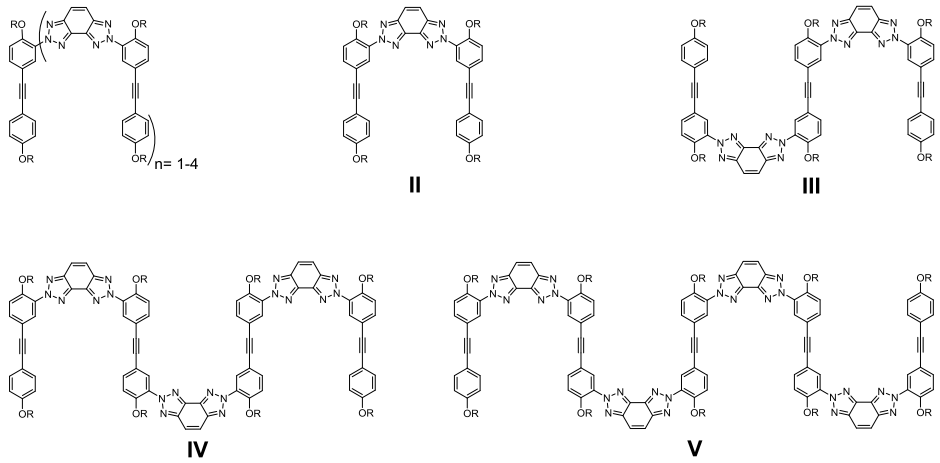

Scheme 1. Chemical structures of *N*-2-aryl-functionalized bis(triazolo)benzenes.

In this system, key steps for stepwise chain growth involve azo coupling following by oxidative cyclization reactions. Compared with alternative synthetic routes, such as deamination (Scheme 4), Sonogashira–Hagihara C–C cross-coupling (Scheme 5), and C–N coupling approaches (Scheme 6), the sequence outlined in Scheme 3 is most attractive in terms of efficiency and selectivity in modular assembly.

While Scheme 4 might appear appealing since it would require only three types of building blocks, our attempts to produce **IV** in this route were not successful, in part due to difficulties in converting the nitro groups of the precursor molecule to amine groups. A standard Sonogashira–Hagihara C–C

Scheme 2. Synthesis of the arylethynyl precursor 4.

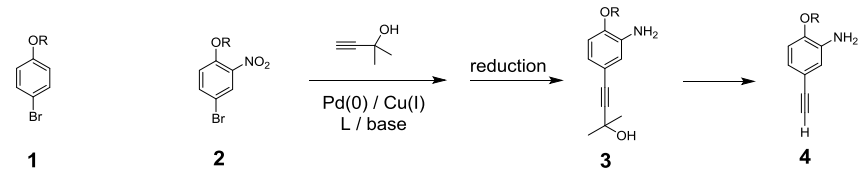

Scheme 3. Stepwise construction of oligomeric bis(triazolo)benzene via azo coupling.

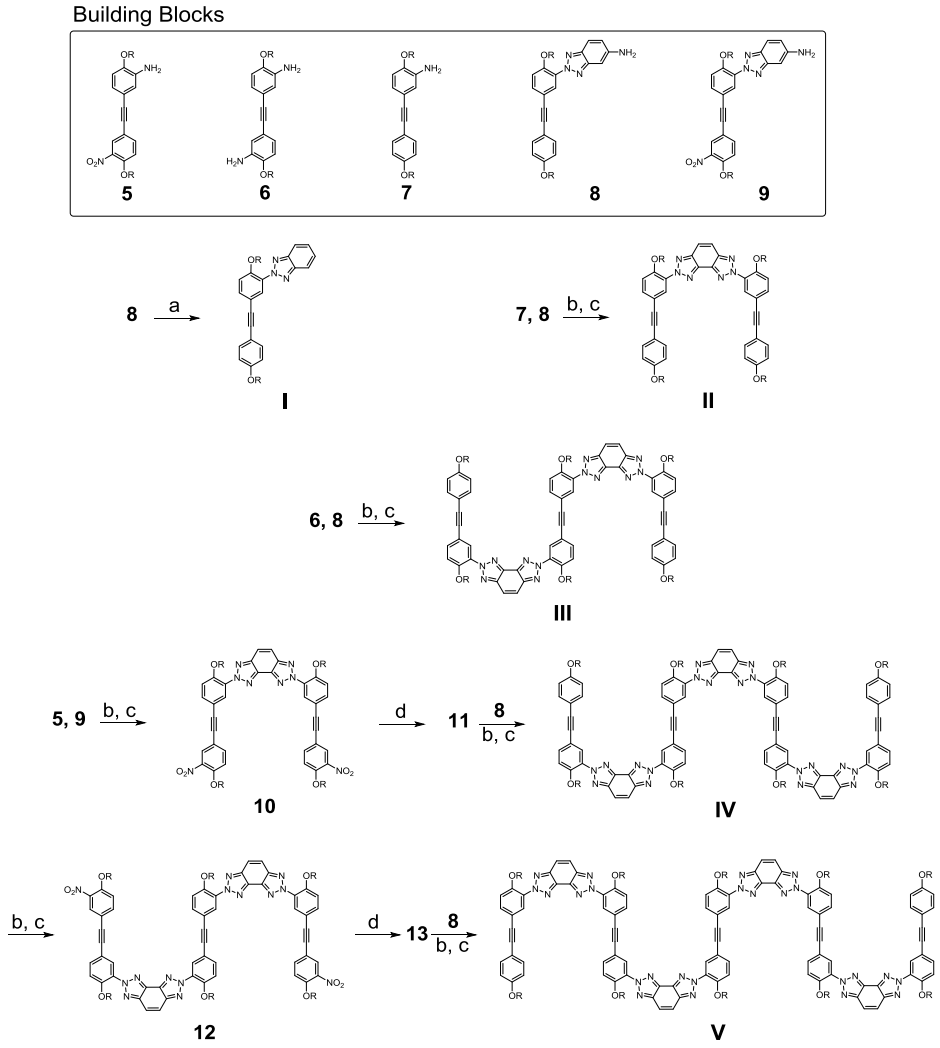

(a) $NaNO_2$, H_3PO_2, 0 ℃. (b) (i) aq HCl/$NaNO_2$, MeOH or THF; (ii) aq NaOH, MeOH, 0 ℃ or pyridine, THF, 0 ℃. (c) $Cu(OAc)_2$, THF, pyridine, 60 ℃. (d) Zn, aq. NH_3, THF.

Scheme 4. Stepwise construction of oligomeric bis(triazolo)benzene via azo coupling and deamination.

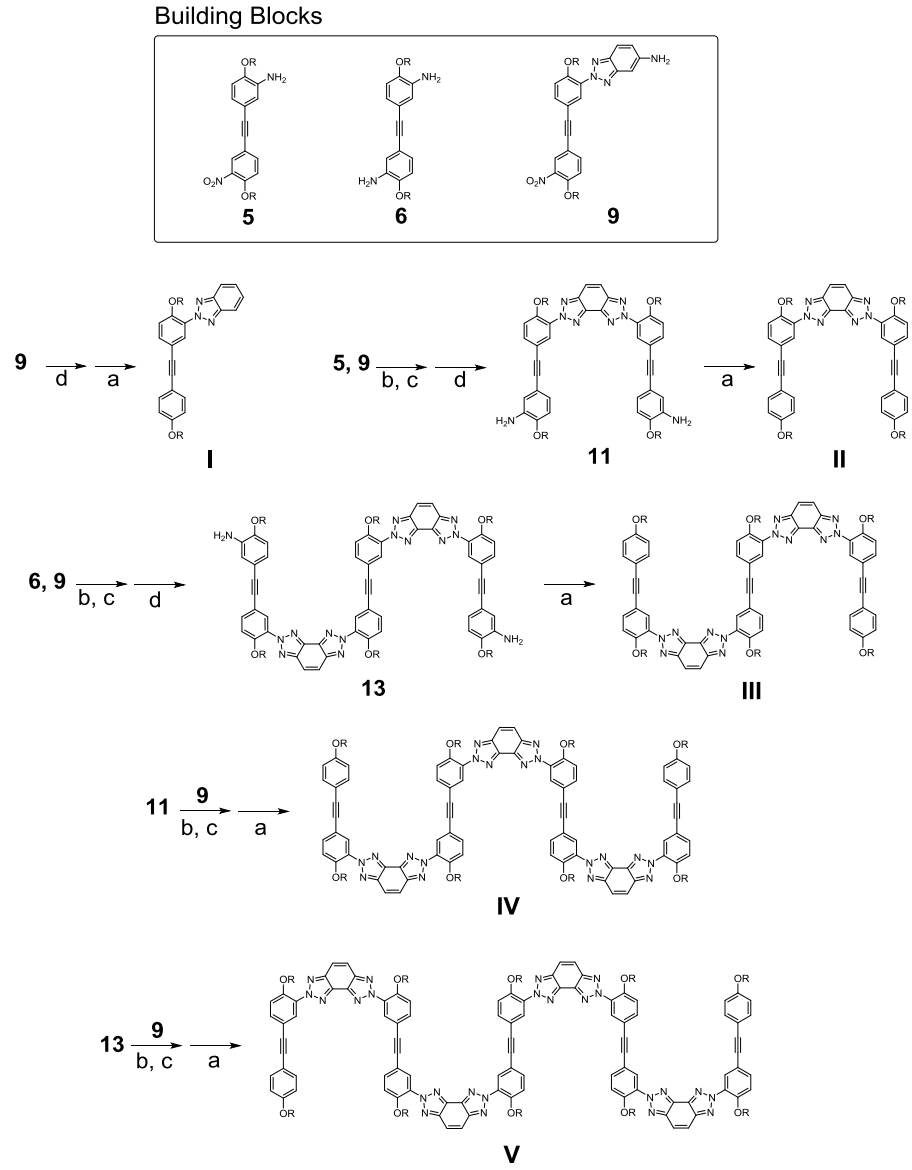

(a) Deamination, (b) azo coupling, (c) oxidative cyclization, and (d) reduction.

Scheme 5. Stepwise construction of oligomeric bis(triazolo)benzene via Sonogashira–Hagihara C–C cross-coupling.

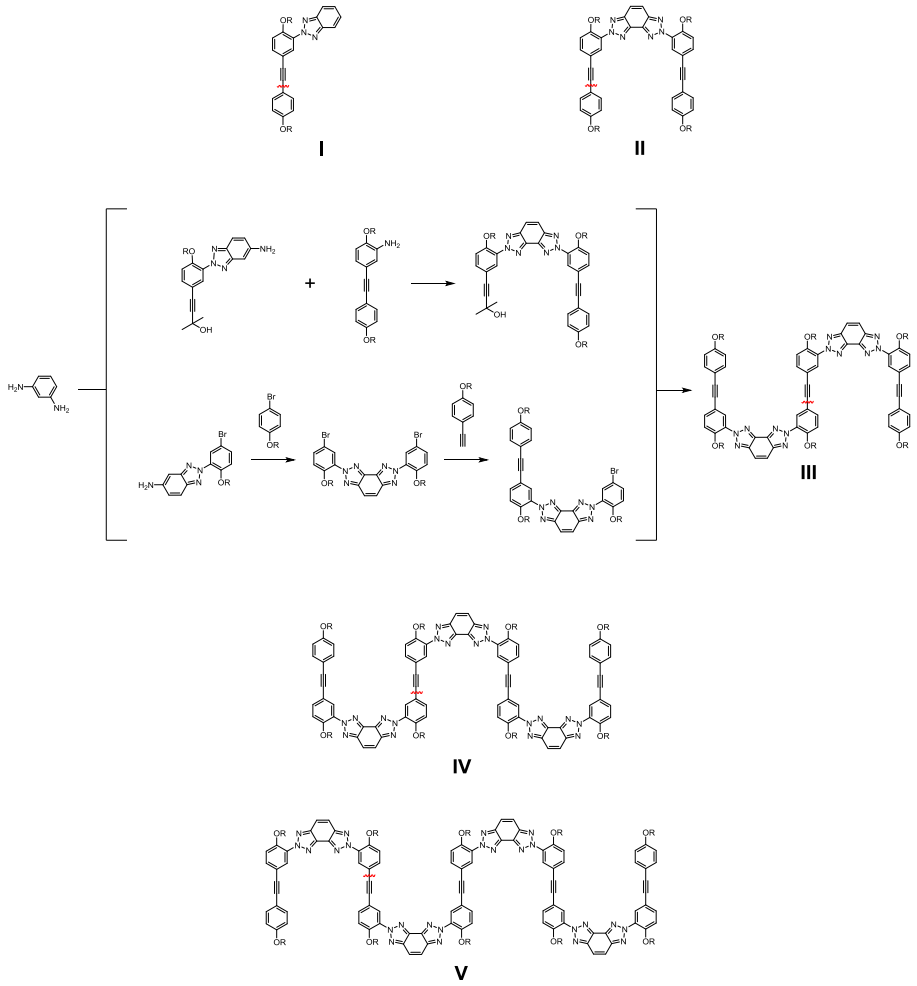

Scheme 6. Stepwise construction of oligomeric bis(triazolo)benzene via C–N cross–coupling.

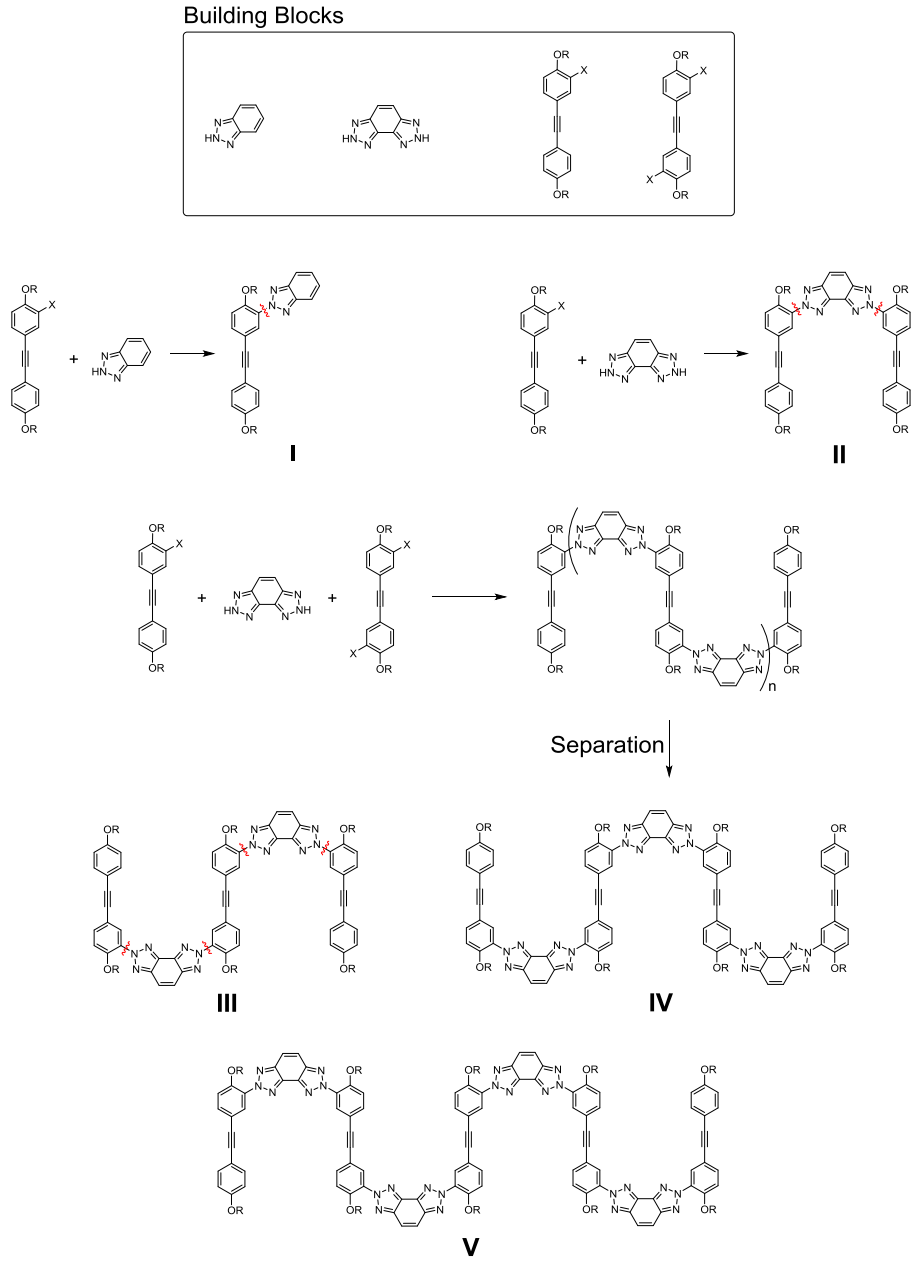

coupling has previously been used for stepwise elongation of foldable oligomers.[2d, 7] A typical problem of this approach is the formation of undesired diethynyl by-products as a result of Glaser coupling, which lowers the product yield. Moreover, this route, as outlined in Scheme 5, would require more building blocks than Scheme 3 in order to arrive at **I**–**V**. For example, the synthesis of **III** by this route (see Scheme 5) entails at least six steps that hardly share common building blocks.

In contrast, the C–N coupling route outlined in Scheme 6 would require only four building blocks to access **I**–**V**. As discussed in Section A.1.1, however, general synthetic protocols are yet to be established to construct aryl-triazole linkage via regioselective C–N coupling. With existing methodologies, the selectivity for *N*-2 over *N*-1 position is still quite low.[8] In addition, this approach would produce a mixture of **III**, **IV**, and **V**. In reality, it would be difficult, if not impossible to separate **III**, **IV**, and **V** having different lengths but with similar polarities and co-existence of regioisomers (from *N*-2 vs *N*-1 substitution).

After careful consideration of the advantages and disadvantages of each strategy summarized above, we decided to take the synthetic route outlined in Scheme 3, which exploits reliable azo coupling reactions as key steps and would suffer less from by-product formation. In addition, azo coupling reaction would result in a significant change in the polarity between the starting material and the product, thereby facilitating the separation step.

One important feature of our synthetic design is the use of nitro groups as "masked amino groups" for the stepwise construction of oligomers (Scheme 7a), rather than uncontrolled formation of oligomer mixtures with varying chain length (Scheme 7b). Since "unmasking" requires reduction of $–NO_2$ to $–NH_2$ groups, we had to screen conditions that would not affect unsaturated C–C bonds within the molecule. A rather mild protocol using

Zn/NH_3 in aqueous THF turned out to be ideal for our purpose.

Scheme 7. Schematic representation of strategies for extending oligomer chain length: (a) amino-nitro pair; (b) amino-amino pair

.

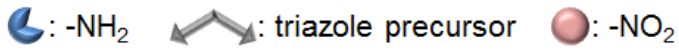

(a)

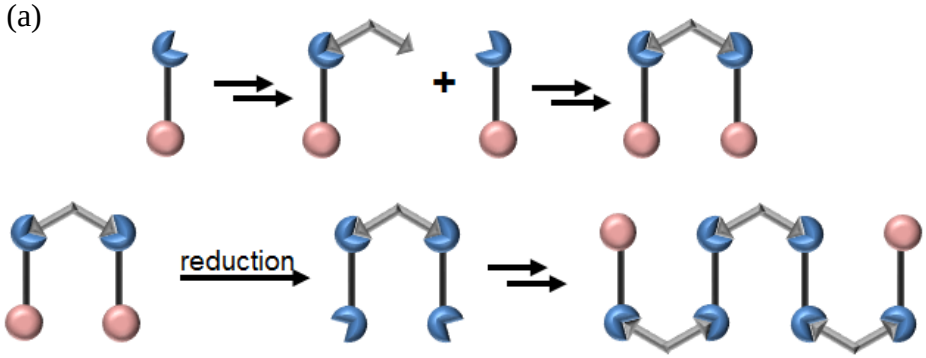

(b)

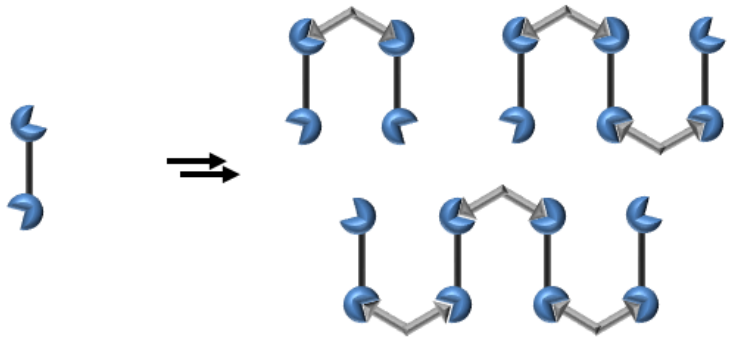

Scheme 8. First-Generation foldamers with bis(triazolo)benzene skeleton.

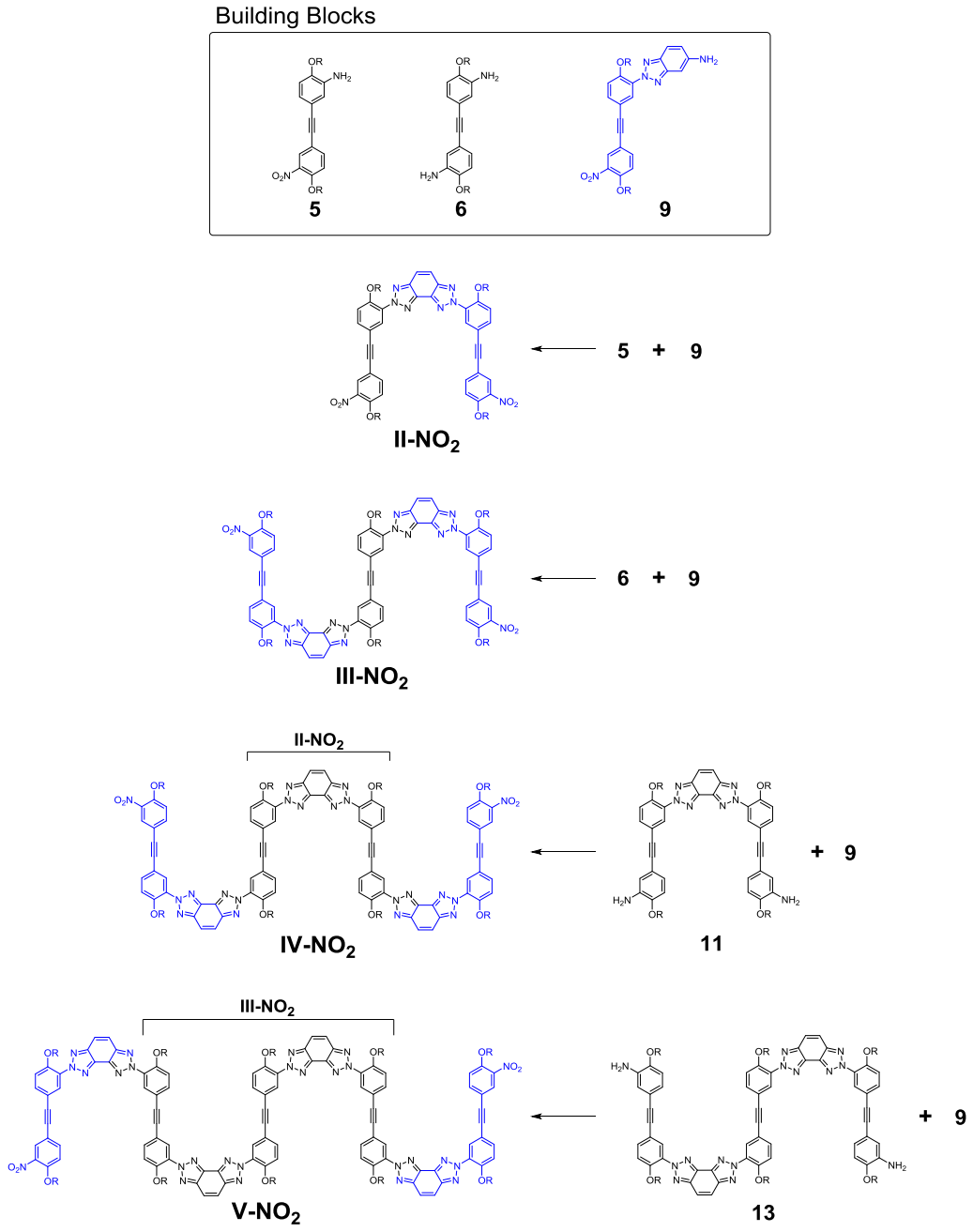

Scheme 9. Second-Generation foldamers with bis(triazolo)benzene skeleton.

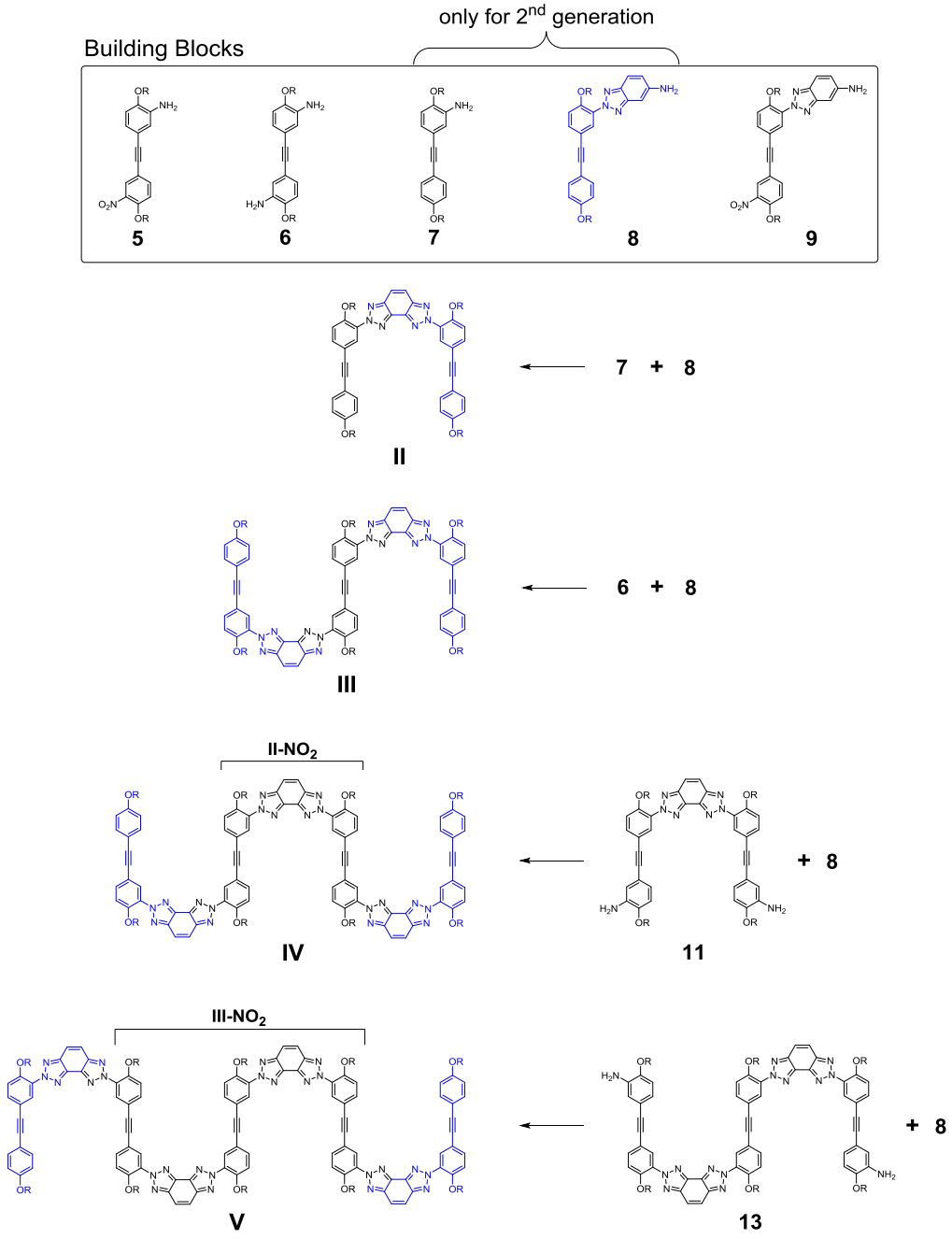

We initially targeted oligomers having nitro groups at each end (Scheme 8) since they could readily be constructed using only three types of building blocks. As it turned out, however, the presence of nitro groups in these molecules significantly compromised their fluorescence properties. With the nitro groups functioning as fluorescence quencher, the diminution of fluorescence quantum yield becomes more pronounced with decreasing chain length. This observation could readily be explained by the fact that each of the oligomers have a fixed number of (i.e. two) nitro groups, and therefore their quenching effects become diminished with increasing chain length when the molecule is comprised of multiple fluorogenic repeats (vide infra). In other words, the fluorescence intensity is enhanced by extending the oligomer length. In order to avoid this problem, second-generation of *N*-2-aryl-1,2,3-bis(triazolo)benzene oligomers were designed (Scheme 9). For this new generation, building block **7** and **8** were newly prepared. By assembling **5**–**9**, oligomers **I**–**V** were successfully synthesized and characterized.

2.2. X-ray Crystallographic Studies

A single crystal of **II** was obtained by vapor diffusion of pentane into chloroform solution and subjected to crystallographic structure analysis. The solid-state structure of **II**, shown in Figure 3, unambiguously confirms the chemical connectivity. While the ring-fused turn motif and π-conjugated linear strands are structurally rigid, rotations around the C_{aryl}–$N_{triazole}$ bonds should still allow the molecule to sample at least three conformations in solution. The solid-state structure **II** is the r-shape conformation (b) in Scheme 10.

The X-ray structure of the nitro-substituted analogue of **III** (Figure 4) is similar to the r-shape conformation (b) with fully stretched backbone. This compound is the synthetic intermediate **12**, and its single crystal was obtained by vapor diffusion of pentane into the ethyl acetate solution. The difference

between **12** and **II** is the presence of the third "pillar". We postulate that solid-state packing enforces a more extended and flattened backbone of **12**.

The possibility of the w-shape conformation (c) in Scheme 10 is suggested by the X-ray structure of **14**, which is a model system of **II**. As shown in Figure 5, the molecule adopts a w-shaped backbone conformation which is stabilized by a H_2O molecule located inside the "cavity" and stabilized by O_{water}–H···$N_{triazole}$ hydrogen bonds (intramolecular fashion) and O_{water}···H–$O_{alcohol}$ hydrogen bonds (intermolecular fashion). If such conformation could be maintained after demethylation of **14**, the molecule could adopt a structure proposed in Figure 6.

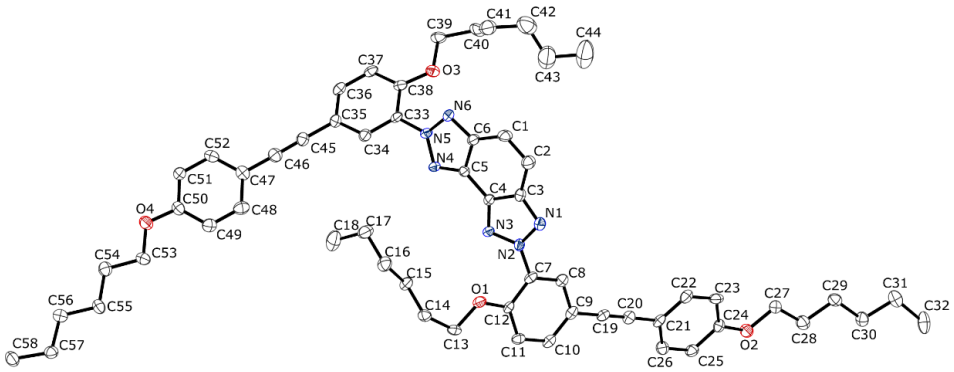

Figure 3. X-ray structure of **II** as ORTEP diagram with 50% thermal ellipsoids. Hydrogen atoms are omitted for clarity.

Scheme 10. Schematic representation of the conformations of **II**.

(a) (b) r-shape (c) w-shape

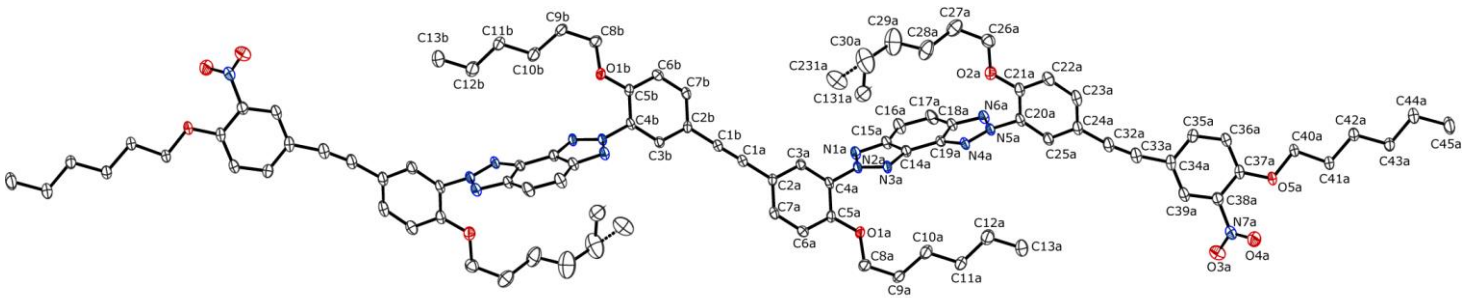

Figure 4. X-ray structure of **12** as ORTEP diagram with 50% thermal ellipsoids. Hydrogen atoms are omitted for clarity.

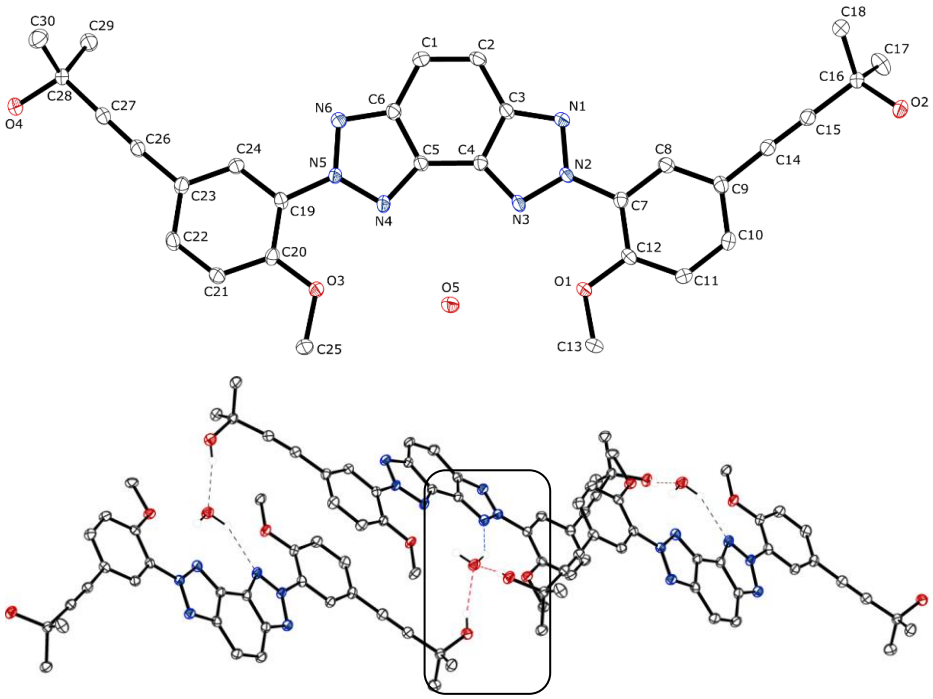

Figure 5. X-ray structure of **14** as ORTEP diagram with 50% thermal ellipsoids (top). Hydrogen bonding among three **14** molecules and one water molecule (bottom). Dotted lines represent hydrogen bond. Hydrogen atoms are omitted for clarity except for those associated with hydrogen bond.

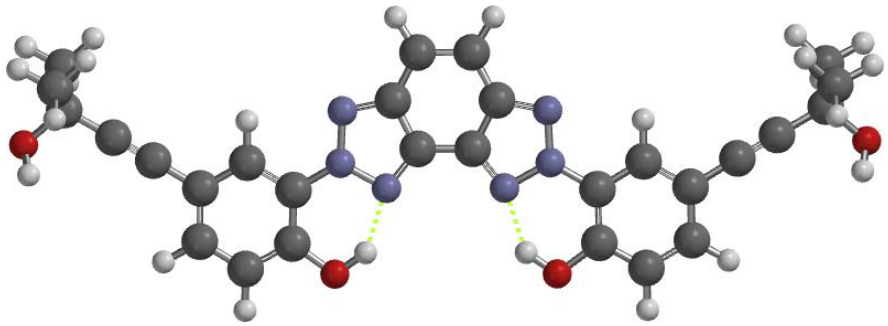

Figure 6. Energy-minimized (DFT/B3LYP) structure of demethylated **14** calculated by Spartan'14 program. Dotted green lines represent hydrogen bonding.

One of the conditions for folding is solvophobic effects that control the interaction between side chains and solvent molecules.[9] If proper conditions are found to enforce the molecule adopt the n-shape conformation (a), folding should occur with short repeating units. This is a merit of the 90° turn motif that we build.

2.3. Photophysical Properties

With a series of compounds **I**–**V** (Scheme 3) synthesized and fully characterized, we first carried out UV–vis spectroscopic studies to investigate their length-dependent light-absorbing properties. Monobenzotriazole functionalized **I** and bis(triazolo)benzenes **II**–**V** in CH_2Cl_2, as shown in Figure 7a, display similar UV–vis spectra. As shown in Figure 7b, the molar absorptivity, $\varepsilon_{320\ nm}$ of **I**–**V** measured at λ = 320 nm show a linear relationship with the number of π-pillar unit. In addition, the normalized electronic absorption spectra of shown in Figure 7a are essentially superimposable with no apparent shifts in λ_{max}. These findings support the notion that the *N*-aryl-triazolobenzene "repeat strand", as defined in Scheme 1, serves as independent light-absorbing unit with no strong electronic coupling to adjacent π-strands across the turn motif. With the *structurally-conjugated-yet-electronically-disjointed* nature of the ground-state electronic properties established for **II**–**V**, we set out to investigate their excited-state electronic properties by fluorescence spectroscopy.

In order to investigate length-dependent light-emitting properties of **II**–**V**, fluorescence measurements were made by fixing the absorbance (at λ = 320 nm) to 0.08. Since the absorbance is proportional to the number of the repeat units that behave as independent chromophores (vide supra), the intensity of the fluorescence spectra is directly proportional to the fluorescence quantum yields, Φ_F. As shown in Figure 7c, the emission spectra of **II**–**V** are essentially superimposable with high (Φ_F = 81–83%) fluorescence quantum

yields. These findings corroborate the notion that each of the ring-fused and *N*-aryl-extended triazole repeat behaves as an independent light-emitting unit as well, despite the seemingly π-conjugated nature of the linear backbone.

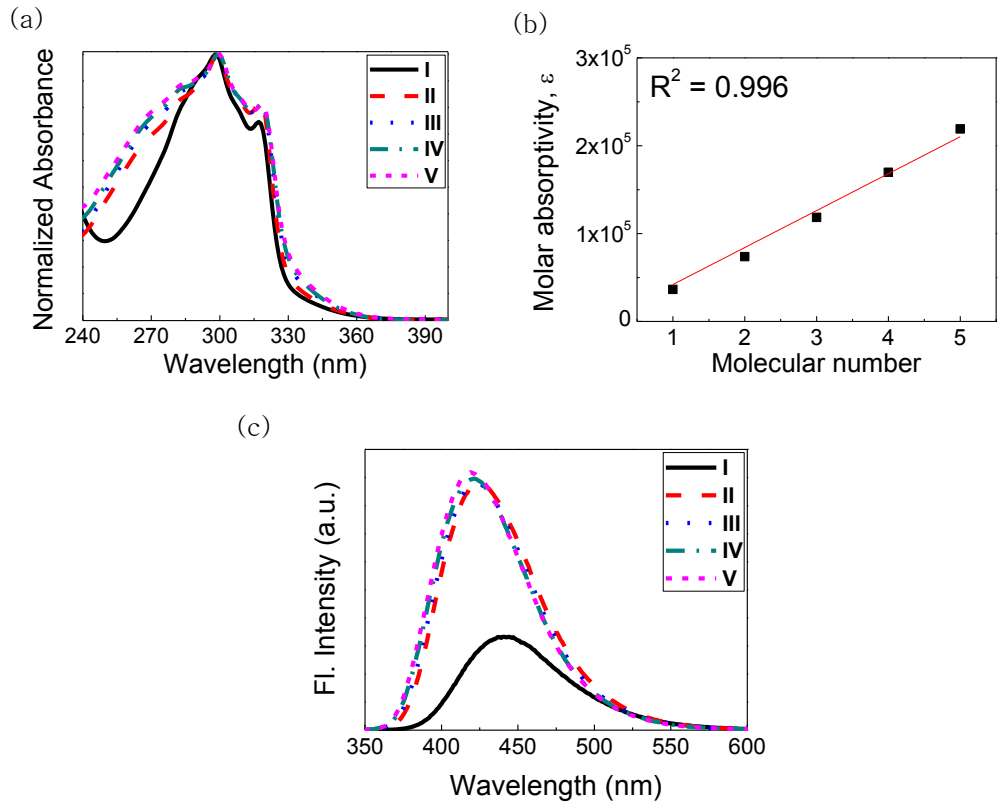

Figure 7. Electronic absorption spectra of **I**–**V**: (a) normalized UV–vis spectra; (b) molar absorptivity, $\varepsilon_{320\ nm}$ vs chain length; (c) fluorescence emission spectra (λ_{ex} = 320 nm) in CH_2Cl_2, T = 293 K.

In the case of **I**, different fluorescence spectrum was obtained, in which the $\lambda_{max,em}$ is red-shifted by $\Delta\lambda$ = 20 nm relative to those of **II**–**V**. This behavior might arise from the increased charge transfer character of **I**. Compared with the symmetrically substituted bis(triazolo)benzene moiety, monotriazolobenzene has only one triazole unit, and therefore could display

CT-type emission with red-shifted $\lambda_{max,em}$. In addition, the fluorescence quantum yield of **I** (Φ_F = 30%) is significantly smaller than those of **II**–**V** (Φ_F = 81–83%). Based on these findings, we conclude that the benzene-fused *N*-aryl-extended triazole behave as an independent fluorophore, but its emission properties can be modified depending on whether it is a part of a mono- (for **I**) vs bis(triazolo)benzene (for **II**–**V**) platform.

Table 1. Photophysical Properties of **I–V.**

compound	$\varepsilon_{320\ nm}$ (10^4 M^{-1} cm^{-1})	$\lambda_{max,ex}$ (nm)	$\lambda_{max,em}$ (nm)	Φ_F (%)
I	3.64	317	441	30
II	7.38	318	426	81
III	11.8	318	421	81
IV	17.0	319	420	82
V	21.9	319	420	83

2.4. Effects of Solvents on the Photophysical Properties

Scheme 11. Schematic representation of the **II** and **V**.

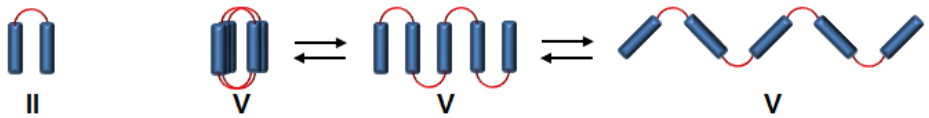

In order to investigate the possible role of molecule-solvent interactions in the conformational dynamics (Scheme 10, 11), we carried out comparative studies on the longest oligomer **V** and the shortest oligomer **II**. Since **V** has multiple turn motifs, *N*-aryl-triazole units could be brought into close proximity by structural folding, while such intramolecular interaction is essentially impossible for **II**. Solution samples of **II** and **V** were prepared with various mixed-solvent systems, and investigated by fluorescence spectroscopy. Due to their limited solubilities in polar organic solvents, samples were prepared by mixing THF stock solutions with other solvents in 2:8 (v/v) ratio

(Figure 8).

As shown in Figure 8, both **II** and **V** show linear correlation between the emission wavenumber and the $E_T(30)$ values of the solvents.[10] With increasing solvent polarity, the emission spectra undergo systematic red-shifts and larger Stokes shifts. This solvent-dependent behavior implicates the involvement of charge separation in the excited-states and CT-type emission.

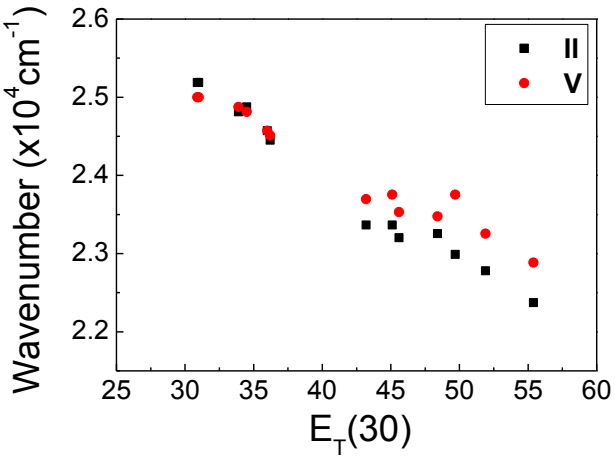

$E_T(30)$	Solvent	$E_T(30)$	Solvent	$E_T(30)$	Solvent
30.9	cyclohexane	36.2	THF	48.4	isopropanol
31.0	n-hexane	43.2	DMF	49.7	n-butanol
33.9	toluene	45.1	DMSO	51.9	EtOH
34.5	Ether	45.6	MeCN	55.4	MeOH
36.0	dioxane				

Figure 8. Polarity-dependent shifts in the emission maximum of 2(■) and 5(●) plotted as wavenumber (cm^{-1}) vs $E_T(30)$ for mixed solvent system. T = 293 K.

Intriguingly, the fluorescence intensity of the **V** decreased over time and stabilized at ca 32–44% of its initial value when cyclohexane, *n*-hexane, or ether was used in the mixed solvent system (Figure 9). In contrast, the shorter

oligomer **II** does not show such spectral change. Under identical conditions, the UV–vis spectra of the samples remained essentially unchanged, indicating that sample decomposition or precipitation is not responsible for the behavior of **V**.

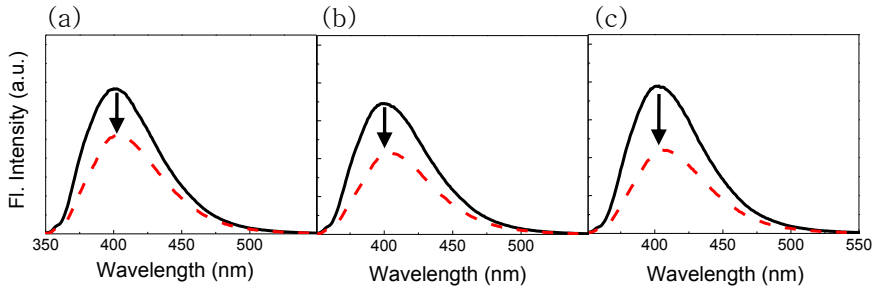

Figure 9. Changes in the fluorescence spectra of **V** in (a) cyclohexane/THF (80:20, v/v); (b) *n*-hexane/THF (80:20, v/v) and (c) ether/THF (80:20, v/v).

In order to investigate whether intermolecular aggregation is involved in this process, the sample concentration was varied in *n*-hexane/THF (80:20, v/v).

For samples of [**V**] = 0.182–3.68 μM (Figure 11), essentially identical behavior was observed. Upon standing at r.t., the intensity of the UV–vis spectra decreased by ca 16–19% (as measured by the absorbance at λ = 300 nm) as a result of hypochromism.[11] This phenomenon is common in biological-type helical polymers showing decrease in electronic absorption intensity upon changing random structure to ordered helical structure.[7] For all the samples, the fluorescence intensity was also decreased by ca 43–50 %. No change in the $\lambda_{max,abs}$ or $\lambda_{max,em}$ was observed. Under similar conditions, samples of [**II**] = 0.527–10.1 μM (Figure 10; note that the sample concentration of **II** was adjusted to ensure that the chromophore concentrations are identical for **II** and **V**) showed no change in either the UV–vis or fluorescence spectra. This striking difference in chain-length dependent

photophysical properties can best be explained by structure-dependent interchromophore interactions that occur in the intramolecular fashion and therefore becomes more pronounced with increasing chain length. Among 15 different mixed-solvent systems that we screened (Figure 8), this behavior was observed particularly for solvents of low polarity (i.e. cyclohexane, *n*-hexane, ether) when mixed with THF. While the detailed nature of this solvent-induced shift in conformational equilibrium (Scheme 10) is yet to be established, its length-dependent but concentration-independent (Figure 10, 11)

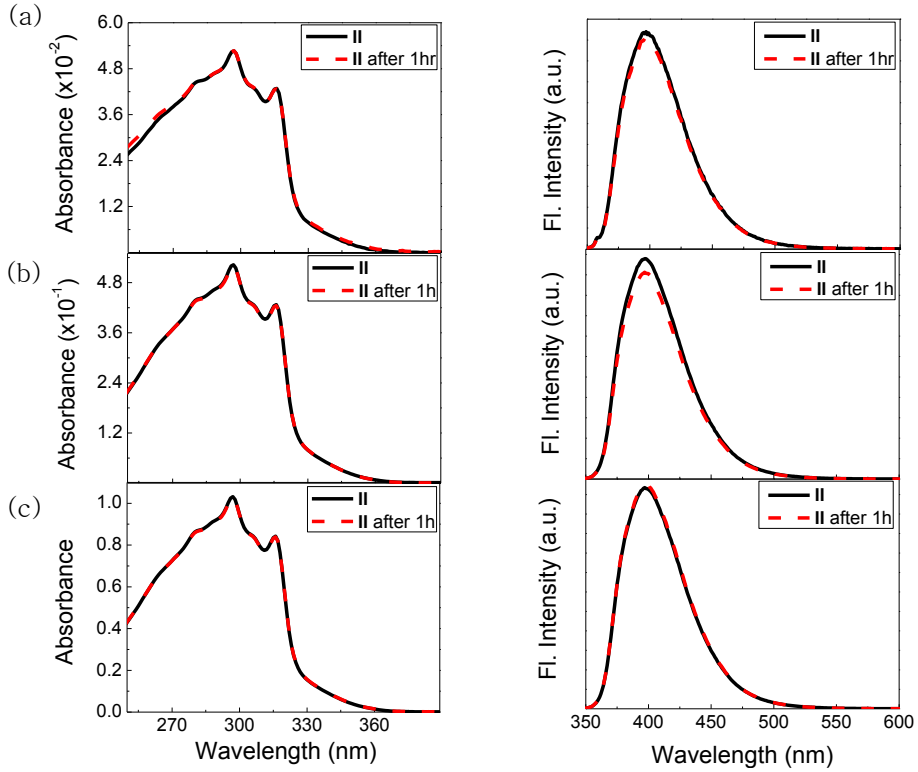

Figure 10. Concentration-dependent UV–vis (left) and fluorescence (right) spectra of **II** in THF/*n*-hexane (20:80, v/v) obtained immediately after mixing (black solid lines) and after 1h (red dashed lines) at T = 293 K. Sample concentrations: (a) 0.527 μM; (b) 5.18 μM; (c) 10.1 μM.

nature strongly suggests the involvement of folding-unfolding of π-conjugated backbone. In addition, the practical utility of the fluorogenic repeats as the foldamer building block has nicely been demonstrated.

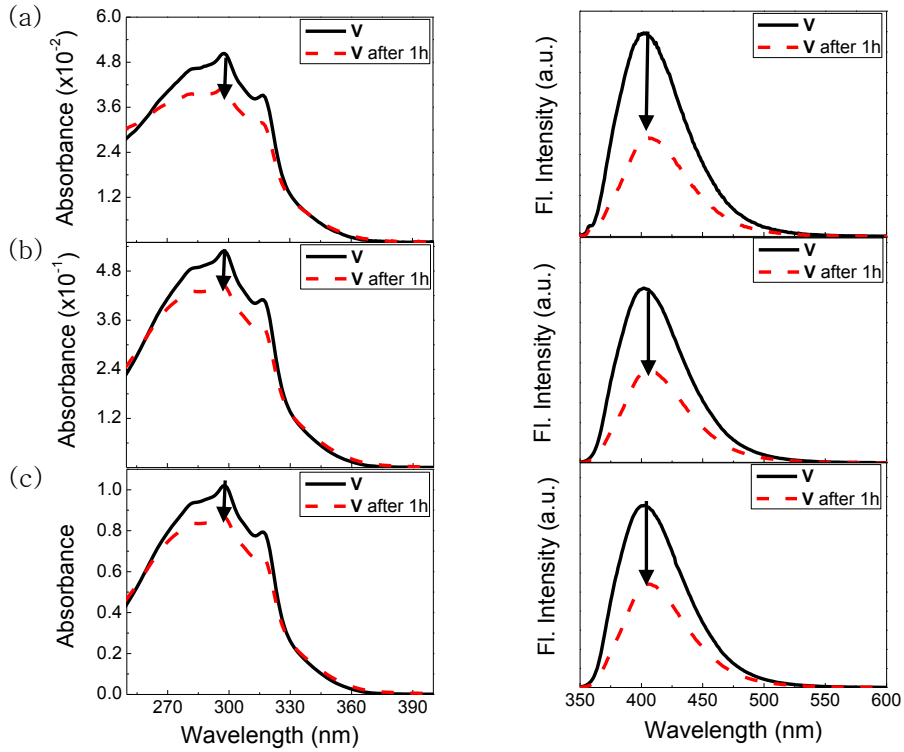

Figure 11. Concentration-dependent UV–vis (left) and fluorescence (right) spectra of **V** in THF/*n*-hexane (20:80, v/v) obtained immediately after mixing (black solid lines) and after 1h (red dashed lines) at T = 293 K. Sample concentrations: (a) 0.182 μM; (b) 1.92 μM; (c) 3.68 μM.

In order to gain further insights into the solvent-dependent spectral changes, we carried out variable-temperature (VT) UV–vis and fluorescence measurements on **II** and **V**. If the experimentally observed hypochromism of **V** (Figure 11) in *n*-hexane/THF (80:20, v/v) arise from structural ordering of chromogenic units through folding, such effect would be diminished at

elevated temperatures that promote unfolding and rapid tumbling. Measurements were made on dilute (0.527 μM) solution samples to minimize the involvement of possible intermolecular interactions.

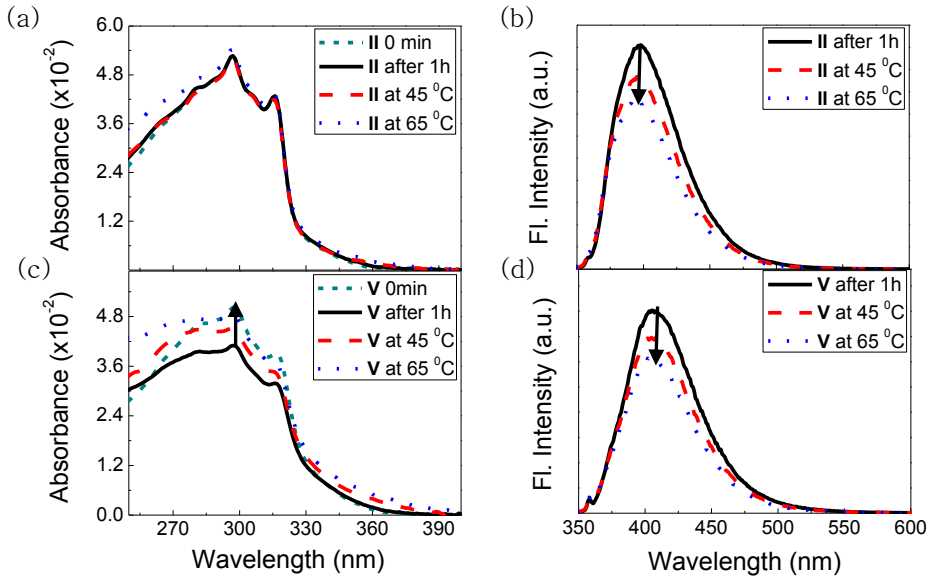

Figure 12. Temperature-dependent spectral changes of **II** (0.527 μM) and **V** (0.182 μM) in *n*-hexane/THF (80:20, v/v): (a) UV–vis and (b) fluorescence spectra of **II**; (c) UV–vis and (d) fluorescence spectra of **V**.

As shown in Figure 12, upon increasing the temperature, the absorbance of **V** was increased to restore the original intensity of the UV–vis spectrum (obtained immediately after mixing). Under similar conditions, the UV–vis spectrum of **II** remained essentially unchanged. Increased thermal motions at elevated temperatures resulted in diminution of the fluorescence intensity, which was observed for both systems (Figure 12).

3. Summary

Using *N*-2-aryl-extended bis(triazolo)benzene as a robust turn motif, we have prepared a series of fluorescent oligomers **I**–**V**. Our synthesis employs a finite number of building blocks that can readily be prepared from common precursors, thereby maximizing modularity in structure assembly without compromising efficiency in synthetic operations. Key steps involve repetitive (i) reduction, (ii) azo coupling, and (iii) oxidative cyclization, which allowed for step-wise construction of oligomers with precise length control. Structural evidence obtained by X-ray crystallography supports the notion of conformational dynamics via C_{aryl}–$N_{triazole}$ rotations.

Comparative spectroscopic studies have revealed that the *N*-aryl-extended bis(triazolo)benzene repeats behave as independent (i.e. uncoupled) light-absorbing and light-emitting units. Moreover, the oligomers display high quantum yields (Φ_F = 81–83%) regardless of chain length, which demonstrates the potential utility of this previously unknown class of linearly extended fluorophores. In addition, the longest oligomer **V** shows hypochromism in the mixed-solvent systems of cyclohexane, *n*-hexane, or ether with THF, which is best explained by structural folding.

4. Experimental Section

4.1. General Considerations

Commercially available reagents were used without further purification. Air sensitive manipulations were carried out under a nitrogen atmosphere by standard Schlenk-line techniques. Thin layer chromatography was performed over Merck silica gel 60 F254 on aluminum foil. Flash chromatography was performed on silica gel (Silicycle Siliaflash P60, 40–63 μm, 230–400 mesh). The compounds 4-bromo-2-nitrophenol and **1** were prepared according to literature procedure.[12]

4.1.1. Physical Measurements

^{1}H and ^{13}C NMR spectra were recorded in $CDCl_3$ on a Bruker DRX 300 NMR (300 MHz) or a Varian/Oxford As-500 (500 MHz) spectrometer. Chemical shifts in ^{1}H NMR spectra were reported in parts per million (ppm) on the δ scale from an internal standard of residual chloroform (δ = 7.27 ppm). Data for ^{1}H NMR are reported as follows: chemical shift, multiplicity (s = singlet, d = doublet, t = triplet, m = multiplet, br s = broad singlet), coupling constant in Hertz (Hz) and integration. Data for ^{13}C NMR spectra are reported in terms of chemical shift in ppm from the central peak of $CDCl_3$ (δ = 77.0 ppm). FTIR spectra were obtained on a Thermoscientific Nicolet iS10 spectrometer equipped with SMART iTR in ATR mode and reported in frequency of the absorption (cm^{-1}). High resolution mass spectra (HRMS) were measured on a JEOL JMS600W spectrometer using electron impact ionization method (EI), JEOL JMS700 spectrometer with fast atom bombardment method (FAB), and MALDI TOF–TOF 5800 System spectrometer using matrix assisted laser desorption ionization time-of flight method (MALDI–TOF). UV–vis spectra were recorded on an Agilent 8453 UV–vis spectrophotometer with ChemStation. Fluorescence spectra were recorded on a Photon Technology International QM–400 spectrofluorometer with FelixGX software. X-ray

crystallographic analysis was performed on a SuperNova, Dual, Cu at zero, AtlasS2 diffractometer.

4.1.2. Fluorescence Quantum Yield Measurements

Quantum yields were determined by standard methods,[13] using trans,trans-1,4-diphenyl-1,3-butadiene (Φ_F = 0.42 in hexane solution; λ_{ex} = 320 nm) as a standard. The sample absorbance was maintained < 0.1 to minimize internal absorption. Corrections were made to account for the differences in solvent refractive indexes.

X-ray Crystallographic Studies on (II)

Single crystals of $C_{58}H_{68}N_6O_4$ **II** were prepared by vapor diffusion of pentane over $CHCl_3$. A suitable crystal was selected and mounted on a nylon loop with paraton-N oil on a SuperNova, Dual, Cu at zero, AtlasS2 diffractometer. The crystal was kept at 99.99(10) K during data collection. Using OLEX2,[14] the structure was solved with the SHELXT[15] structure solution program using Direct Methods and refined with the SHELXL[16] refinement package using Least Squares minimization.

A clear pale-pink crystal data for $C_{58}H_{68}N_6O_4$ (approximate dimensions 0.1 × 0.1 × 0.1 mm^3, M =913.18 g/mol): monoclinic, space group $P2_1/n$ (no. 14), a = 7.6783(5) Å , b = 15.8409(13) Å , c = 41.956(3) Å , β = 94.895(7)°, V = 5084.6(7) $Å^3$, Z = 4, T = 99.95(17) K, μ(MoKα) = 0.075 mm^{-1}, *Dcalc* = 1.193 g/cm^3, 23170 reflections measured (6.796° ≤ 2Θ ≤ 59.346°), a frame time of 17.9 to 71.6 seconds collected with 1° steps in ω and ϕ scans, 11308 unique (R_{int} = 0.0554, R_{sigma} = 0.0769) which were used in all calculations. The final R_1 was 0.1429 (I > 2σ(I)) and wR_2 was 0.3987 (all data).

X-ray Crystallographic Studies on (12)

Single crystals of $C_{90}H_{100}N_{14}O_{10}$ **12** were prepared by vapor diffusion of pentane over EA. A suitable crystal was selected and mounted on a nylon loop with paraton-N oil on a SuperNova, Dual, Cu at zero, AtlasS2 diffractometer. The crystal was kept at 99.99(10) K during data collection. Using OLEX2,[14] the structure was solved with the SHELXS[17] structure solution program using Direct Methods and refined with the SHELXL[16] refinement package using Least Squares minimization.

A clear yellow crystal data for $C_{90}H_{100}N_{14}O_{10}$ (approximate dimensions 0.2 × 0.1 × 0.1 mm^3, M =1537.83 g/mol): triclinic, space group $P\bar{1}$ (no. 2), a = 10.1895(4) Å, b = 12.3027(4) Å, c = 17.0591(6) Å, α = 103.278(3)°, β = 97.210(3)°, γ = 98.163(3)°, V = 2032.31(13) $Å^3$, Z = 1, T = 99.95(13) K, μ(MoKα) = 0.083 mm^{-1}, *Dcalc* = 1.257 g/cm^3, 14209 reflections measured (6.732° ≤ 2Θ ≤ 59.092°), a frame time of 13.0 to 130.0 seconds collected with 1° steps in ω and ϕ scans, 9183 unique (R_{int} = 0.0254, R_{sigma} = 0.0520) which were used in all calculations. The final R_1 was 0.0679 (I > 2σ(I)) and wR_2 was 0.1796 (all data).

X-ray Crystallographic Studies on (14)

Single crystals of $C_{30}H_{30}N_6O_5$ **14** were prepared by vapor diffusion of pentane over EA. A suitable crystal was selected and mounted on a nylon loop with paraton-N oil on a SuperNova, Dual, Cu at zero, AtlasS2 diffractometer. The crystal was kept at 99.99(10) K during data collection. Using OLEX2,[14] the structure was solved with the olex2.solve[18] structure solution program using Charge Flipping and refined with the SHELXL[15] refinement package using Least Squares minimization.

A clear pink crystal data for $C_{30}H_{30}N_6O_5$ (approximate dimensions 0.1 × 0.08 × 0.07 mm^3, M =554.60 g/mol): monoclinic, space group $P2_1/c$ (no. 14), a = 8.5118(4) Å, b = 21.5727(10) Å, c = 14.8041(7) Å, β = 98.907(5)°, V = 2685.6(2) $Å^3$, Z = 4, T = 99.99(10) K, μ(MoKα) = 0.096 mm^{-1}, *Dcalc* =

1.372 g/cm^3, 11390 reflections measured (6.794° ≤ 2Θ ≤ 59.326°), a frame time of 32.0 to 127.9 seconds collected with 1° steps in ω and ϕ scans, 6229 unique (R_{int} = 0.0277, R_{sigma} = 0.0479) which were used in all calculations. The final R_1 was 0.0488 (I > 2σ(I)) and wR_2 was 0.1366 (all data).

4.2. Synthesis

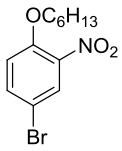

4-Bromo-2-nitro-1-*n*-hexyloxy-benzene (2). A suspension of 4-bromo-2-nitrophenol (18.0 g, 82.6 mmol), 1-bromohexane (16.4 g, 99.1 mmol) and potassium carbonate (22.8 g, 165 mmol) in DMF (180 mL) was stirred at reflux for 2 h, and poured into water (400 mL). The mixture was extracted with diethyl ether (100 mL x 4) and the combined organic phase was dried over anhyd $MgSO_4$. Volatile fractions were removed under reduced pressure to afford crude product, which was purified by silica gel column chromatography with n-hexane: CH_2Cl_2 (5:1, *v*:*v*) as an eluent to obtain **2** as a pale yellow solid (yield = 22.9g, 75.8 mmol, 91.8%). ^{1}H NMR (500Mz, $CDCl_3$, 298 K, ppm): δ 7.94 (d, J = 2.5 Hz, 1H), 7.60 (dd, J = 8.8 Hz, 2.5 Hz, 1H), 6.97 (d, J = 8.8 Hz, 1H), 4.08 (t, J = 6.4 Hz, 2H), 1.85–1.79 (m, 2H), 1.50–1.44 (m, 2H), 1.36–1.32 (m, 4H), 0.92–0.89 (m, 3H); ^{13}C NMR (125 MHz, $CDCl_3$,298 K): δ 14.0, 22.5, 25.4, 28.8, 31.4, 70.0, 111.5, 116.0, 128.2, 136.7, 151.7. FT-IR (neat): ν_{max} 3083, 2955, 2932, 2859, 1605, 1568, 1530, 1488, 1466, 1394, 1350, 1283, 1253, 1161, 1103, 1079, 1005, 937, 876, 813. HRMS (EI$^+$) [M = $C_{12}H_{16}BrNO_3$]$^+$ calculated 301.0313, found 301.0317.

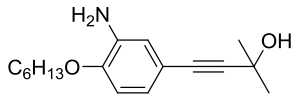

4-(3-Amino-4-hexyloxy-phenyl)-2-methylbut-3-yn-2-ol (3). To a three-necked flask was added **2** (11.6 g, 38.2 mmol), $Pd(PPh_3)_4$ (1.33 g, 1.15 mmol) and CuI (364 mg, 1.91 mmol). The reaction vessel was evacuated and back-filled with nitrogen three times to remove dioxygen. Dry triethyl amine (55.0 mL) and 2-methylbut-3-yn-2-ol (11.0 mL, 76.4 mmol) were delivered into the flask by using a syringe. The reaction mixture was stirred at 60 ℃ for 3 h, allowed to cool to r.t. and filtered through a plug of a Celite. The filtrate was concentrated under reduced pressure, and water (40 mL) was added. The crude mixture was extracted with EtOAc (50 mL x 3). The combined organic layer was dried over anhyd $MgSO_4$, filtered, and concentrated under reduced pressure to afford a brown oil, which was carried on to the next step without purification.

Into a THF solution (90 mL) of the above material was added zinc powder (20.0 g, 306 mmol) and aq NH_3 (30%, 160 mL). The mixture was heated at reflux for 3 h, cooled to r.t., and filtered through a Celite pad to remove insoluble materials. The filtrate was concentrated under reduced pressure, and the residual material was triturated with EtOAc (3 x 80 mL). The organic phase was washed with brine (60 mL), dried over anhyd Na_2SO_4, and filtered. The filtrate was concentrated under reduced pressure. The residual material was purified by silica gel column chromatography using hexanes to *n*-hexane/CH_2Cl_2 (4:1, *v*:*v*) gradient to obtain **3** as a light brown oil. The overall yield over the two steps was quantitative. ^{1}H NMR (500Mz, $CDCl_3$, 298 K, ppm): δ 6.81 (dd, J = 8.3 Hz, J = 2.0 Hz, 1H), 6.78 (d, J = 2.0Hz, 1H), 6.68 (d, J = 8.3Hz, 1H), 3.98 (t, J = 6.5 Hz, 2H), 3.80 (br s, 2H), 1.83–1.78 (m, 2H), 1.60 (s, 6H), 1.50–1.44 (m, 2H), 1.36–1.33 (m, 4H), 0.93–0.90 (m, 3H); ^{13}C NMR (125 MHz, $CDCl_3$,298 K): δ 14.0, 22.6, 25.8, 29.2, 31.6, 65.6, 68.3, 76.8, 77.0, 77.3, 82.5, 91.7, 110.9, 114.7, 117.7, 122.5, 136.0,

147.0. FT-IR (neat): ν_{max} 3379, 3359, 2982, 2934, 2872, 2224, 1615, 1514, 1471, 1436, 1377, 1306, 1245, 1145, 1102, 1017, 950, 884. HRMS (EI^+) [M = $C_{17}H_{25}NO_2]^+$ calculated 275.1885, found 275.1886.

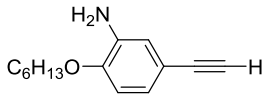

5-Ethynyl-2-hexyloxy-phenylamine (4). To a two-necked flask was added **3** (4.55 g, 16.5 mmol), KOH (926 mg, 16.5 mmol), K_3PO_4 (3.50 g, 16.5 mmol), and anhyd toluene (50 mL). The reaction vessel was evacuated and back-filled with nitrogen three times to remove dioxygen. The reaction vessel was immersed in a pre-heated oil bath and heaeted at reflux until complete conversion was confirmed by TLC. The mixtures was allowed to cool to r.t. and filtered through a Celite pad, which was washed several times with toluene. Combined filtrates were concentrated under reduced pressure, and the residual material was purified by column purification on SiO_2 using *n*-hexane/CH_2Cl_2 (3:1, *v*:*v*) to *n*-hexane/CH_2Cl_2 (1:3, *v*:*v*) as gradient to obtain **4** as a light yellow oil (yield = 2.98 g, 13.7mmol, 83.0%). ^{1}H NMR (500Mz, $CDCl_3$, ppm) δ 6.89 (dd, *J* = 8.1 Hz, *J* = 2.0 Hz, 1H), 6.85 (d, *J* = 2.0Hz, 1H), 6.70 (d, *J* = 8.1Hz, 1H), 4.00 (t, *J* = 6.5 Hz, 2H), 3.82 (br s, 2H), 2.95 (s, 1H), 1.84–1.79 (m, 2H), 1.51–1.45 (m, 2H), 1.37–1.33 (m, 4H), 0.93–0.90 (m, 3H); ^{13}C NMR (75 MHz, $CDCl_3$,298 K): δ 14.0, 22.6, 25.8, 29.2, 31.6, 68.3, 75.0, 76.6, 77.1, 77.5, 84.3, 110.9, 114.0, 118.0, 123.0, 136.1, 147.4. FT-IR (neat): ν_{max} 3481, 3379, 3309, 2932, 2870, 2099, 1614, 1513, 1470, 1432, 1391, 1324, 1294, 1231, 1146, 1087, 1022, 956, 934, 863. HRMS (EI^+) [M = $C_{14}H_{19}NO]^+$ calculated 217.1467, found 217.1465.

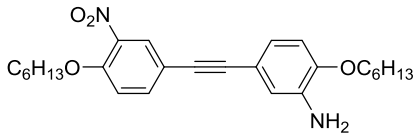

2-Hexyloxy-5-[2-(4-hexyloxy-3-nitrophenyl)ethynyl]-benzenamine (5). A Shlenk flask was loaded with **4** (1.50 g, 6.90 mmol), **2** (2.09 g, 6.90 mmol), $Pd(PPh_3)_4$ (399 mg, 0.345 mmol) and CuI (263 mg, 1.38 mmol). The reaction flask was evacuated and back-filled with nitrogen three times to remove dioxygen. A portion of dry triethyl amine (60 mL) was added by syringe. The reaction mixture was stirred at 55 ℃ for 9 h. Insoluble fractions were removed by filtration through a Celite pad, and the filtrate was concentrated under reduced pressure. Water (40 mL) was added, and the mixture was extracted with EtOAc (50 mL x 3). The combined organic layer was washed with water (50 mL) and brine (50 mL) and dried over anhyd Na_2SO_4. Volatile fractions were removed under reduced pressure, and the residual material was purified by column chromatography on SiO_2 using *n*-hexane to *n*-hexane/EtOAc (10:1, *v*:*v*) as gradient to obtain **5** as a yellow powder (yield = 2.00 g, 4.56 mmol, 66.1%). ^{1}H NMR (500Mz, $CDCl_3$, ppm) δ 7.95 (d, J = 2.0 Hz, 1H), 7.60 (dd, J = 8.8 Hz, J = 2.2 Hz, 1H), 7.02 (d, J = 8.8 Hz, 2H), 6.91 (dd, J = 8.3 Hz, J = 2.0 Hz, 1H), 6.87 (d, J = 2.0 Hz, 1H), 6.74 (d, J = 8.3 Hz, 1H), 4.12 (t, J = 6.5 Hz, 2H), 4.02 (t, J = 6.6 Hz, 2H), 3.85 (br s, 2H), 1.87–1.80 (m, 4H), 1.52–1.45 (m, 4H), 1.38–1.33 (m, 8H), 0.93–0.90 (m, 6H); ^{13}C NMR (75 MHz, $CDCl_3$,298 K): δ 13.99, 14.03, 22.5, 22.6, 25.5, 25.8, 28.9, 29.2, 31.4, 31.6, 68.3, 69.9, 84.9, 90.6, 111.0, 114.3, 116.1, 117.4, 122.6, 128.3, 136.2, 136.6, 147.4, 151.8. FT-IR (neat): ν_{max} 3482, 3378, 2934, 2872, 2207, 1618, 1576, 1533, 1515, 1498, 1467, 1437, 1355, 1390, 1333, 1286, 1270, 1247, 1223, 1161, 1133, 1088, 1041, 991, 933, 905, 861, 822, 808. HRMS (EI^+) [M = $C_{26}H_{34}N_2O_4$]$^+$ calculated 438.2518, found 438.2515.

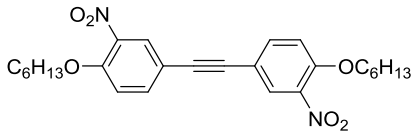

1,1'-(1,2-Ethynediyl)bis[4-(hexyloxy)-3-nitrobenzene] (6-1). To a suspension of $Pd(PPh_3)_2Cl_2$ (140 mg, 0.200 mmol), 1,4-bis(diphenylphosphino)butane (168 mg, 0.393 mmol), 4-bromo-2-nitrophenol (2.37 g, 7.86 mmol), and propiolic acid (825 mg, 11.8 mmol) in DMSO (20.0 mL) was added DBU (1.20 g, 7.86 mmol). The flask was sealed with a septum and heated at 80 ℃ for 12 h. The reaction mixture was poured into sat'd aq NH_4Cl (30 mL), and extracted with CH_2Cl_2 (4 x 20 mL). The combined organic layer was washed with brine (100 mL), dried over anhyd $MgSO_4$, and filtered. Volatile fractions were removed under reduced pressure, and the residual material was purified by silica gel column chromatography with n-hexane:EtOAc (20:1, *v*:*v*) as eluent to obtain **6-1** as a brownish yellow powder (yield = 0.800g, 1.71 mmol, 43.5%). ^{1}H NMR (500Mz, $CDCl_3$, ppm) δ7.98 (d, *J* = 2.0 Hz, 2H), 7.64 (dd, *J* = 8.8 Hz, *J* = 2.2 Hz, 2H), 7.06 (d, *J* = 8.8 Hz, 2H), 4.14 (t, *J* = 6.4 Hz, 4H), 1.88–1.83 (m, 4H), 1.53–1.47 (m, 4H), 1.37–1.34 (m, 8H), 0.95–0.90 (m, 6H); ^{13}C NMR (75 MHz, $CDCl_3$,298 K): δ 14.0, 22.5, 25.5, 28.8, 31.4, 70.0, 87.4, 114.5, 114.8, 128.6, 136.8, 139.7, 152.5. FT-IR (neat): ν_{max} 2961, 2926, 2858, 1617, 1537, 1507, 1481, 1406, 1364, 1327, 1287, 1275, 1249, 1165, 1086, 1012, 982, 902, 822, 805. HRMS (EI^+) $[M = C_{26}H_{32}N_2O_6]^+$ calculated 468.2260, found 468.2257.

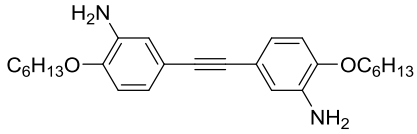

5,5'-(1,2-Ethynediyl)bis[2-(hexyloxy)benzenamine] (6). To a solution of **6-1** (150 mg, 0.320 mmol) in THF (10 mL) was added zinc powder (335 mg, 5.12 mmol) and aq NH_3 (30%, 15 mL). The mixture was heated at reflux for 2.5 h.

Insoluble fractions were removed by filtration through a Celite pad, and the filtrate was concentrated under reduced pressure. The residual material was triturated with EtOAc (4 x 40 mL). The organic phase was washed with brine (50 mL), dried over anhyd Na_2SO_4, filtered, and concentrated. Flash column chromatography on SiO_2 with CH_2Cl_2:EtOAc (10:1, *v*:*v*) as eluent furnished **6** as a yellowish-white powder (yield = 0.100g, 0.245 mmol, 76.6%). ^{1}H NMR (500Mz, $CDCl_3$, ppm) δ6.89 (dd, *J* = 8.3 Hz, *J* = 2.0 Hz, 2H), 6.87 (d, *J* = 1.7 Hz, 2H), 6.72 (d, *J* = 8.3 Hz, 2H), 4.01 (t, *J* = 6.6 Hz, 2H), 3.81 (br s, 4H), 1.85–1.79 (m, 4H), 1.51–1.46 (m, 4H), 1.38–1.34 (m, 8H), 0.95–0.90 (m, 6H); ^{13}C NMR (125 MHz, $CDCl_3$,298 K): δ 14.0, 22.6, 25.8, 29.3, 31.6, 68.3, 87.8, 111.0, 115.8, 117.6, 122.4, 136.1, 146.8. FT-IR (neat): ν_{max} 3474, 3456, 3342, 3054, 2928, 2855, 1615, 1518, 1471, 1441, 1392, 1335, 1291, 1264, 1244, 1205, 1150, 1072, 1045, 1015, 995, 980, 935, 859, 815, 801. HRMS (EI^+) [M = $C_{26}H_{36}N_2O_2]^+$ calculated 408.2777, found 408.2779.

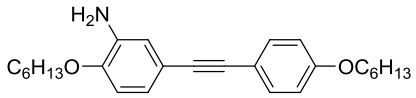

2-Hexyloxy-5-[2-(4-hexyloxyphenyl)ethynyl]-benzenamine (7). A Shlenk flask was loaded with **4** (1.72 g, 7.92 mmol), **1** (2.04 g, 7.92 mmol), $Pd(PPh_3)_4$ (458 mg, 0.396 mmol), and CuI (159 mg, 0.832 mmol). The reaction flask was evacuated and back-filled with nitrogen three times to remove dioxygen. Dry triethyl amine (20 mL) was added by syringe. The reaction mixture was heated at 55 ℃ for 12 h. Insoluble materials were removed by filtration through a Celite pad, and the filtrate was concentrated under reduced pressure. Water (40 mL) was added, and the aqueous layer was extracted with CH_2Cl_2 (50 mL x 3). The combined organic layer was washed with water (50 mL) and brine (50 mL), dried over anhyd $MgSO_4$, and filtered. Volatile fractions were removed under reduced pressure, and the residual material was purified by

silica gel chromatography using *n*-hexane/methylene chloride (1:1, *v*:*v*) as eluent to obtain **7** as a pale yellow powder (yield = 1.09 g, 2.76 mmol, 34.8%). ^{1}H NMR (500Mz, $CDCl_3$, ppm) δ 7.42 (d, J = 8.8 Hz, 1H), 6.92–6.84 (m, 4H), 6.73 (d, J = 8.4 Hz, 1H), 4.01 (t, J = 6.6 Hz, 2H), 3.97 (t, J = 6.6 Hz, 2H), 3.82 (br s, 2H), 1.85–1.76 (m, 4H), 1.52–1.45 (m, 4H), 1.39–1.33 (m, 8H), 0.93–0.91 (m, 6H); ^{13}C NMR (75 MHz, $CDCl_3$,298 K): δ 14.05, 14.09, 22.6, 22.7, 25.7, 25.8, 29.2, 29.3, 31.6, 68.1, 68.3, 87.4, 88.4, 111.1, 114.5, 115.7, 117.6, 120.0, 122.4, 132.8, 136.1, 146.9, 158.9. FT-IR (neat): ν_{max} 3477, 3389, 3342, 2928, 2855, 1607, 1518, 1470, 1436, 1393, 1331, 1305, 1286, 1262, 1248, 1220, 1176, 1152, 1108, 1076, 1045, 995, 934, 862, 833, 802. HRMS (EI^+) [M = $C_{26}H_{35}NO_2$]$^+$ calculated 393.2668, found 393.2670.

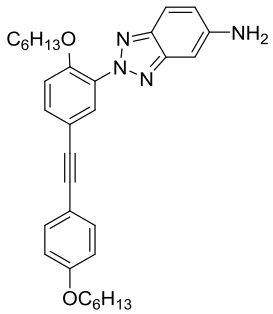

1-(5-Amino-2*H*-benzotriazol-2-yl)-2-hexyloxy-5-[2-(4-hexyloxyphenyl)ethynyl]-benzene (8). To a stirred MeOH solution (10 mL) of **7** (250 mg, 0.635 mmol) was added slowly conc. HCl (0.30 mL). The reaction mixture was kept at 0 ℃ using an ice bath. An aqueous solution (1 mL) of $NaNO_2$ (65.7 mg, 0.952 mmol) was added dropwise to generate the diazonium intermediate, and the reaction mixture was stirred for 15 min. A solution of *m*-phenylenediamine (137.3 mg, 1.27 mmol) and sodium hydroxide (400 mg) in water (2 mL) was kept at 0 ℃. With stirring, the diazonium intermediate was added dropwise to the *m*-phenylenediamine solution. After stirring for 1 h, volatile fractions were removed under reduced pressure, and water (40 mL) was added to the residual material, which was

extracted with CH_2Cl_2 (50 mL x 3). The combined organic layer was washed with water (50 mL) and brine (50 mL), dried over anhyd Na_2SO_4, and filtered. Volatile fractions were removed under reduced pressure.

To a pyridine solution (10 mL) of the azo coupling product described above was added $Cu(OAc)_2 \cdot H_2O$ (567 mg, 2.84 mmol). The reaction mixture was heated at 60 ℃ for 1 h. The mixture was cooled to r.t., and volatile fractions were removed under reduced pressure. After addition of water (20 mL), the aqueous layer was extracted with dichloromethane (30 mL x 3). The combined organic layer was dried over anhyd Na_2SO_4, filtered, and concentrated under reduced pressure. The crude product was purified by silica gel column chromatography with CH_2Cl_2 as eluent to furnish **8** as a yellow oil. The overall yield over the two steps was 63.9% (207 mg, 0.406 mmol). ^{1}H NMR (500Mz, $CDCl_3$, ppm): δ 7.81 (d, J = 2.0 Hz, 1H), 7.76 (d, J = 9.0 Hz, 1H), 7.56 (dd, J = 8.4 Hz, J = 2.0 Hz, 1H), 7.41 (d, J = 8.9 Hz, 2H), 7.06 (d, J = 8.5 Hz, 1H), 6.98 (s, 1H), 6.92 (dd, J = 9.3 Hz, J = 2.0 Hz, 1H), 6.85 (d, J = 8.9 Hz, 2H), 4.04 (t, J = 6.5 Hz, 2H), 3.96 (t, J = 6.6 Hz, 2H), 3.92 (br s, 2H), 1.81–1.75 (m, 2H), 1.70–1.65 (m, 2H), 1.49–1.43 (m, 2H), 1.35–1.29 (m, 6H), 1.23–1.18 (m, 4H), 0.92–0.89 (m, 3H), 0.82–0.79 (m, 3H); ^{13}C NMR (75 Hz, $CDCl_3$,298 K): δ 13.9, 14.0, 22.5, 22.6, 25.4, 25.7, 28.8, 29.2, 31.3, 31.6, 68.1, 69.6, 76.8, 77.1, 77.4, 86.7, 89.2, 96.5, 114.1, 114.6, 115.0, 116.1, 119.1, 121.4, 130.4, 130.6, 132.9, 133.5, 140.7, 145.4, 146.3, 152.9, 159.2. FT-IR (neat): ν_{max} 3464, 3357, 3231, 3042, 2931, 2869, 2535, 2206, 1887, 1635, 1611, 1567, 1516, 1470, 1393, 1361, 1318, 1288, 1248, 1174, 1142, 1108, 1066, 1016, 976, 939, 904, 892, 832, 809. HRMS (EI^+) [M = $C_{32}H_{38}N_4O_2$]$^+$ calculated 510.2994, found 510.2999.

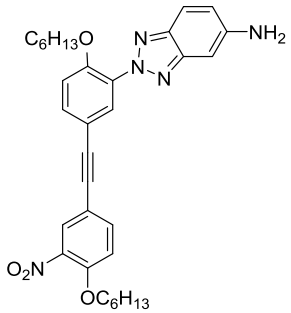

1-(5-Amino-2*H*-benzotriazol-2-yl)-2-hexyloxy-5-[2-(4-hexyloxy-3-nitrophenyl)ethynyl]-benzene (9). To a stirred MeOH solution (15 mL) of **5** (400 mg, 0.912 mmol) was added slowly conc. HCl (0.36 mL). The reaction mixture was kept at 0 ℃ using an ice bath. An aqueous solution (1 mL) of $NaNO_2$ (82.1 mg, 1.19 mmol) was added dropwise to generate the diazonium intermediate, and the reaction mixture was stirred for 10 min. A solution of *m*-phenylenediamine (197 mg, 1.82 mmol) and sodium hydroxide (400 mg) in water (2 mL) was kept at 0 ℃. With stirring, the diazonium intermediate was added dropwise to the *m*-phenylenediamine solution. After stirring for 1 h, volatile fractions were removed under reduced pressure, and water (40 mL) was added to the residual material, which was extracted with CH_2Cl_2 (50 mL x 3). The combined organic layer was washed with water (50 mL) and brine (50 mL), dried over anhyd Na_2SO_4, and filtered. Volatile fractions were removed under reduced pressure.

To a pyridine solution (10 mL) of the azo coupling product described above was added $Cu(OAc)_2{\cdot}H_2O$ (792 mg, 3.97 mmol). The reaction mixture was heated at 60 ℃ for 1 h. The mixture was cooled to r.t., and volatile fractions were removed under reduced pressure. After addition of water (20 mL), the aqueous layer was extracted with CH_2Cl_2 (30 mL x 3). The combined organic layer was dried over anhyd Na_2SO_4, filtered, and concentrated under reduced pressure. The crude product was purified by silica gel column chromatography with CH_2Cl_2 as eluent to furnish **9** as a yellow oil. The overall yield over the two steps was 58.0% (294 mg, 0.529 mmol). ^{1}H NMR

(500Mz, $CDCl_3$, ppm): δ 7.93 (d, J = 2.0 Hz, 1H), 7.81 (d, J = 2.0 Hz, 1H), 7.73 (d, J = 8.8 Hz, 1H), 7.61 (dd, J = 8.8 Hz, J = 2.2 Hz, 1H), 7.59 (dd, J = 8.6 Hz, J = 2.2 Hz, 1H), 7.09 (d, J = 8.6 Hz, 1H), 7.04 (d, J = 8.8 Hz, 1H), 6.98 (d, J = 2.2 Hz, 1H), 6.94 (dd, J = 8.8 Hz, J = 2.0 Hz, 1H), 4.13 (t, J = 6.4 Hz, 2H), 4.07 (t, J = 6.6 Hz, 2H), 3.94 (br s, 2H), 1.87–1.82 (m, 2H), 1.73–1.67 (m, 2H), 1.52–1.46 (m, 2H), 1.37–1.28 (m, 6H), 1.24–1.19 (m, 4H), 0.93–0.90 (m, 3H), 0.83–0.81 (m, 3H); ^{13}C NMR (75 MHz, $CDCl_3$,298 K): δ 13.9, 14.0, 22.47, 22.53, 25.4, 25.5, 28.79, 28.83, 31.3, 31.4, 69.7, 69.9, 86.6, 88.6, 96.5, 114.1, 114.4, 115.0, 115.4, 119.2, 121.5, 128.4, 130.7, 133.7, 136.8, 139.7, 140.7, 145.4, 146.3, 152.2, 153.5. FT-IR (neat): ν_{max} 3465, 3377, 3232, 3062, 2953, 2931, 2870, 2858, 2551, 2213, 1890, 1636, 1618, 1557, 1513, 1469, 1405, 1352, 1322, 1289, 1224, 1150, 1082, 1066, 1041, 1004, 979, 939, 894, 813. HRMS (EI^+) [M = $C_{32}H_{37}N_5O_4$]$^+$ calculated 555.2846, found 555.2852.

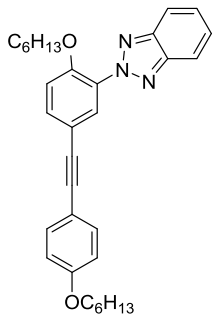

1-(2*H*-benzotriazol-2-yl)-2-hexyloxy-5-[2-(4-hexyloxyphenyl)ethynyl]-benzene (I). To a THF solution (10 mL) of **8** (113 mg, 0.221 mmol) was slowly added conc HCl (0.25 mL), and the reaction mixture was cooled to 0 ℃. An aqueous solution (1 mL) of $NaNO_2$ (22.9 mg, 0.332 mmol) was added dropwise, and the mixture was stirred at 0 ℃ for 20 min. A portion of urea (4.00 mg, 0.0663 mmol) and aq hypophosphorous acid (50% *w*/*w*, 1 mL) were added, and the resulting mixture was stirred at 0 ℃ for 5 h. The reaction

mixture was extracted three times with CH_2Cl_2. The combined organic layer was dried over anhyd $MgSO_4$, filtered, and concentrated under reduced pressure. The residual material was purified by flash column chromatography on SiO_2 with CH_2Cl_2:*n*-hexane (1:1, *v*:*v*) as eluent to afford **I** as a pale yellow powder (yield = 78.0 mg, 0.157 mmol, 71.2%). ^{1}H NMR (300Mz, $CDCl_3$, ppm): δ 8.00–7.94 (m, 2H), 7.85 (d, J = 2.1 Hz, 1H), 7.62 (dd, J = 8.6 Hz, J = 2.1 Hz, 1H), 7.48–7.41 (m, 4H), 7.10 (d, J = 8.6 Hz, 1H), 6.89–6.84 (m, 2H), 4.07 (t, J = 6.5 Hz, 2H), 3.97 (t, J = 6.5 Hz, 2H), 1.84–1.75 (m, 2H), 1.72–1.63 (m, 2H), 1.52–1.42 (m, 2H), 1.39–1.25 (m, 6H), 1.24–1.17 (m, 4H), 0.94–0.89 (m, 3H), 0.82–0.77 (m, 3H); ^{13}C NMR (75 MHz, $CDCl_3$,298 K): δ 13.9, 14.0, 22.5, 22.6, 25.4, 25.7, 29.2, 31.3, 31.6, 68.1, 69.7, 76.7, 77.1, 77.5, 86.5, 89.4, 114.1, 114.6, 114.9, 116.3, 118.4, 126.8, 130.5, 130.6, 133.0, 134.0, 144.8, 153.0, 159.3. FT-IR (neat): ν_{max} 3058, 2927, 2859, 2741, 1612, 1569, 1517, 1467, 1347, 1288, 1248, 1174, 1142, 1069, 1015, 969, 938, 904, 831. HRMS (EI$^+$) [M = $C_{32}H_{37}N_3O_2$]$^+$ calculated 495.2886, found 495.2888.

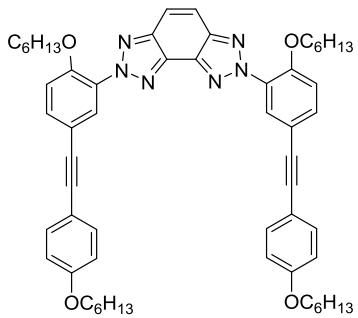

2,7-Bis-{5-[2-(4-hexyloxyphenyl)ethynyl]-2-hexyloxyphenyl}-2,7-dihydro-benzo[1,2,-*d*:3,4-*d*']bistriazole (II). To a stirred THF solution (6 mL) of **7** (192 mg, 0.487 mmol) was added slowly conc. HCl (0.25 mL). The reaction mixture was kept at 0 ℃ using an ice bath. An aq solution (1 mL) of $NaNO_2$ (60.5 mg, 0.877 mmol) was added dropwise to generate the diazonium intermediate, and the reaction mixture was stirred for 15 min. A solution of **8** (207 mg, 0.406 mmol) in pyridine-THF (1:6 v/v, 7 mL) was kept at 0 ℃.

With stirring, the diazonium intermediate was added dropwise to the solution of **8**. After stirring for 1 h, water (40 mL) was added to the reaction mixture. The aqueous layer was extracted with CH_2Cl_2 (50 mL x 3). Combined extracts were washed with water (50 mL) and brine (50 mL), dried over anhyd Na_2SO_4, filtered, and concentrated under reduced pressure.

To a pyridine-THF (2:1, v/v, 15 mL) solution of the crude azo coupling product described above was added $Cu(OAc)_2 \cdot H_2O$ (343 mg, 1.72 mmol). The reaction mixture was heated at 60 ℃ for 1 h. The reaction mixture was cooled to r.t., and volatile fractions were removed under reduced pressure. After addition of water (40 mL), the aqueous layer was extracted with CH_2Cl_2 (50 mL x 3). The combined organic layer was washed with H_2O (50 mL x 3) and aq citric acid (50 mL), dried over anhyd $MgSO_4$. After filtration, the filtrate was concentrated under reduced pressure. The residual material was purified by silica gel column chromatography with CH_2Cl_2 as eluent to furnish **II** as an orange powder. The overall yield over the two steps was 55.0% (204 mg, 0.223 mmol). ^{1}H NMR (500Mz, $CDCl_3$, ppm): δ 7.92 (d, J = 2.0 Hz, 2H), 7.88 (s, 2H), 7.62 (dd, J = 8.6 Hz, J = 2.0 Hz, 2H), 7.45 (d, J = 8.8 Hz, 4H), 7.11 (d, J = 8.8 Hz, 2H), 6.87 (d, J = 8.6 Hz, 4H), 4.11 (t, J = 6.6 Hz, 4H), 3.98 (t, J = 6.6 Hz, 4H), 1.82–1.77 (m, 4H), 1.75–1.69 (m, 4H), δ1.50–1.44 (m, 4H), 1.39–1.33 (m, 12H), 1.27–1.21 (m, 8H), 0.93–0.91 (m, 6H), δ0.80–0.78 (m, 6H); ^{13}C NMR (75 MHz, $CDCl_3$,298 K): δ 13.9, 14.0, 22.5, 22.6, 25.4, 25.7, 28.9, 29.2, 31.4, 31.6, 68.1, 69.7, 86.5, 89.3, 114.1, 114.6, 115.0, 116.3, 118.8, 130.3, 130.5, 133.0, 133.8, 136.2, 145.0, 152.9, 159.3. FT-IR (neat): ν_{max} 2930, 2870, 1612, 1568, 1517, 1468, 1360, 1287, 1249, 1174, 1152, 1115, 1058, 1018, 969, 937, 892, 832. HRMS (FAB^+) [M = $C_{58}H_{69}N_6O_4]^+$ calculated 913.5380, found 913.5377.

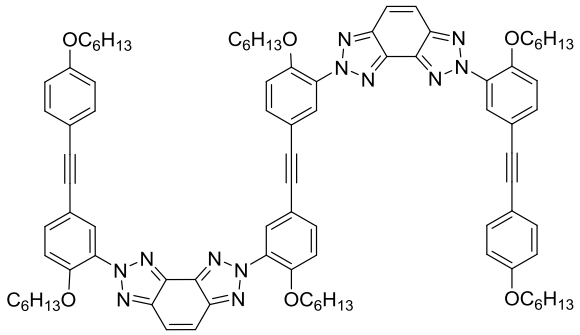

1,1'-(1,2-Ethynediyl)bis{3-[7-(5-(2-(4-hexyloxyphenyl)ethynyl)2-hexyloxyphenyl)benzo[1,2,-*d*:3,4-*d*']bistriazol-2(7*H*)-yl]-4-hexyloxybenzene} (III). To a stirred THF solution (10 mL) of **6** (73.5 mg, 0.180 mmol) was added slowly conc. HCl (0.20 mL). The reaction mixture was kept at 0 ℃ using an ice bath. An aq solution (1 mL) of $NaNO_2$ (51.7 mg, 0.749 mmol) was added dropwise to generate the diazonium intermediate, and the reaction mixture was stirred for 15 min. A solution of **8** (202 mg, 0.395 mmol) in pyridine-THF (1:10, v/v 11 mL) was kept at 0 ℃. With stirring, the diazonium intermediate was added dropwise to the solution of **8**. After stirring for 1 h, water (40 mL) was added to the reaction mixture. The aqueous layer was extracted with CH_2Cl_2 (50 mL x 3). Combined extracts were washed with water (50 mL) and brine (50 mL), dried over anhyd Na_2SO_4, filtered, and concentrated under reduced pressure.

To a pyridine-THF (2:1, v/v, 15 mL) solution of the crude azo coupling product described above was added $Cu(OAc)_2 \cdot H_2O$ (474 mg, 2.38 mmol). The reaction mixture was heated at 60 ℃ for 1 h. The reaction mixture was cooled to r.t., and volatile fractions were removed under reduced pressure. After addition of water (40 mL), the aqueous layer was extracted with CH_2Cl_2 (50 mL x 3). The combined organic layer was washed with H_2O (50 mL x 3) and aq. citric acid (50 mL), and dried over anhyd $MgSO_4$. After filtration, the filtrate was concentrated under reduced pressure. The residual material was purified by silica gel column chromatography with CH_2Cl_2 as an eluent to

furnish **III** as a pale red powder. The overall yield over the two steps was 57.2% (149 mg, 103 mmol). ^{1}H NMR (500Mz, $CDCl_3$, ppm) δ 7.94 (d, J = 2.0 Hz, 2H), 7.92 (d, J = 2.0 Hz, 2H), 7.88 (m, 4H), 7.64–7.60 (m, 4H), 7.44 (d, J = 8.8 Hz, 4H), 7.13–7.09 (m, 4H), 6.87 (d, J = 8.8 Hz, 4H), 4.12–4.08 (m, 8H), 3.97 (t, J = 6.6 Hz, 4H), 1.82–1.76 (m, 4H), 1.75–1.69 (m, 8H), 1.50–1.44 (m, 4H), 1.36–1.35 (m, 16H), 1.27–1.20 (m, 16H), 0.93–0.90 (m, 6H), δ0.80–0.77 (m, 12H); ^{13}C NMR (125 MHz, $CDCl_3$,298 K): δ 13.9, 14.0, 22.5, 22.6, 25.4, 25.7, 28.8, 29.2, 31.4, 31.6, 68.1, 69.7, 86.6, 87.8, 89.3, 114.08, 114.12, 114.6, 115.0, 115.7, 116.2, 118.80, 118.82, 130.25, 130.28, 130.5, 130.6, 133.0, 133.8, 134.0, 136.18, 136.22, 145.0, 152.9, 153.3, 159.2. FT-IR (neat): ν_{max} 2931, 2871, 1613, 1567, 1517, 1468, 1360, 1288, 1249, 1174, 1151, 1115, 1058, 1014, 969, 937, 893, 831, 816. HRMS (FAB$^+$) [M = $C_{90}H_{102}N_{12}O_6$]$^+$ calculated 1446.8045, found 1446.8046.

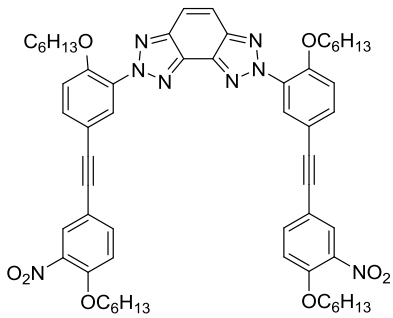

2,7-Bis-{5-[2-(4-hexyloxy-3-nitrophenyl)ethynyl]-2-hexyloxyphenyl}-2,7-dihydro-benzo[1,2-*d*:3,4-*d*']bistriazole (10). To a stirred THF solution (4 mL) of **9** (349 mg, 0.795 mmol) was added slowly conc. HCl (0.30 mL). The reaction mixture was kept at 0 ℃ using an ice bath. An aq solution (1 mL) of $NaNO_2$ (71.3 mg, 1.03 mmol) was added dropwise to generate the diazonium intermediate, and the reaction mixture was stirred for 10 min. A solution of *m*-phenylenediamine (442 mg, 0.795 mmol) in pyridine-THF (1:2, v/v, 6 mL) was kept at 0 ℃. With stirring, the diazonium intermediate was added

dropwise to the *m*-phenylenediamine solution. After stirring for 1 h, water (40 mL) was added to the reaction mixture. The aqueous layer was extracted with CH_2Cl_2 (50 mL x 3). Combined extracts were washed with water (50 mL) and brine (50 mL), dried over anhyd Na_2SO_4, filtered, and concentrated under reduced pressure.

To a pyridine-THF (2:1, v/v, 15 mL) solution of the crude azo coupling product described above (630 mg, 0.627 mmol) was added $Cu(OAc)_2 \cdot H_2O$ (876 mg, 4.39 mmol). The reaction mixture was heated at 60 ℃ for 1 h. The reaction mixture was cooled to r.t., and volatile fractions were removed under reduced pressure. After addition of water (40 mL), the aqueous layer was extracted with CH_2Cl_2 (50 mL x 3). The combined organic layer was washed with H_2O (50 mL x 3) and aq citric acid (50 mL), and dried over anhyd $MgSO_4$. After filtration, the filtrate was concentrated under reduced pressure. The residual material was purified by silica gel column chromatography with CH_2Cl_2 as eluent to furnish **10** as a yellow powder. The overall yield over the two steps was 78.9%. ^{1}H NMR (500Mz, $CDCl_3$, ppm): δ 7.97 (d, J = 2.0 Hz, 2H), 7.93 (d, J = 2.0 Hz, 2H), 7.88 (S, 2H), 7.63 (d, J = 2.0 Hz, 2H), 7.61 (d, J = 2.0 Hz, 2H), 7.13 (d, J = 8.6 Hz, 2H), 7.04 (d, J = 8.8 Hz, 2H), 4.12 (t, J = 6.4 Hz, 4H), 4.11 (t, J = 6.6 Hz, 4H), 1.86–1.80 (m, 4H), 1.75–1.69 (m, 4H), 1.51–1.45 (m, 4H), 1.39–1.29 (m, 12H), 1.26–1.18 (m, 8H), 0.92–0.89 (m, 6H), 0.80–0.77 (m, 6H); ^{13}C NMR (125 MHz, $CDCl_3$,298 K): δ 13.9, 14.0, 22.46, 22.52, 25.4, 25.5, 28.8, 31.35, 31.4, 69.7, 69.9, 86.7, 88.5, 114.1, 114.5, 115.1, 115.3, 118.9, 128.5, 130.3, 130.7, 134.0, 136.2, 136.8, 139.7, 145.0, 152.2, 153.4. FT-IR (neat): ν_{max} 3067, 2954, 2931, 2870, 2567, 1686, 1417, 1534, 1513, 1467, 1356, 1287, 1152, 1099, 1082, 1059, 1005, 971, 936, 893, 817. HRMS (FAB^+) [M = $C_{58}H_{67}N_8O_8$]$^+$ calculated 1003.5082, found 1003.5098.

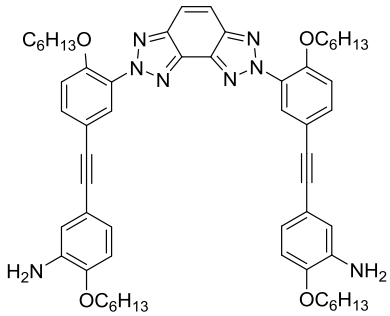

2,7-Bis-{5-[2-(3-amino-4-hexyloxyphenyl)ethynyl]-2-hexyloxyphenyl}-2,7-dihydro-benzo[1,2-*d*:3,4-*d*']bistriazole (11). To a solution of **10** (655 mg, 0.653 mmol) in THF (7 mL) was added zinc (1.51 g, 19.6 mmol) and aq NH_3 (30%, 10 mL). The mixture was heated at reflux for 2.5 h. Insoluble fractions were removed by filtration through a Celite pad, and the filtrate was concentrated under reduced pressure. The residual material was triturated with CH_2Cl_2 (3 x 40 mL). The organic phase was washed with brine (50 mL), dried over anhyd Na_2SO_4, filtered, and concentrated. Flash column chromatography on SiO_2 with *n*-hexane to *n*-hexane/EtOAc (5:1, *v*:*v*) as eluent furnished **11** as a white powder (yield = 0.444g, 0.471 mmol, 72.1%). ^{1}H NMR (300Mz, $CDCl_3$, ppm): δ 7.91 (d, J = 2.0 Hz, 2H), 7.88 (s, 2H), 7.73 (dd, J = 8.6 Hz, J = 2.0 Hz, 2H), 7.10 (d, J = 8.7 Hz, 2H), 6.92 (dd, J = 8.2 Hz, J = 2.0 Hz, 2H), 6.88 (d, J = 1.9 Hz, 2H), 6.74 (d, J = 8.3 Hz, 2H), 4.10 (t, J = 6.5 Hz, 4H), 4.01 (t, J = 6.5 Hz, 4H), 3.83 (br s, 2H), 1.87–1.78 (m, 4H), 1.76–1.67 (m, 4H), 1.51–1.46 (m, 4H), 1.40–1.30 (m, 12H), 1.27–1.19 (m, 8H), 0.94–0.89 (m, 6H), δ0.81–0.76 (m, 6H); ^{13}C NMR (125 MHz, $CDCl_3$,298 K): δ 13.9, 14.0, 22.5, 22.6, 25.4, 25.8, 28.9, 29.2, 31.4, 31.6, 68.3, 69.7, 85.9, 89.8, 111.1, 114.0, 115.1, 116.4, 117.5, 118.8, 122.5, 130.2, 130.5, 133.8, 136.14, 136.17, 144.9, 147.1, 152.8. FT-IR (neat): ν_{max} 3486, 3352, 2931, 2868, 1612, 1518, 1468, 1359, 1328, 1288, 1248, 1222, 1151, 1059, 1018, 960, 936, 889, 862, 803. HRMS (FAB$^+$) [M = $C_{58}H_{71}N_8O_4$]$^+$ calculated 943.5598, found 943.5593.

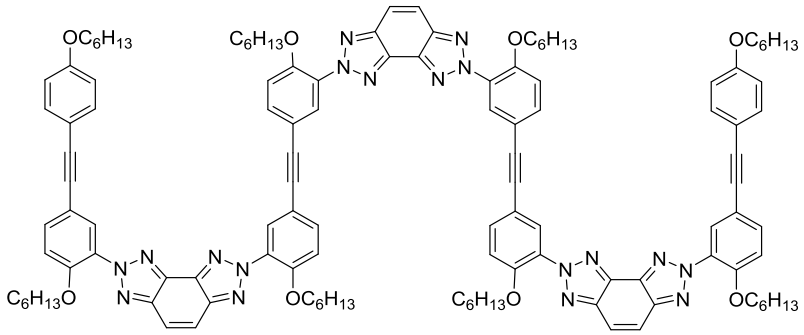

2,7-Bis{5-[2-(3-(7-(5-(2-(4-hexyloxyphenyl)ethynyl)-2-hexyloxyphenyl)-7*H*-benzo[1,2-*d*:3,4-*d*']bistriazol-2-yl)-4-hexyloxyphenyl)ethynyl]-2-hexyloxyphenyl}-2,7-dihydro-benzo[1,2-*d*:3,4-*d*']bistriazole (IV). To a stirred THF solution (10 mL) of the **11** (106 mg, 0.112 mmol) was added slowly conc. HCl (0.20 mL). The reaction mixture was kept at 0 ℃ using an ice bath. An aq solution (1 mL) of $NaNO_2$ (23.2 mg, 0.336 mmol) was added dropwise to generate the diazonium intermediate, and the reaction mixture was stirred for 15 min. A solution of **8** (143 mg, 0.279 mmol) in pyridine-THF (1:10, v/v, 11 mL) was kept at 0 ℃. With stirring, the diazonium intermediate was added dropwise to the solution of **8**. After stirring for 1 h, water (40 mL) was added to the reaction mixture. The aqueous layer was extracted with CH_2Cl_2 (50 mL x 3). Combined extracts were washed with water (50 mL) and brine (50 mL), dried over anhyd Na_2SO_4, filtered, and concentrated under reduced pressure.

To a pyridine-THF (4:1, v/v, 10 mL) solution of the crude azo coupling product described above was added $Cu(OAc)_2 \cdot H_2O$ (280 mg, 1.40 mmol). The reaction mixture was heated at 60 ℃ for 1 h. The reaction mixture was cooled to r.t., and volatile fractions were removed under reduced pressure. After addition of water (40 mL), the aqueous layer was extracted with CH_2Cl_2 (50 mL x 3). The combined extracts were washed with H_2O (50 mL x 3) and aq citric acid (50 mL), dried over anhyd $MgSO_4$. After filtration, the filtrate was concentrated under reduced pressure. The residual material was purified by

silica gel column chromatography with CH_2Cl_2 as eluent to furnish **IV** as a red powder. The overall yield over the two steps was 89.3% (198 mg, 0.100 mmol). ^{1}H NMR (300Mz, $CDCl_3$, ppm) δ 7.95–7.93 (m, 6H), 7.89 (m, 6H), 7.65–7.59 (m, 6H), 7.44 (d, J = 8.6 Hz, 4H), 7.14–7.09 (m, 6H), 6.87 (d, J = 8.4 Hz, 4H), 4.12–4.07 (m, 12H), 3.96 (t, J = 6.5 Hz, 4H), 1.83–1.67 (m, 16H), 1.51–1.44 (m, 4H), 1.38–1.31 (m, 20H), 1.24–1.19 (m, 24H), 0.93–0.89 (m, 6H), 0.80–0.76 (m, 18H); ^{13}C NMR (125 MHz, $CDCl_3$,298 K): δ 13.9, 14.0, 22.5, 22.6, 25.4, 25.6, 28.8, 29.2, 31.4, 31.6, 68.1, 69.7, 86.5, 87.8, 89.3, 114.07, 114.11, 114.6, 115.0, 115.6, 116.2, 118.8, 130.2, 130.3, 130.5, 130.6, 133.0, 133.8, 134.0, 136.18, 136.23, 145.0, 152.9, 153.3, 159.2. FT-IR (neat): ν_{max} 3055, 2930, 2870, 2538, 1613, 1567, 1517, 1467, 1360, 1288, 1249, 1174, 1151, 1099, 1058, 1014, 969, 937, 916, 892, 831, 814. HRMS (FAB$^+$) [M = $C_{122}H_{136}N_{18}O_8]^+$ calculated 1981.0789, found 1981.0776.

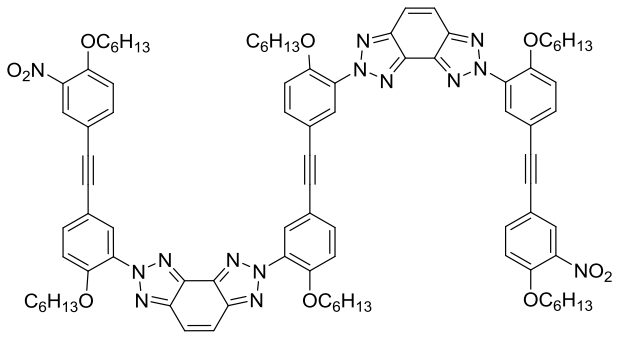

1,1'-(1,2-Ethynediyl)bis{3-[7-(5-(2-(4-hexyloxy-3-nitrophenyl)ethynyl)-2-hexyloxyphenyl)benzo[1,2,-*d*:3,4-*d*']bistriazol-2(7*H*)-yl]-4-hexyloxybenzene} (12). To a stirred THF solution (5 mL) of **6** (287 mg, 0.707 mmol) was added slowly conc. HCl (0.56 mL). The reaction mixture was kept at 0 ℃ using an ice bath. An aq solution (1 mL) of $NaNO_2$ (117 mg, 1.70 mmol) was added dropwise to generate the diazonium intermediate, and the reaction mixture was stirred for 10 min. A solution of **9** (904 mg, 1.63 mmol) in pyridine-THF (1:3, v/v, 8 mL) was kept at 0 ℃. With stirring, the

diazonium intermediate was added dropwise to the solution of **9**. After stirring for 1 h, water (40 mL) was added to the reaction mixture. The aqueous layer was extracted with CH_2Cl_2 (50 mL x 3). Combined extracts were washed with water (50 mL) and brine (50 mL), dried over anhyd Na_2SO_4, filtered, and concentrated under reduced pressure.

To a pyridine-THF (4:1, v/v, 20 mL) solution of the crude azo coupling product described above was added $Cu(OAc)_2 \cdot H_2O$ (1.63 g, 8.16 mmol). The reaction mixture was heated at 60 ℃ for 1 h. The reaction mixture was cooled to r.t., and volatile fractions were removed under reduced pressure. After addition of EtOAc (40 mL), the organic layer was washed with H_2O (50 mL x 3), dried over anhyd $MgSO_4$. After filtration, the filtrate was concentrated under reduced pressure. The residual material was purified by silica gel column chromatography with CH_2Cl_2 to CH_2Cl_2/EtOAc (30:1, *v*:*v*) as eleuent to obtain **12** as a yellow powder. The overall yield over the two steps was 55.3%. ^{1}H NMR (500Mz, $CDCl_3$, ppm): δ 7.97 (d, J = 2.2 Hz, 2H), 7.93 (d, J = 2.0 Hz, 4H), 7.88 (s, 4H), 7.65–7.61 (m, 6H), 7.13 (dd, J = 8.8 Hz, J = 2.0 Hz, 6H), 7.04 (d, J = 8.8 Hz, 2H), 4.14–4.10 (m, 12H), 1.87–1.82 (m, 4H), 1.75–1.70 (m, 8H), 1.52–1.46 (m, 4H), 1.38–1.33 (m, 16H), 1.24–1.21 (m, 16H), 0.93–0.90 (m, 6H), 0.80–0.77 (m, 12H); ^{13}C NMR (75 MHz, $CDCl_3$,298 K): δ 13.9, 14.0, 22.46, 22.52, 25.41, 25.47, 28.8, 31.35, 31.41, 69.7, 69.9, 86.7, 87.8, 88.5, 114.1, 114.5, 115.1, 115.4, 115.6, 118.8, 118.9, 128.5, 130.25, 130.27, 130.57, 130.67, 134.0, 136.19, 136.25, 136.8, 139.7, 145.00, 145.02, 152.2, 153.3, 153.5. FT-IR (neat): ν_{max} 3056, 2953, 2932, 2870, 1617, 1557, 1534, 1515, 1467, 1357, 1288, 1249, 1151, 1099, 1081, 1058, 1006, 970, 936, 917, 893, 816. HRMS (FAB$^+$) [M = $C_{90}H_{100}N_{14}O_{10}$]$^+$ calculated 1536.7747, found 1536.7749.

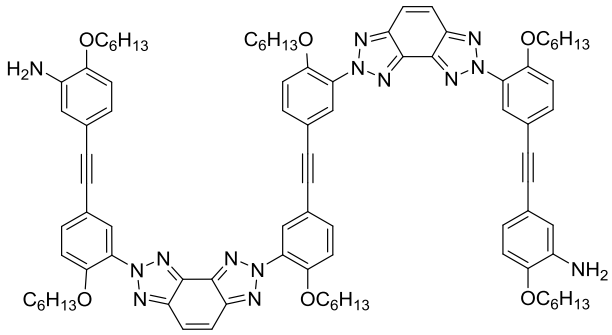

1,1'-(1,2-Ethynediyl)bis{3-[7-(5-(2-(3-amino-4-hexyloxyphenyl)ethynyl)-2-hexyloxyphenyl)benzo[1,2,-*d*:3,4-*d*']bistriazol-2(7*H*)-yl]-4-hexyloxybenzene} (13). To a solution of **12** (308 mg, 0.200 mmol) in THF (10 mL) was added zinc (0.600 g, 9.18 mmol) and aq NH_3 (30%, 10 mL). The mixture was heated at reflux for 6 h. Insoluble fractions were removed by filtration through a Celite pad, the filtrate was concentrated under reduced pressure. The residual material was triturated with CH_2Cl_2 (3 x 40 mL). The organic phase was washed with brine (50 mL), dried over anhyd Na_2SO_4, filtered, and concentrated. Flash column chromatography on SiO_2 with CH_2Cl_2 as eluent furnished **13** as a yellow powder (yield = 0.210g, 0.142 mmol, 71.0%). ^{1}H NMR (300Mz, $CDCl_3$, ppm): δ 7.95 (d, J = 2.1 Hz, 2H), 7.91 (d, J = 2.1 Hz, 2H), 7.89 (m, 4H), 7.66–7.59 (m, 4H), 7.15–7.09 (m, 4H), 6.92 (dd, J = 8.2 Hz, J = 2.0 Hz, 2H), 6.88 (d, J = 1.9 Hz, 2H), 6.74 (d, J = 8.4 Hz, 1H), 4.14–4.08 (m, 8H), 4.02 (t, J = 6.6 Hz, 4H), 3.85 (br s, 4H), δ1.87–1.78 (m, 4H), 1.78–1.67 (m, 8H), 1.54–1.44 (m, 4H), 1.41–1.32 (m, 16H), 1.26–1.19 (m, 16H), 0.95–0.90 (m, 6H), δ0.82–0.76 (m, 12H); ^{13}C NMR (75 MHz, $CDCl_3$,298 K): δ 13.9, 14.0, 22.5, 22.6, 25.4, 25.8, 28.84, 28.86, 29.24, 31.4, 31.6, 68.3, 69.7, 86.0, 87.8, 89.8, 111.1, 114.05, 114.11, 115.1, 115.6, 116.4, 117.5, 118.8, 118.9, 122.5, 130.2, 130.3, 130.5, 130.6, 133.8, 134.0, 136.2, 136.3, 144.96, 144.99, 147.1, 152.9, 153.3. FT-IR (neat): ν_{max} 3480, 3372, 3054, 2932, 2870, 2533, 2208, 1613, 1571, 1517, 1468, 1359, 1328, 1288, 1248, 1222, 1151, 1099, 1058, 1015, 962, 937, 918, 891, 860, 803.

HRMS (FAB$^+$) [M = $C_{90}H_{104}N_{14}O_6$]$^+$ calculated 1476.8263, found 1476.8263.

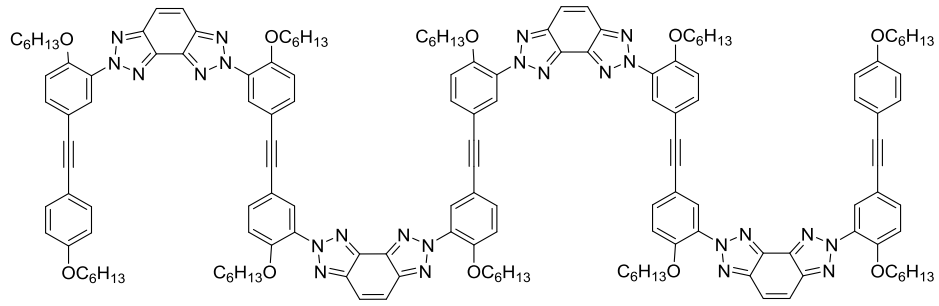

1,1'-(1,2-Ethynediyl)bis{3-[7-(5-(2-(3-(7-(5-(2-(4-hexyloxyphenyl)ethynyl)-2-hexyloxyphenyl)benzo[1,2-*d*:3,4-*d*']bistriazol-2(7*H*)-yl)-4-hexyloxyphenyl)ethynyl)-2-hexyloxyphenyl)benzo[1,2-*d*:3,4-*d*']bistriazol-2(7*H*)-yl]-4-hexyloxybenzene} (V). To a THF solution (10 mL) of **13** (182 mg, 0.123 mmol) was slowly added conc. HCl (0.20 mL), and the reaction mixture was cooled to 0 ℃. An aqueous solution (1 mL) of $NaNO_2$ (25.5 mg, 0.369 mmol) was added dropwise to generate the diazonium intermediate, and the reaction mixture was stirred for 10 min. A solution of **8** (187 mg, 0.366 mmol) in pyridine-THF (1:10, v/v, 11 mL) was kept at 0 ℃. With stirring, the diazonium intermediate was added dropwise to the solution of **8**. After stirring for 1 h, water (40 mL) was added to the reaction mixture. The aqueous layer was extracted with CH_2Cl_2 (50 mL x 3). Combined extracts were washed with water (50 mL) and brine (50 mL), dried over anhyd Na_2SO_4, filtered, and concentrated under reduced pressure.

To a pyridine-THF (2:1, v/v, 15 mL) solution of the crude azo coupling product described above was added $Cu(OAc)_2 \cdot H_2O$ (174 mg, 0.872 mmol). The reaction mixture was heated at 60 ℃ for 1 h. The reaction mixture was cooled to r.t., and volatile fractions were removed under reduced pressure. After addition of water (40 mL), the aqueous layer was extracted with CH_2Cl_2 (50 mL x 3). The combined organic layer was washed with H_2O (50 mL x 3) and aq citric acid (50 mL), and dried over anhyd $MgSO_4$. After filtration, the

filtrate was concentrated under reduced pressure. The residual material was purified by silica gel column chromatography with CH_2Cl_2 as eluent furnished **V** as a pale red powder. The overall yield over the two steps was 50.6% (0.157 mg, 0.0623 mmol). ^{1}H NMR (500Mz, $CDCl_3$, ppm) δ 7.93–7.91 (m, 8H), 7.64–7.60 (m, 8H), 7.44 (d, *J*=9.06 Hz, 4H), 7.13–7.10 (m, 8H), 6.87 (d, *J* = 8.8 Hz, 4H), 4.12–4.08 (m, 16H), 3.97 (t, *J* = 6.6 Hz, 4H), 1.82–1.76 (m, 4H), 1.74–1.69 (m, 16H), 1.49–1.43 (m, 4H), 1.36–1.34 (m, 24H), 1.23–1.20 (m, 32H), 0.93–0.90 (m, 6H), δ0.79–0.76 (m, 24H); ^{13}C NMR (75 MHz, $CDCl_3$,298 K): δ 13.9, 14.0, 22.5, 22.6, 25.4, 25.7, 28.8, 29.2, 31.4, 31.6, 68.1, 69.7, 86.6, 87.8, 89.3, 114.1, 114.6, 115.0, 115.6, 116.2, 118.8, 118.9, 130.2, 130.3, 130.5, 130.6, 133.0, 133.8, 134.0, 136.20, 136.24, 145.0, 152.9, 153.3, 159.2. FT-IR (neat): ν_{max} 3051, 2931, 2870, 2538, 2404, 2210, 1891, 1748, 1613, 1567, 1515, 1467, 1394, 1360, 1288, 1249, 1174, 1151, 1099, 1058, 1013, 969, 937, 915, 892, 831, 814. HRMS (MALDI) [M = $C_{154}H_{170}N_{24}O_{10}]^+$ calculated 2516.3565, found 2516.3202.

4.3. NMR Spectra

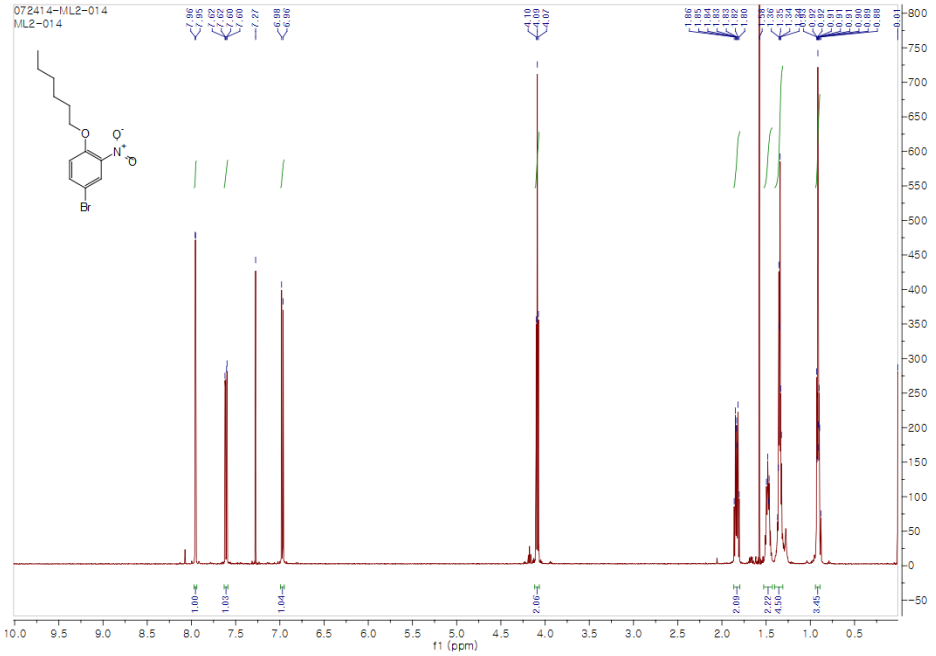

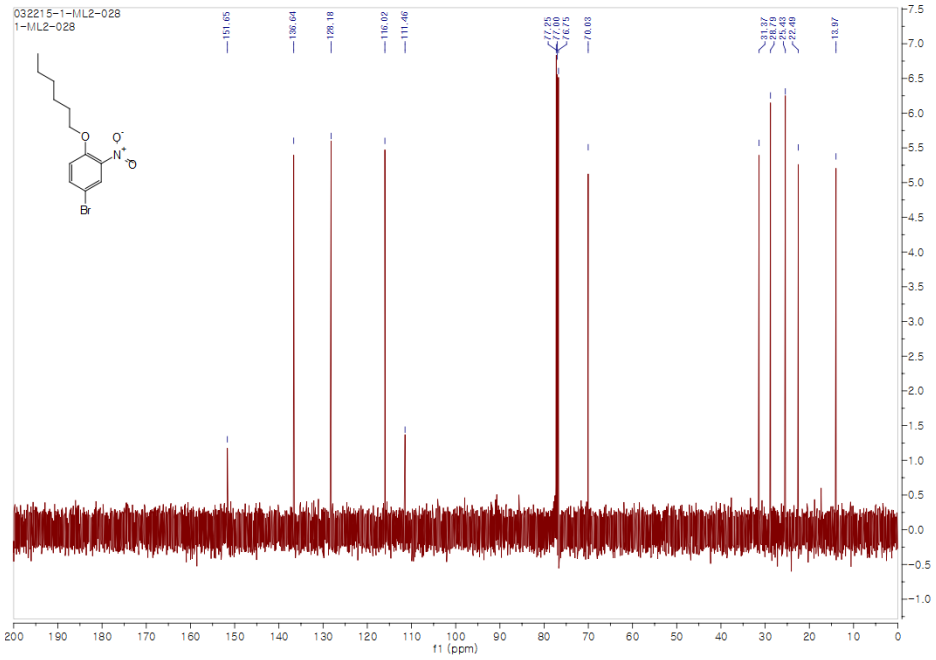

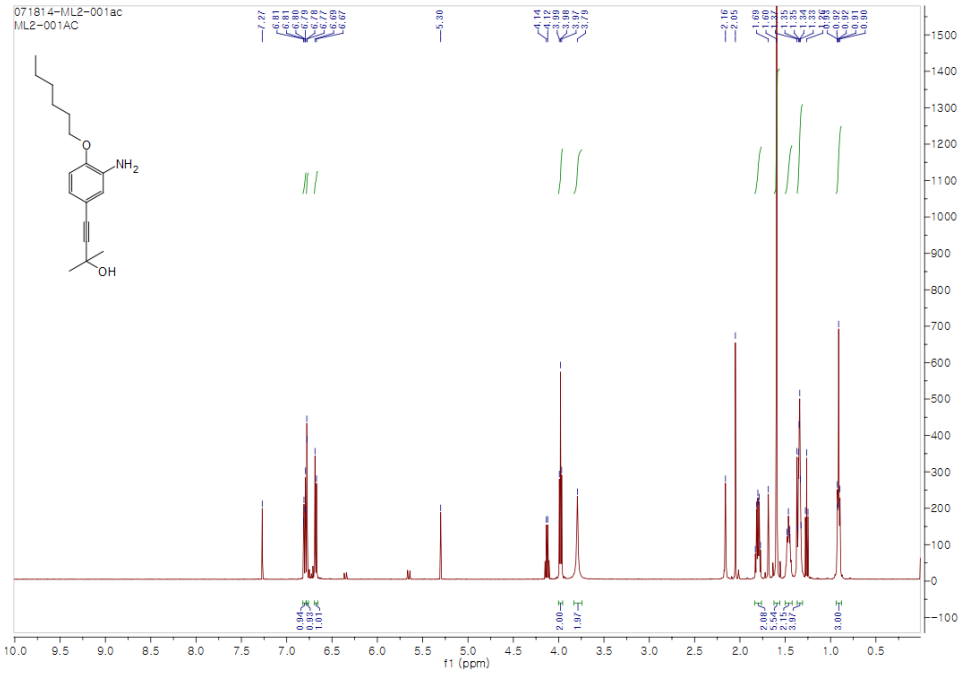
071814-ML2-001ac
ML2-001AC
NH2
OH
f1 (ppm)

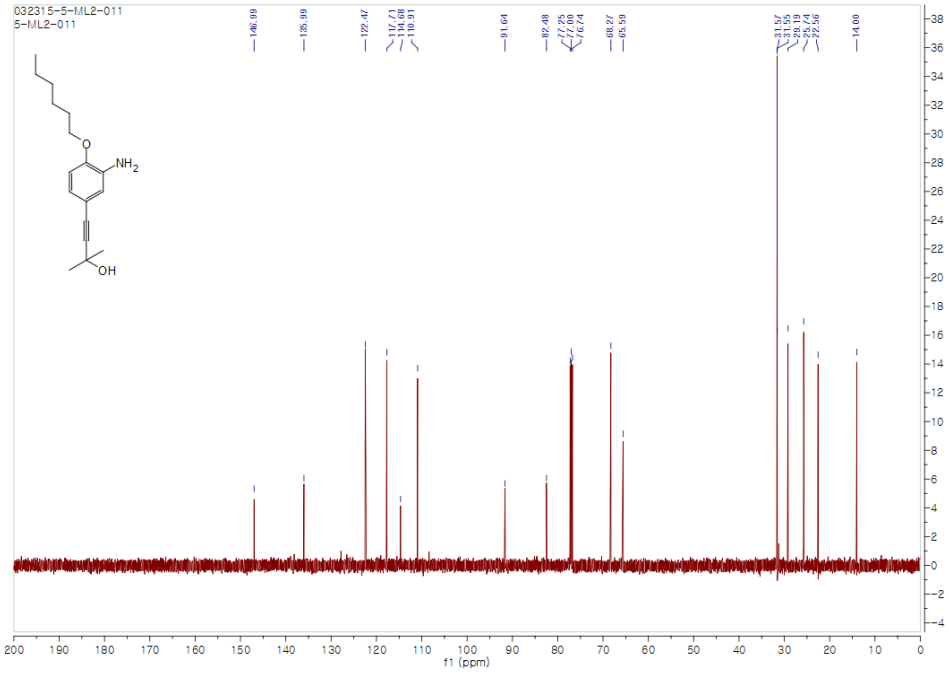
032315-5-ML2-011
5-ML2-011
NH2
OH
f1 (ppm)

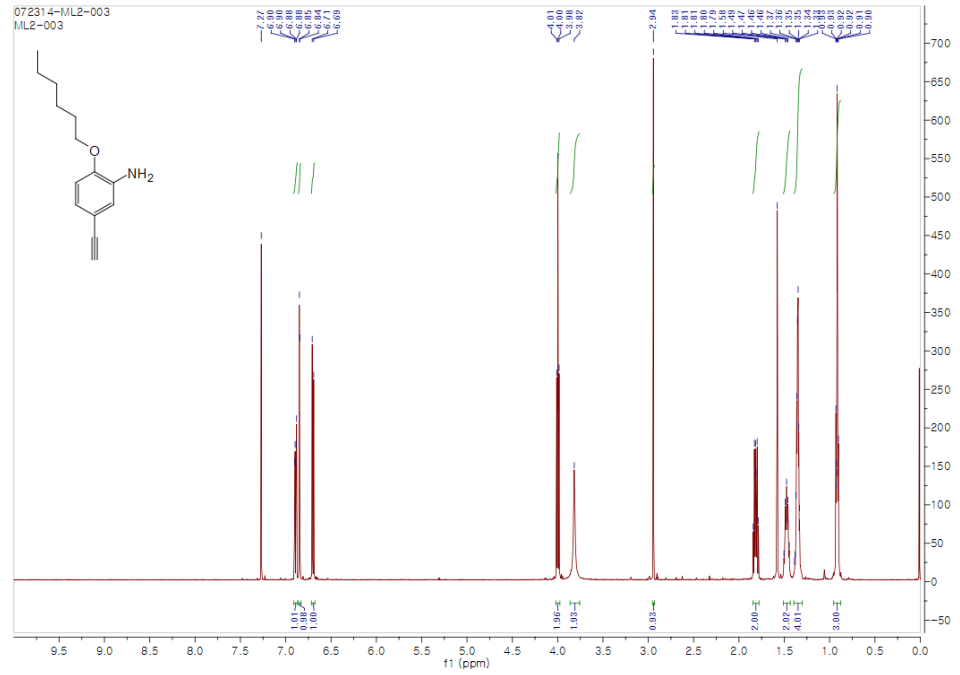
072314-ML2-003
ML2-003
NH2
f1 (ppm)

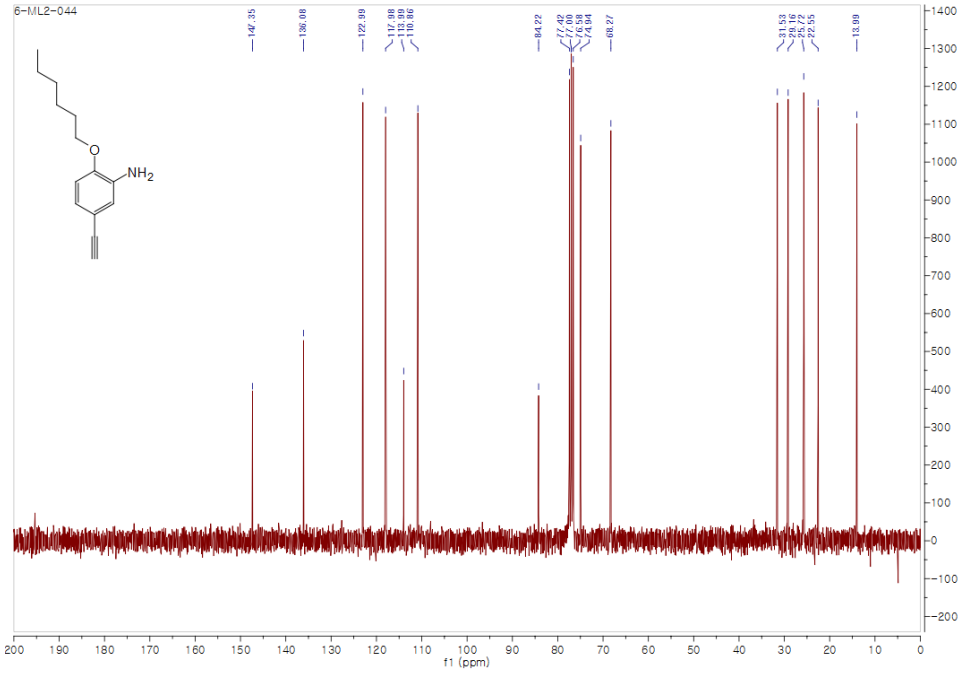
6-ML2-044
NH2
f1 (ppm)

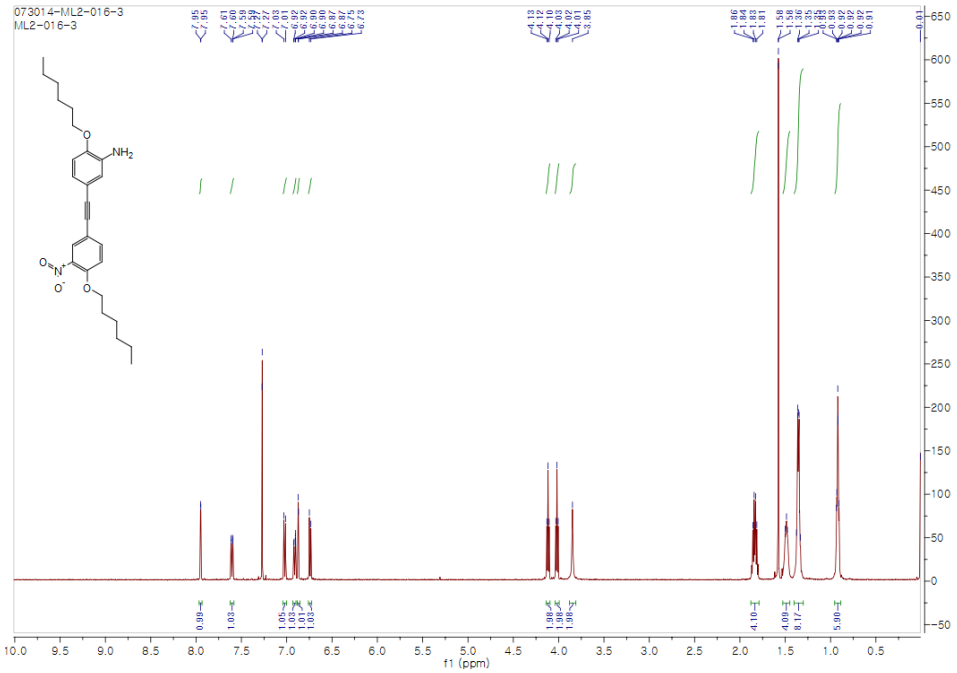
073014-ML2-016-3
ML2-016-3
f1 (ppm)

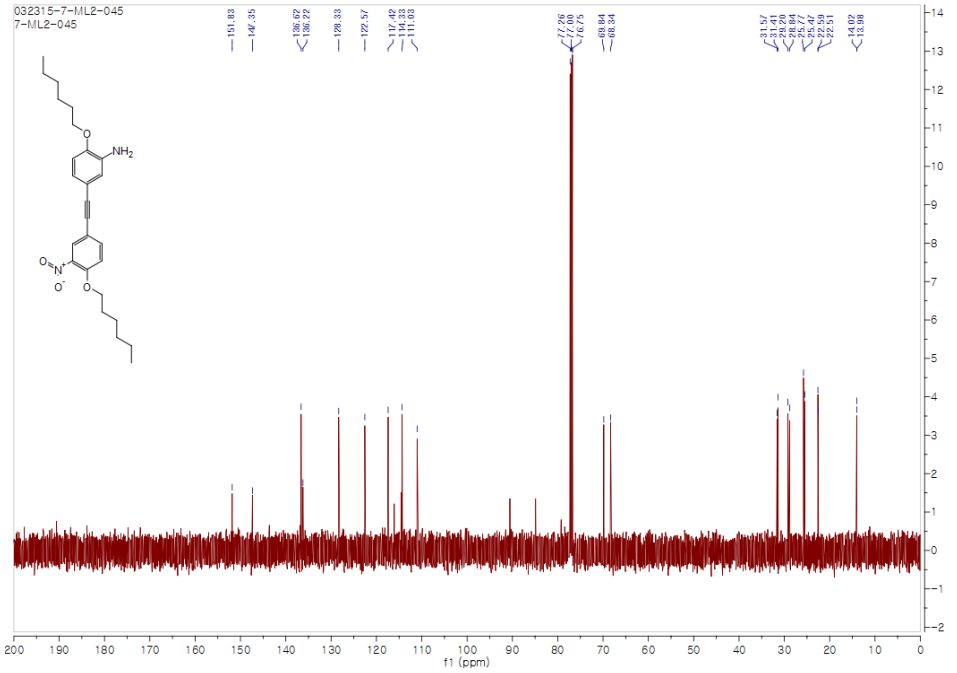
032315-7-ML2-045
7-ML2-045
f1 (ppm)

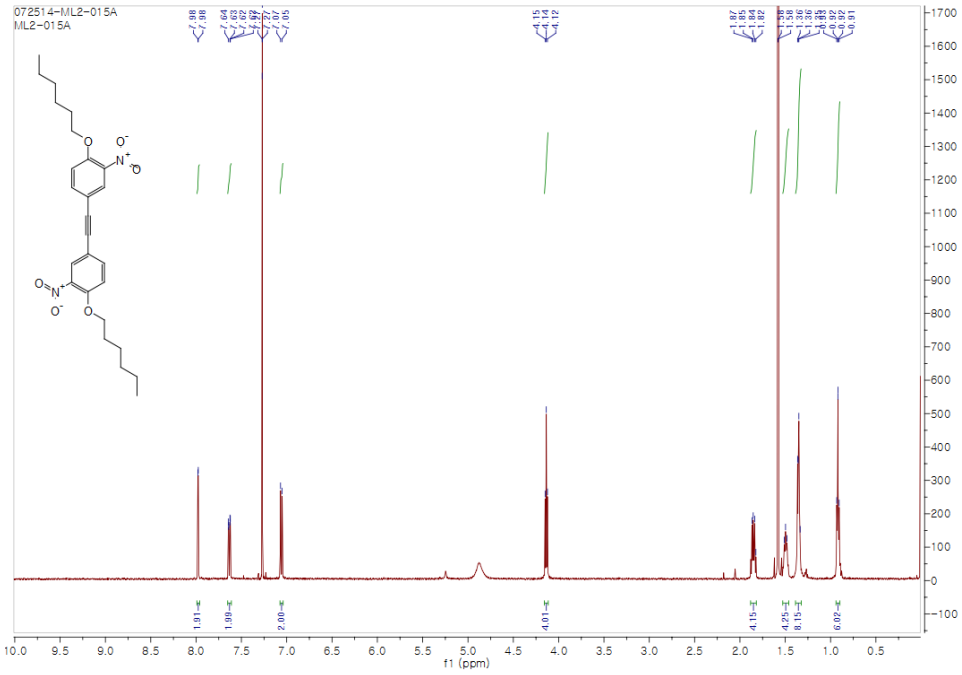
072514-ML2-015A
ML2-015A
f1 (ppm)

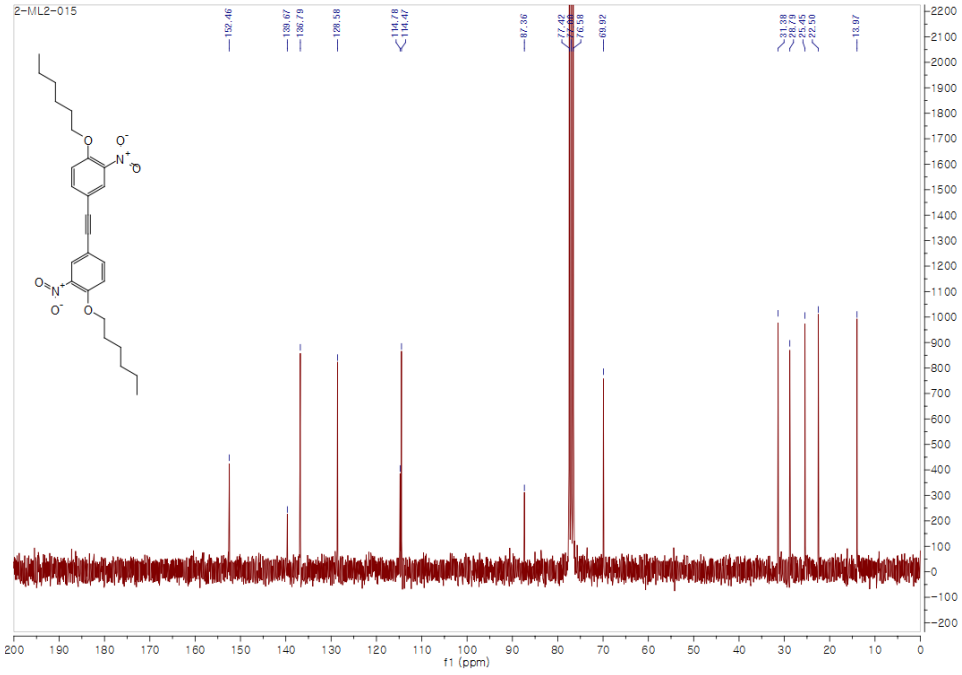
2-ML2-015
f1 (ppm)

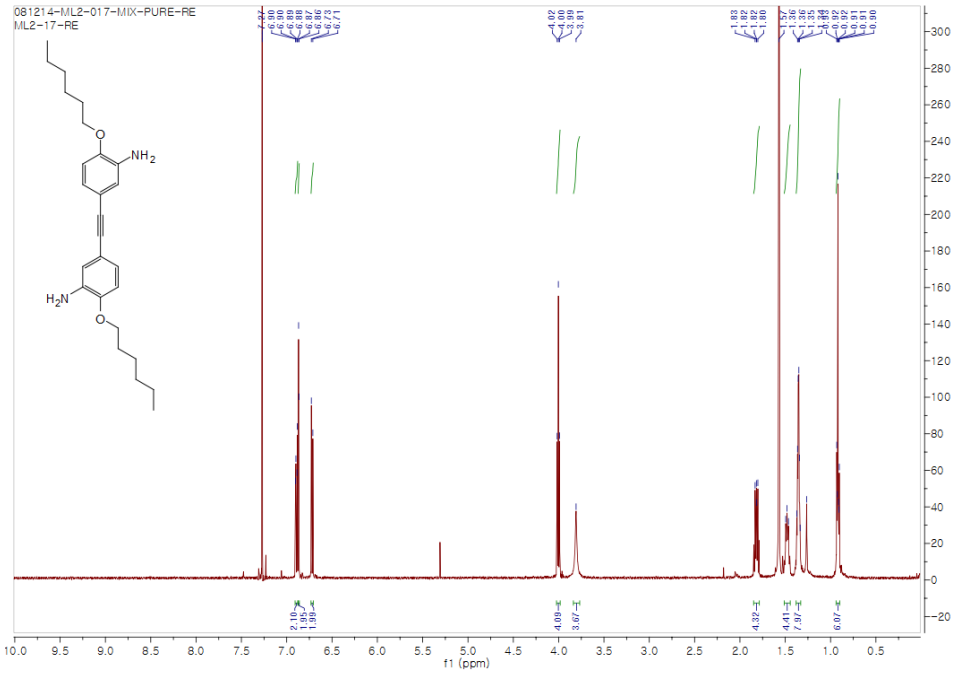
081214-ML2-017-MIX-PURE-RE
ML2-17-RE
NH2
H2N
f1 (ppm)

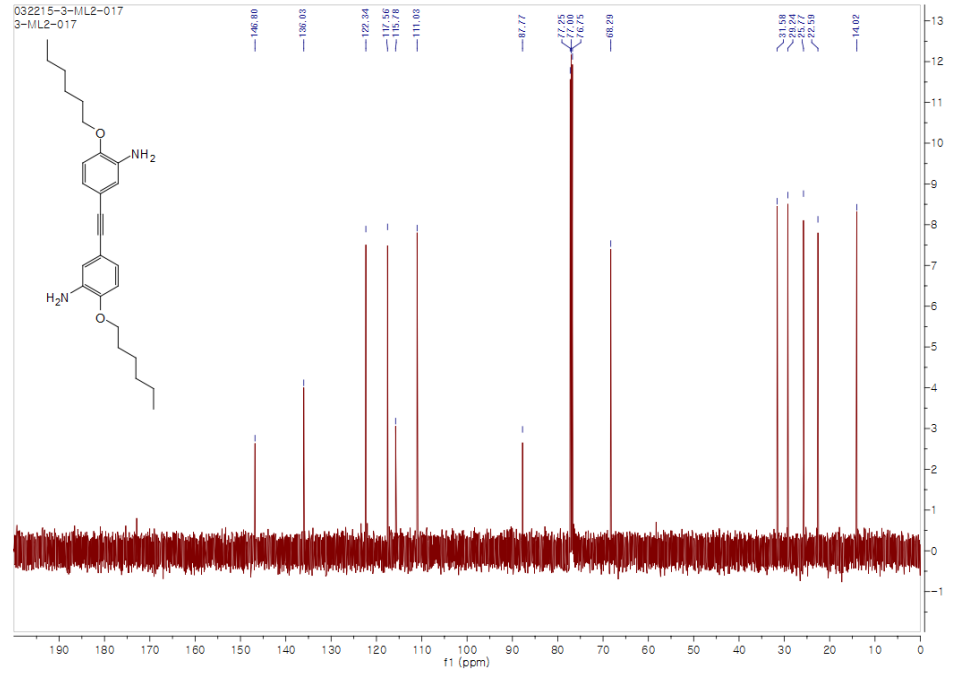
032215-3-ML2-017
3-ML2-017
NH2
H2N
f1 (ppm)

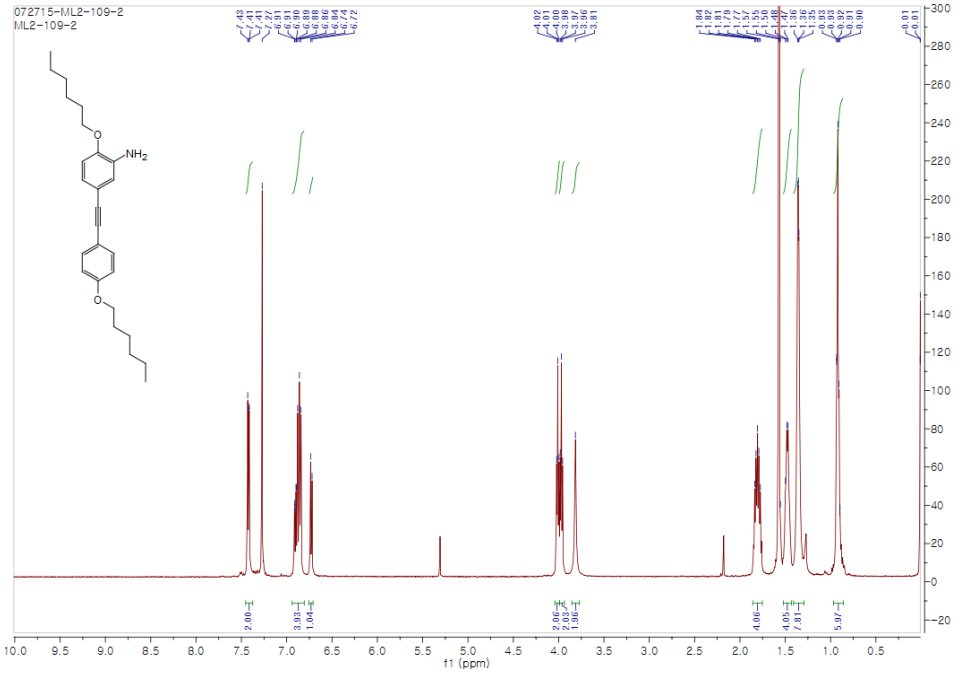
072715-ML2-109-2
ML2-109-2
NH2
f1 (ppm)

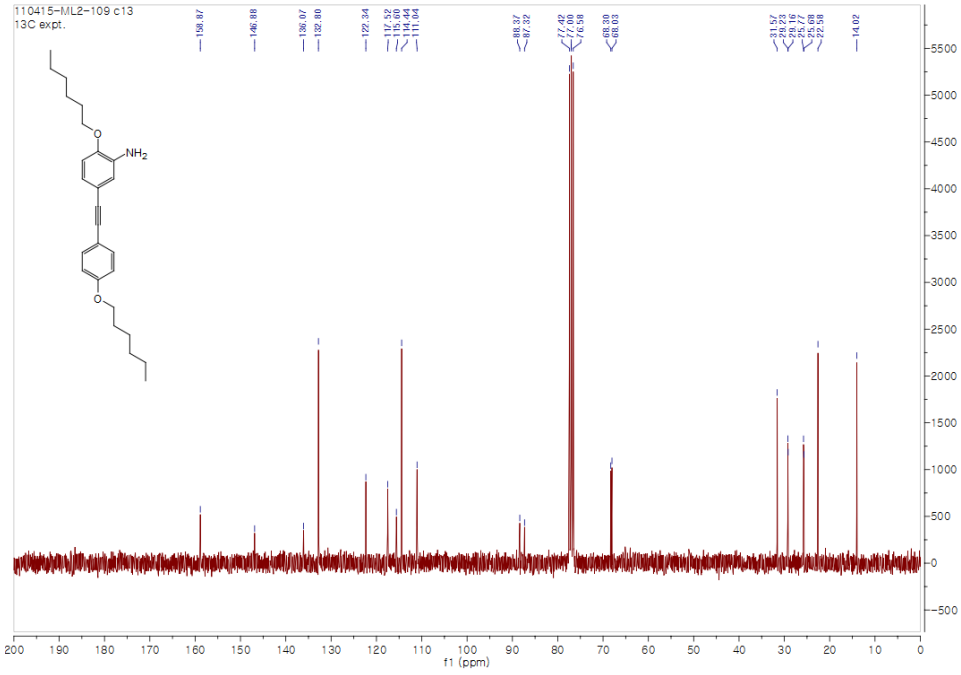
110415-ML2-109 c13
13C expt.
NH2
f1 (ppm)

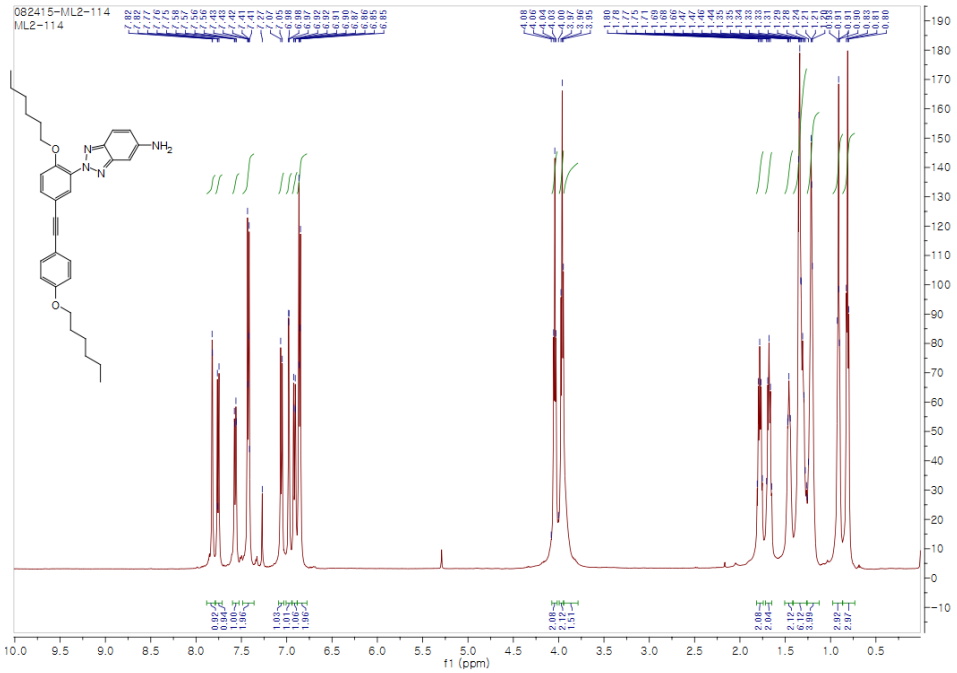
082415-ML2-114
ML2-114
f1 (ppm)

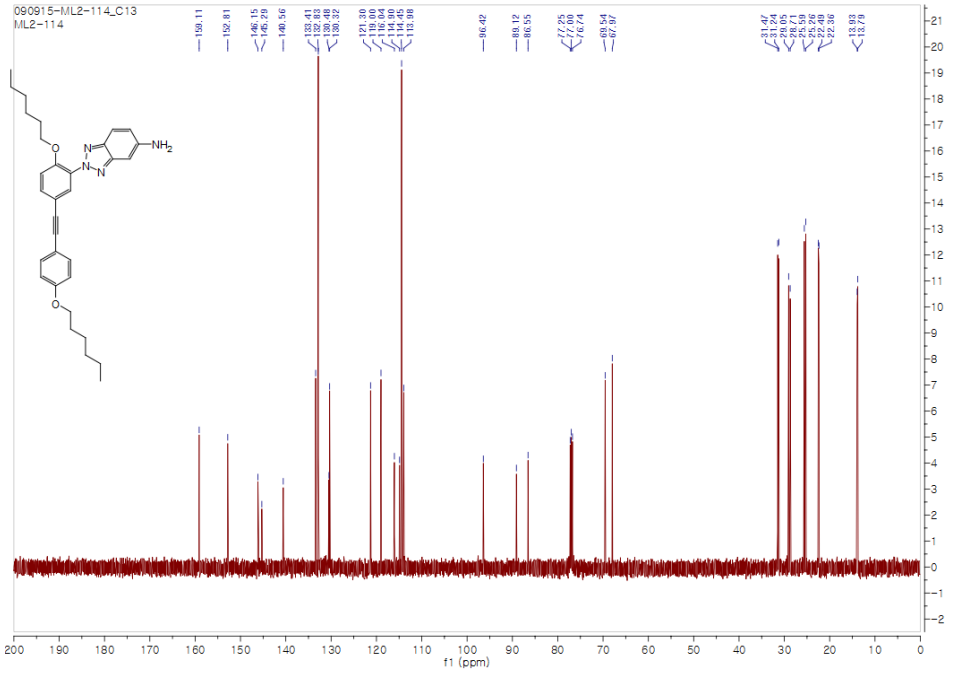
090915-ML2-114_C13
ML2-114
f1 (ppm)

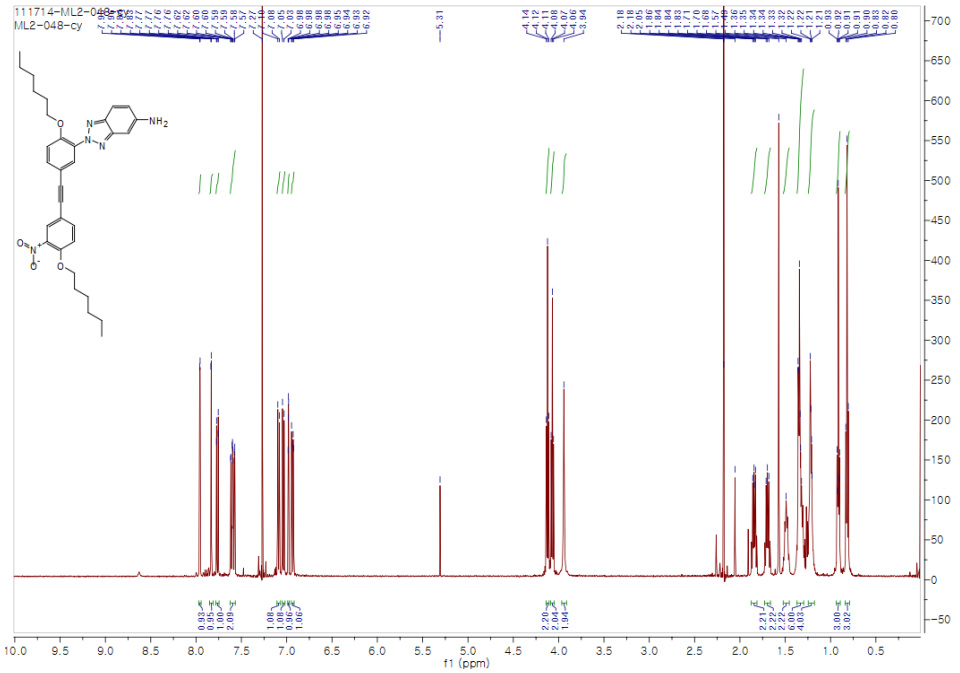
111714-ML2-048-cy
ML2-048-cy
NH2
f1 (ppm)

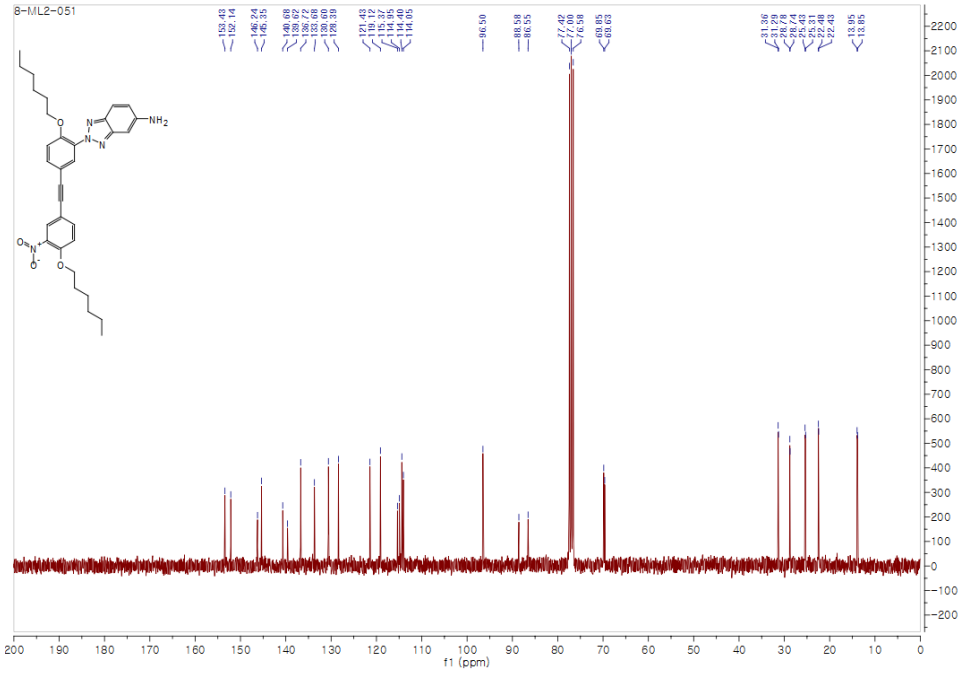
8-ML2-051
NH2
f1 (ppm)

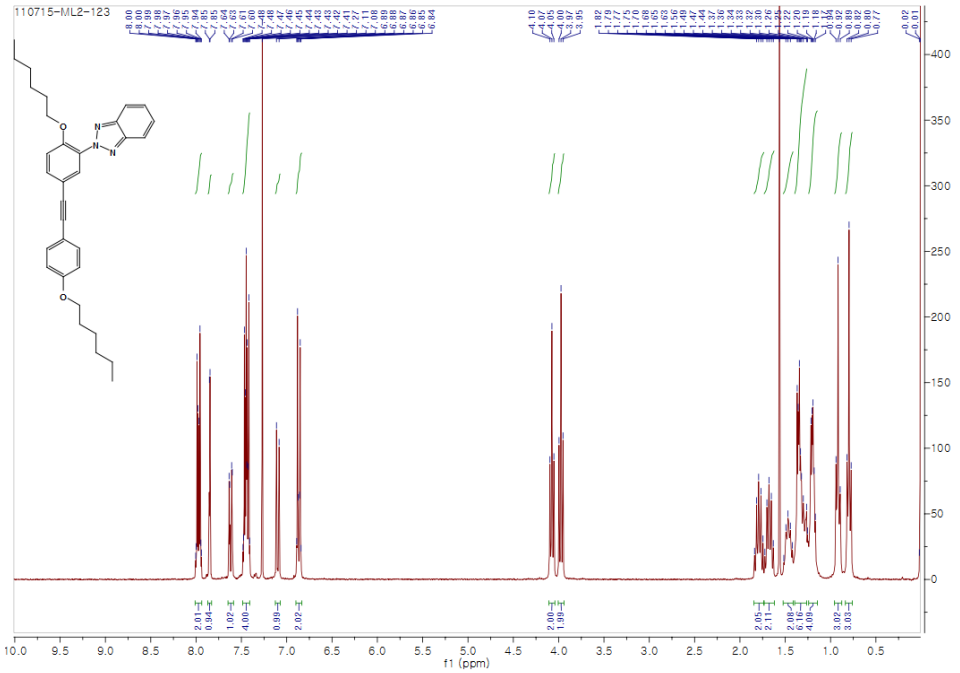
110715-ML2-123
f1 (ppm)

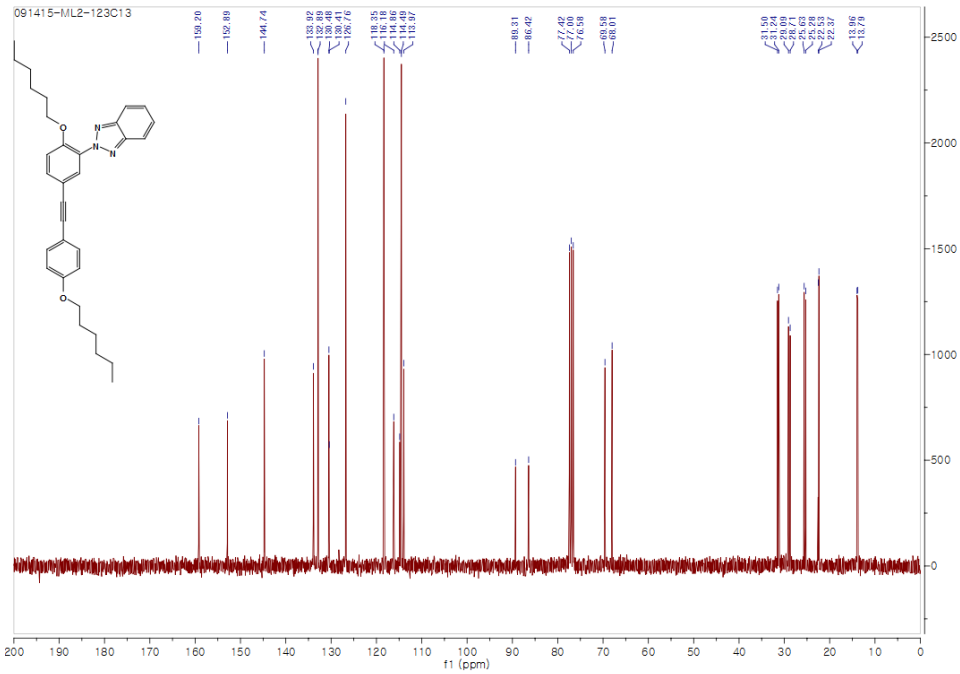
091415-ML2-123C13
f1 (ppm)

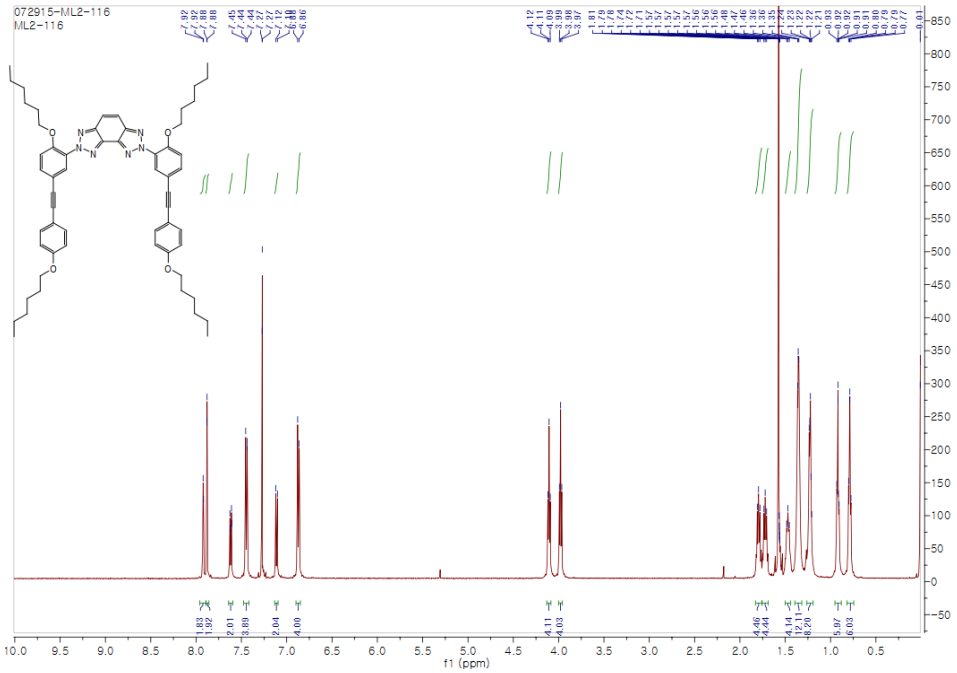
072915-ML2-116
ML2-116
f1 (ppm)

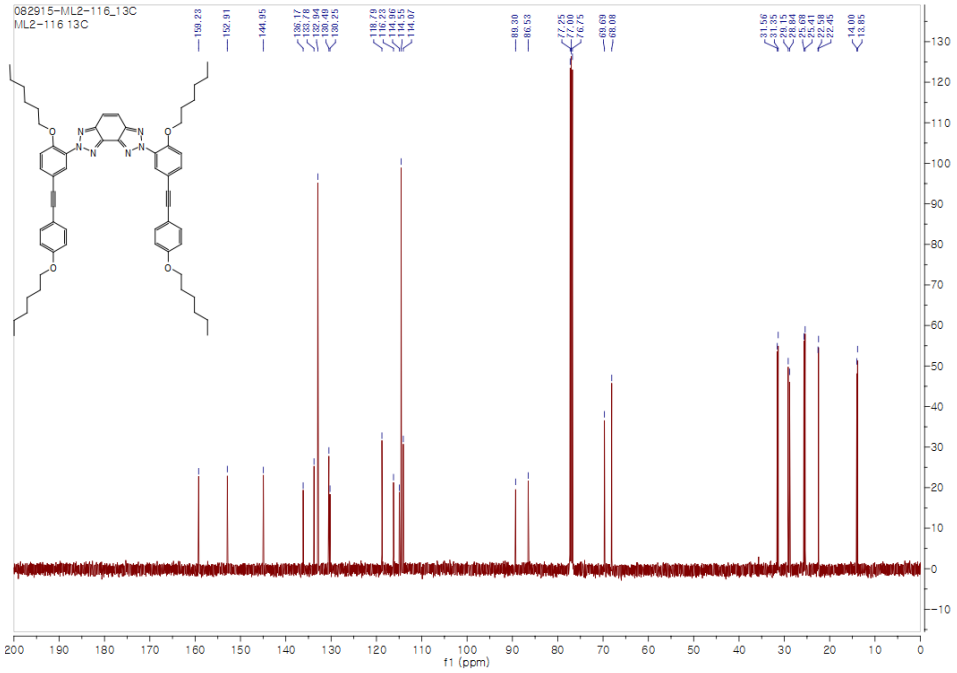
082915-ML2-116_13C
ML2-116 13C
f1 (ppm)

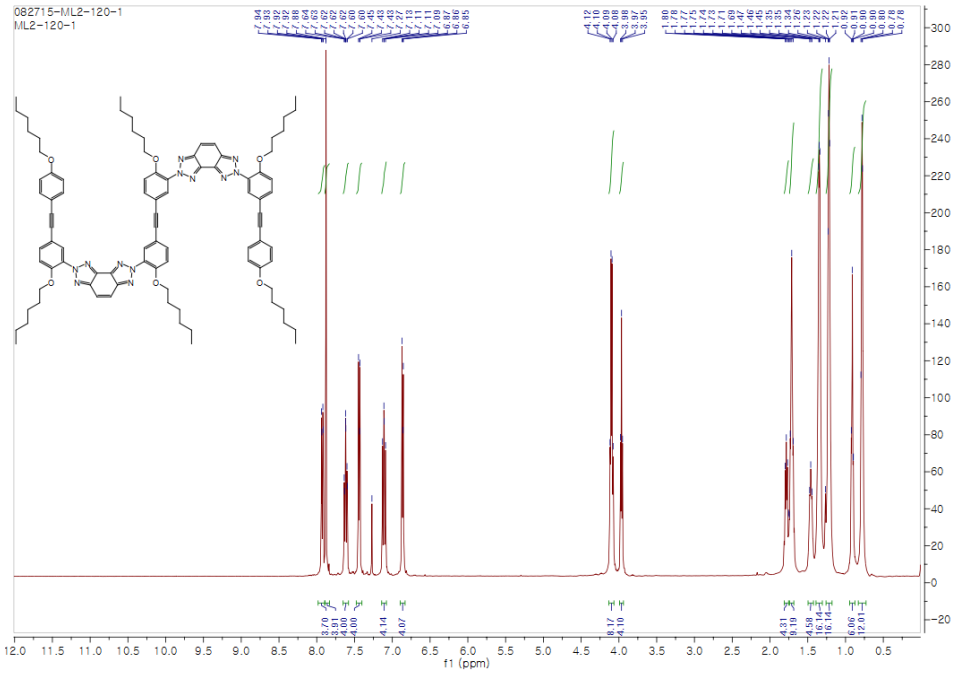
082715-ML2-120-1
ML2-120-1
f1 (ppm)

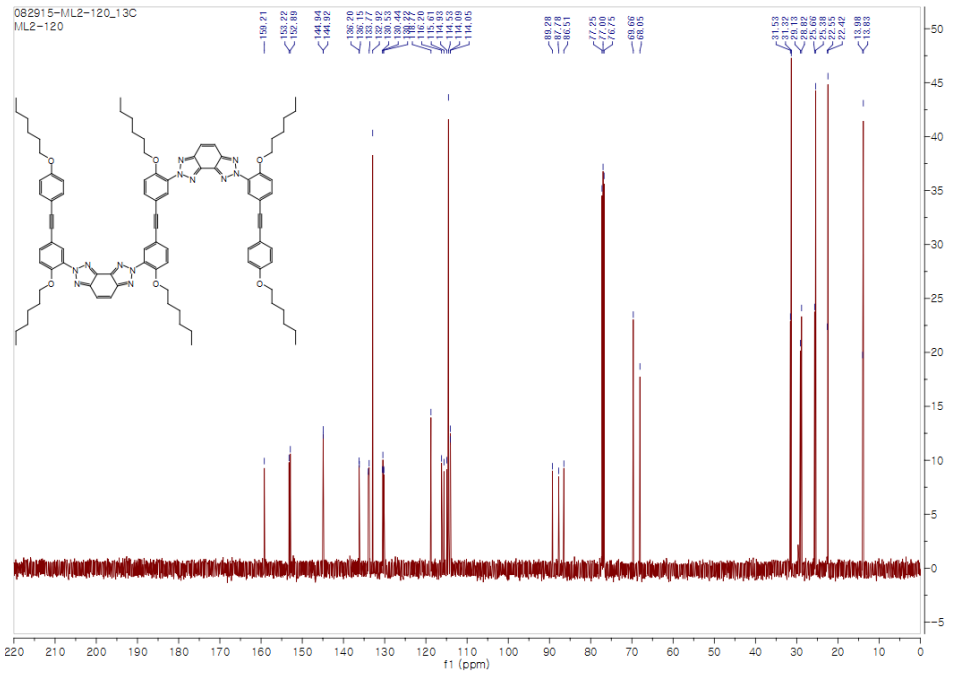
082915-ML2-120_13C
ML2-120
f1 (ppm)

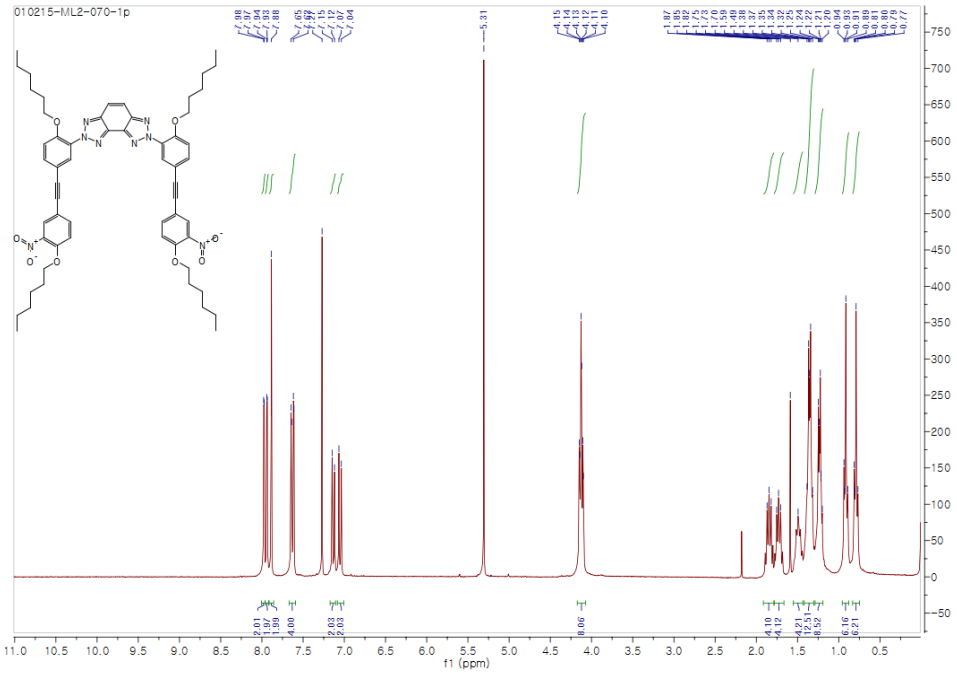
010215-ML2-070-1p
f1 (ppm)

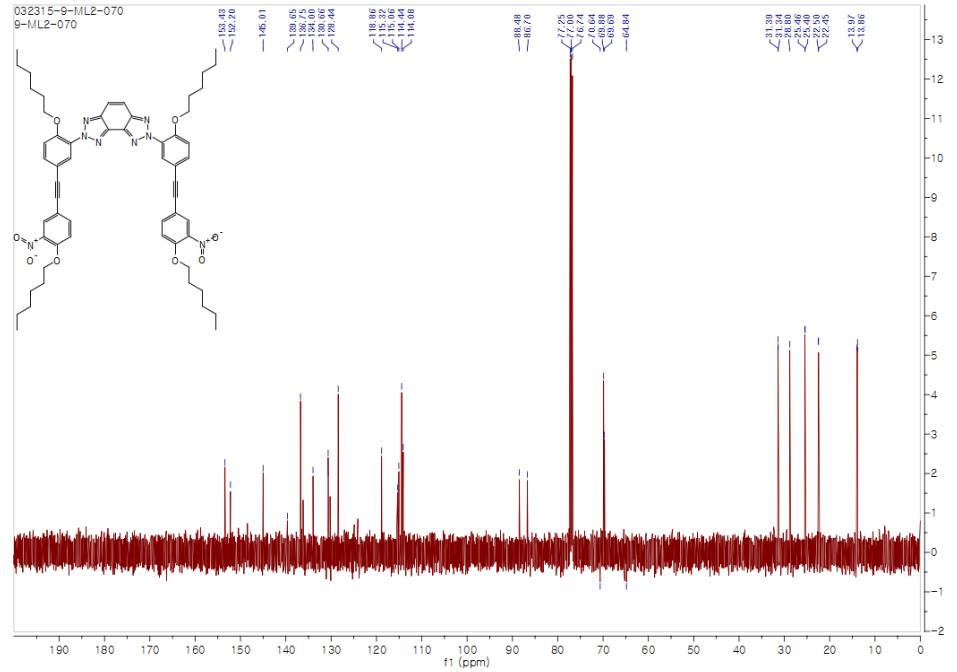
032315-9-ML2-070
9-ML2-070
f1 (ppm)

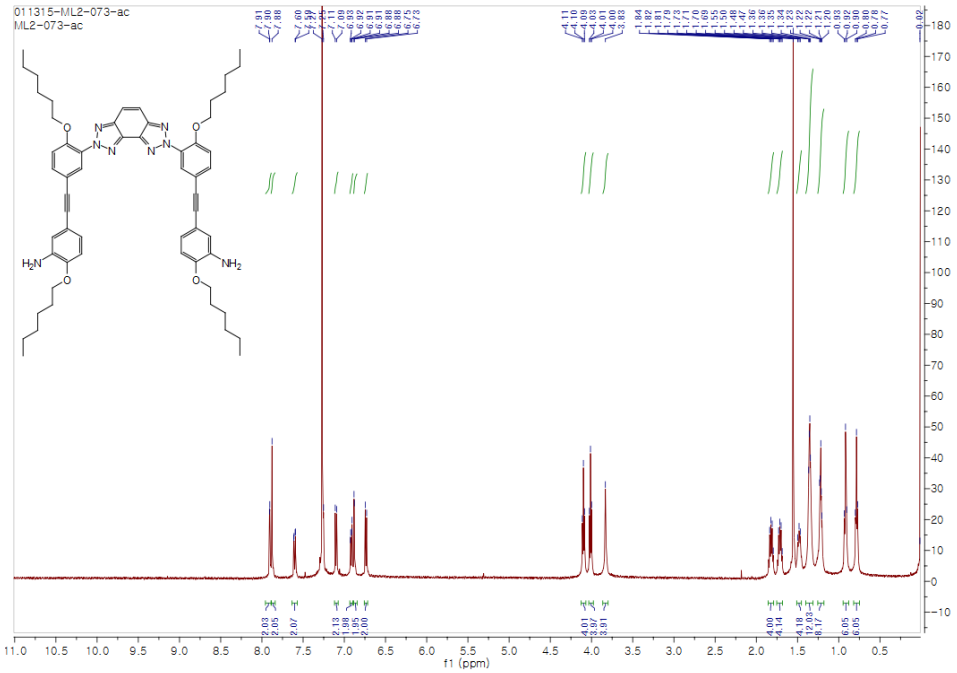
011315-ML2-073-ac
ML2-073-ac
f1 (ppm)

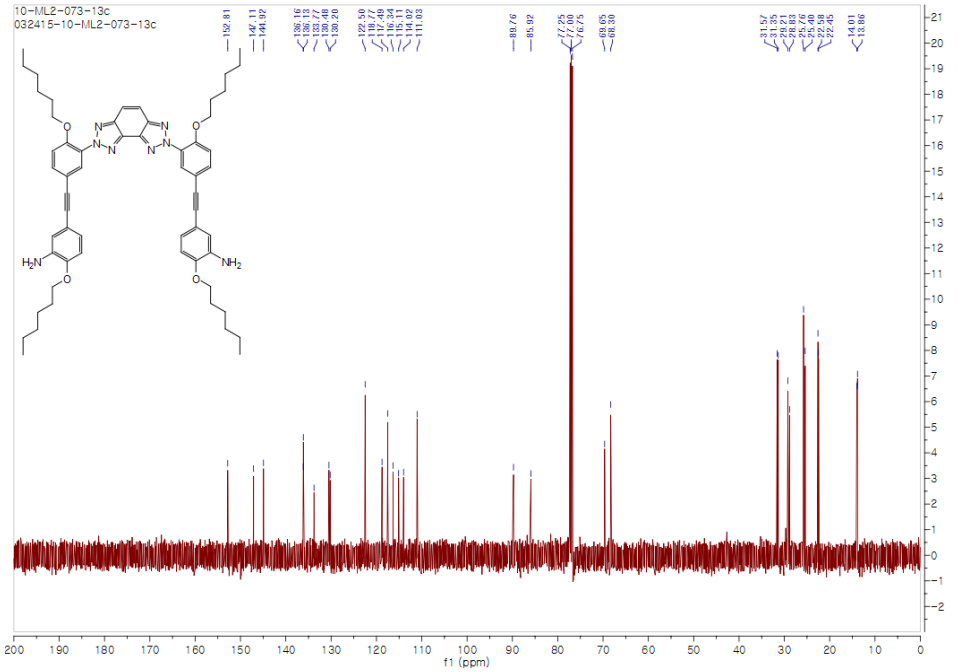
10-ML2-073-13c
03241S-10-ML2-073-13c
f1 (ppm)

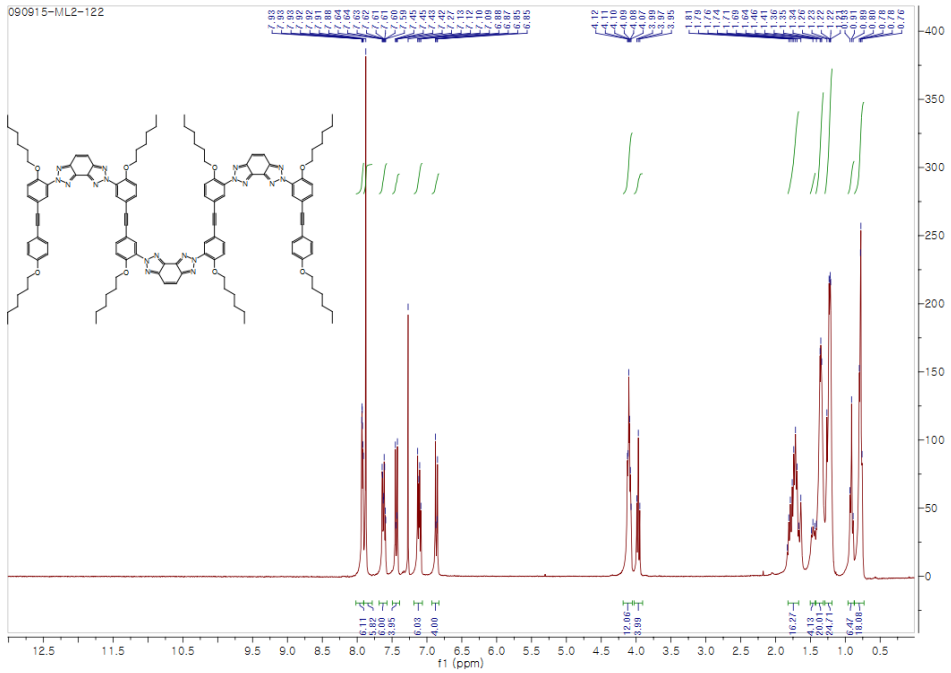
090915-ML2-122
f1 (ppm)

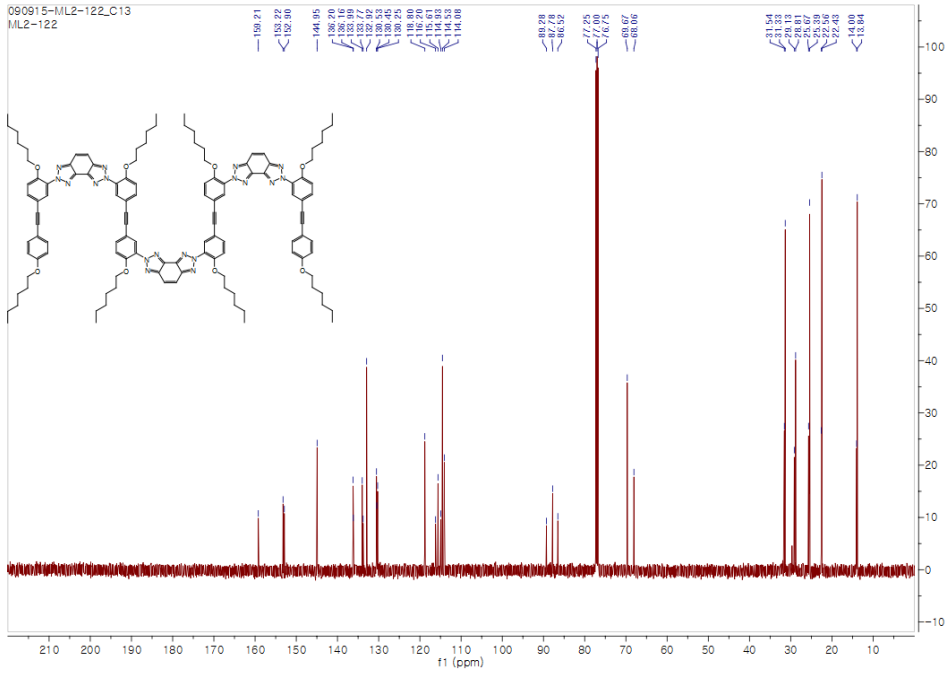
090915-ML2-122_C13
ML2-122
f1 (ppm)

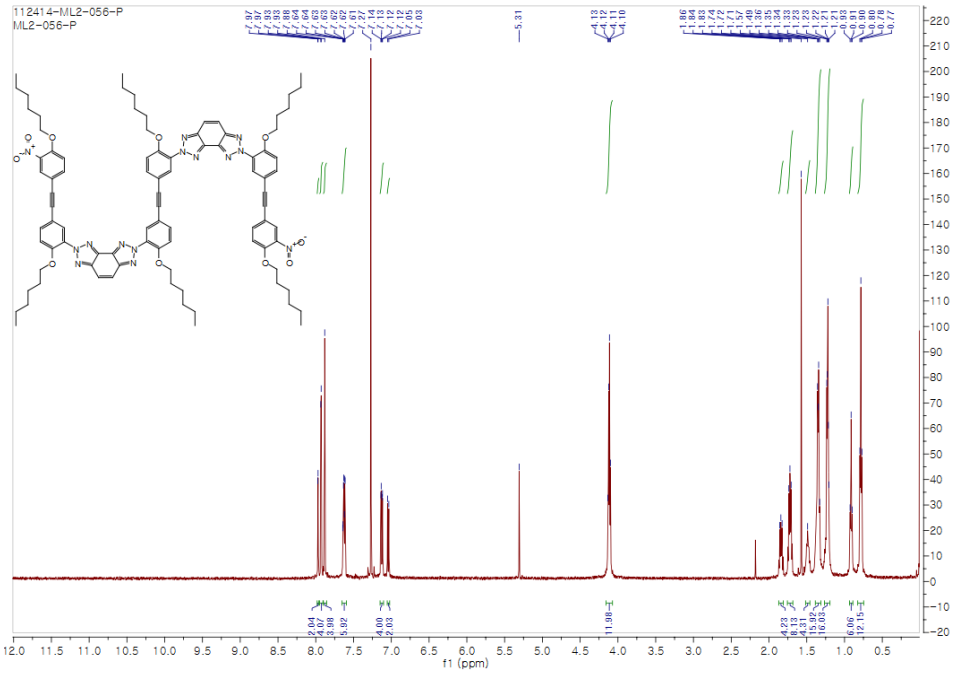
112414-ML2-056-P
ML2-056-P
f1 (ppm)

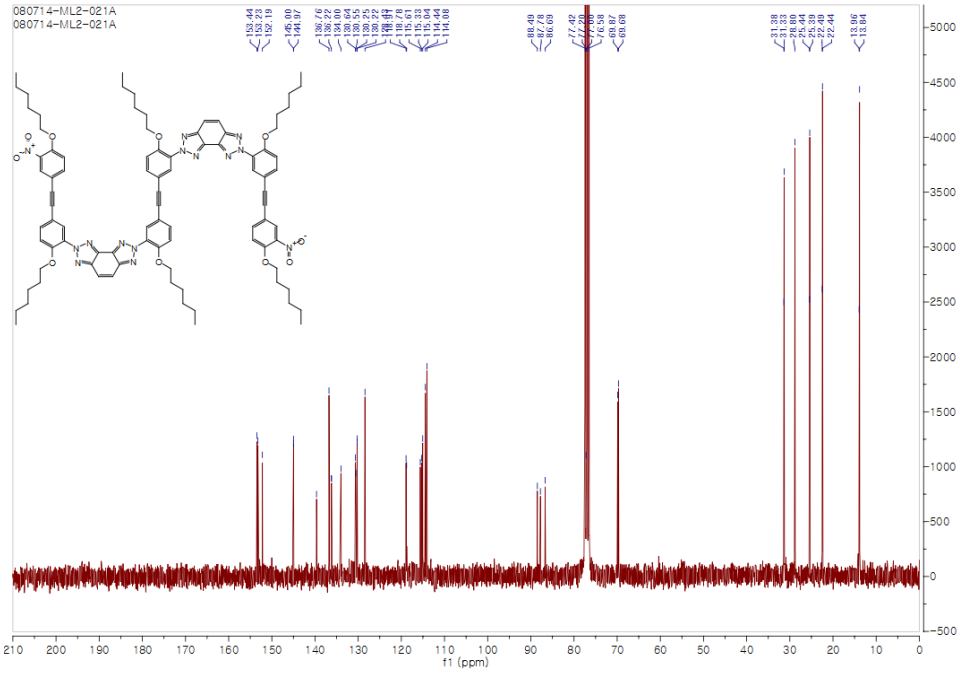
080714-ML2-021A
080714-ML2-021A
f1 (ppm)

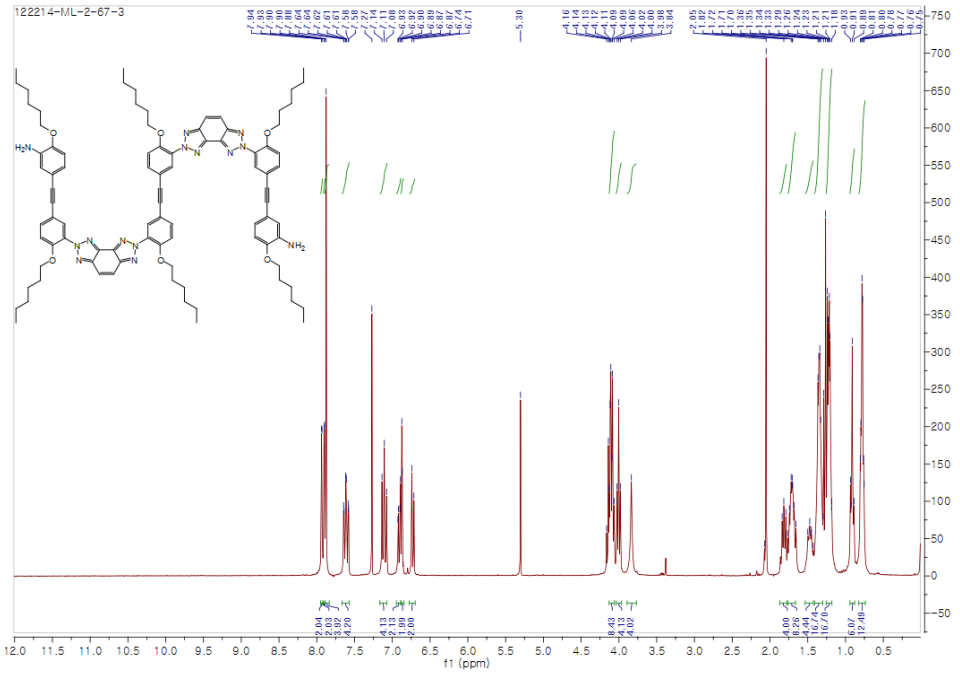
122214-ML-2-67-3
f1 (ppm)

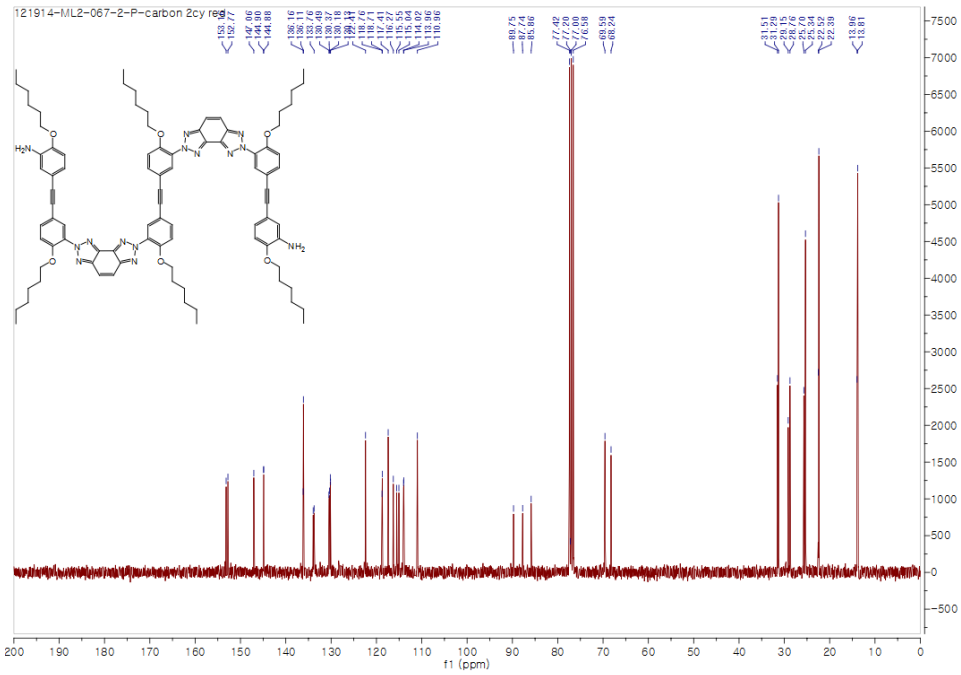
121914-ML2-067-2-P-carbon 2cy reg
f1 (ppm)

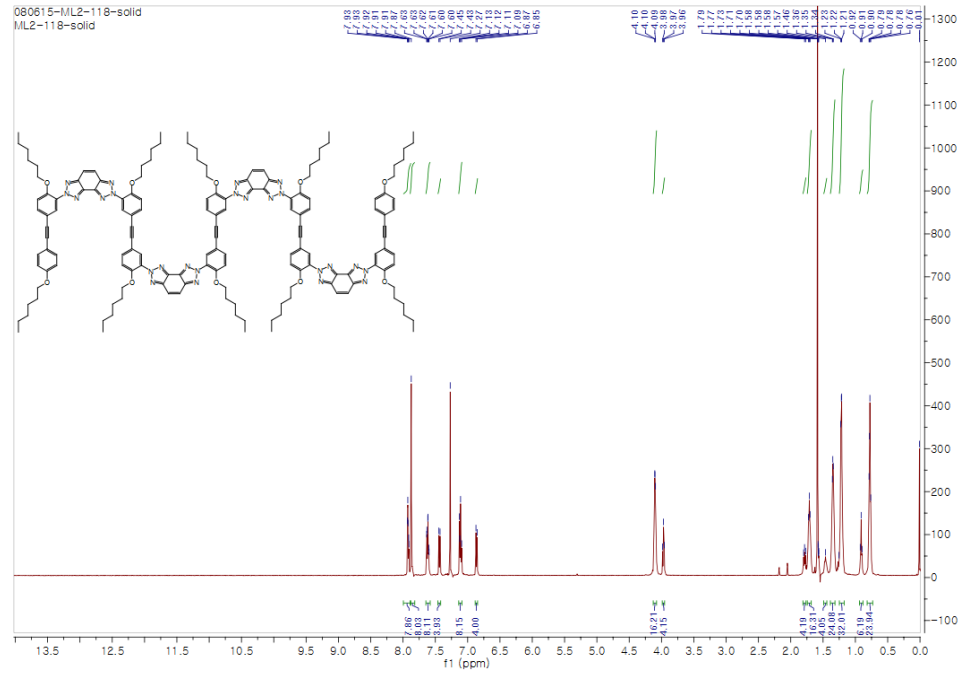
080615-ML2-118-solid
ML2-118-solid
f1 (ppm)

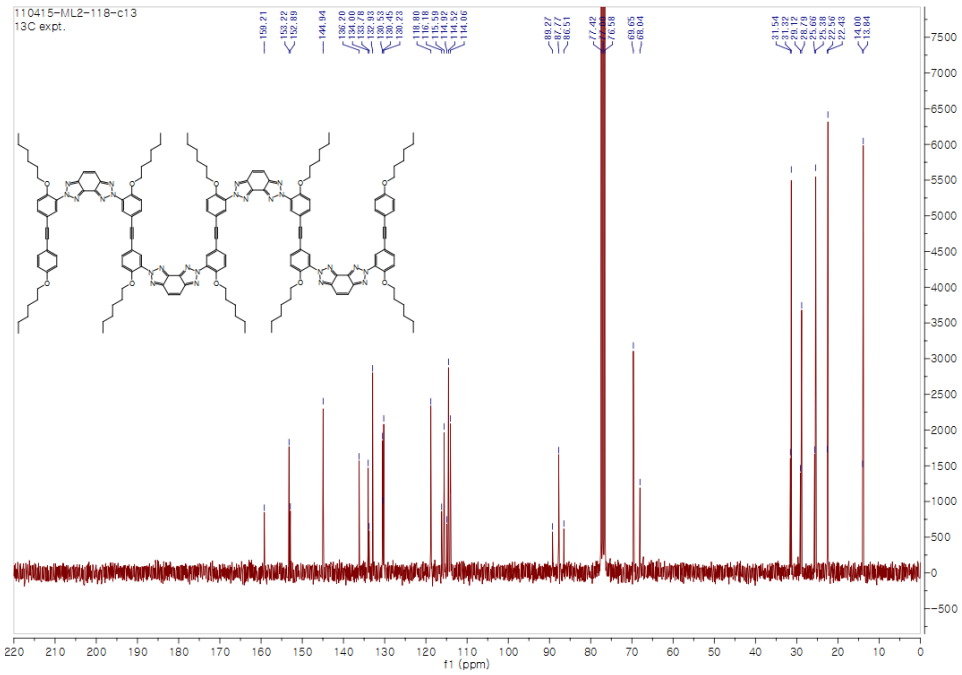
110415-ML2-118-c13
13C expt.
f1 (ppm)

5. References

1. Pelay-Gimeno, M.;Glas, A.;Koch, O.;Grossmann, T. N. *Angew. Chem., Int. Ed.* **2015**, *54*, 8896–8927.
2. (a)Kim, H.;So, S. M.;Yen, C. P.;Vinhato, E.;Lough, A. J.;Hong, J. I.;Kim, H. J.;Chin, J. *Angew. Chem., Int. Ed.* **2008**, *47*, 8657–8660; (b)Hu, H. Y.;Xiang, J. F.;Cao, J.;Chen, C. F. *Org. Lett.* **2008**, *10*, 5035–5038; (c)Hu, H. Y.;Xiang, J. F.;Yang, Y.;Chen, C. F. *Org. Lett.* **2008**, *10*, 69–72; (d)Kim, U. I.;Suk, J. M.;Naidu, V. R.;Jeong, K. S. *Chem. Eur. J.* **2008**, *14*, 11406–11414; (e)Dydio, P.;Zielinski, T.;Jurczak, J. *Chem. Commun.* **2009**, *45*, 4560–4562; (f)Peterson, S. S.;Kirby, T.;Kadarkaraisamy, M.;Hartshorn, R. M.;Sykes, A. G. *Polyhedron* **2009**, *28*, 3031–3035; (g)Gale, P. A.;Hiscock, J. R.;Moore, S. J.;Caltagirone, C.;Hursthouse, M. B.;Light, M. E. *Chem. Asian J.* **2010**, *5*, 555–561; (h)Kim, M. J.;Lee, H. W.;Moon, D.;Jeong, K. S. *Org. Lett.* **2012**, *14*, 5042–5045; (i)Zhu, K.;Vukotic, V. N.;Loeb, S. J. *Angew. Chem., Int. Ed.* **2012**, *51*, 2168–2172; (j)Shang, J.;Si, W.;Zhao, W.;Che, Y.;Hou, J. L.;Jiang, H. *Org. Lett.* **2014**, *16*, 4008–4011; (k)Hwang, I.-h.;Hong, k.-I.;Jeong, K.-S.;Jang, W.-D. *RSC Adv.* **2015**, *5*, 1097–1102.
3. (a)Caltagirone, C.;Gale, P. A.;Hiscock, J. R.;Brooks, S. J.;Hursthouse, M. B.;Light, M. E. *Chem. Commun.* **2008**, 3007–3009; (b)Caltagirone, C.;Hiscock, J. R.;Hursthouse, M. B.;Light, M. E.;Gale, P. A. *Chem. Eur. J.* **2008**, *14*, 10236–10243.
4. (a)Bautista, A. D.;Craig, C. J.;Harker, E. A.;Schepartz, A. *Curr. Opin. Chem. Biol.* **2007**, *11*, 685–692; (b)Cheng, R. P. *Curr. Opin. Struct. Biol.* **2004**, *14*, 512–520; (c)Gellman, S. H. *Acc. Chem. Res.* **1998**, *31*, 173–180; (d)Hill, D. J.;Mio, M. J.;Prince, R. B.;Hughes, T. S.;Moore, J. S. *Chem. Rev.* **2001**, *101*, 3893–4012; (e)Horne, W. S. *Expert. Opin. Drug Dis.* **2011**, *6*, 1247–1262; (f)Li, Z.-T. *Beilstein J. Org. Chem.* **2015**, *11*, 2057–2071; (g)Martinek, T. A.;Fulop, F. *Chem. Soc. Rev.* **2012**, *41*, 687–702; (h)Nair, R. V.;Vijayadas, K. N.;Roy, A.;Sanjayan, G. J. *Eur. J. Org. Chem.* **2014**, *2014*, 7763–7780; (i)Zhang, D. W.;Zhao, X.;Li, Z. T. *Acc. Chem. Res.* **2014**, *47*, 1961–1970.
5. (a)Arunkumar, E.;Ajayaghosh, A.;Daub, J. *J. Am. Chem. Soc.* **2005**, *127*,

3156–3164; (b)Chou, C.;Wang, D.;Hsu, J. F.;Liu, Y.;Peng, Z. *Synthetic Met.* **2009**, *159*, 1657–1663; (c)Dehm, V.;Büchner, M.;Seibt, J.;Engel, V.;Würthner, F. *Chem. Sci.* **2011**, *2*, 2094–2100; (d)Lu, Z.;Zhu, Y.;Lin, J.;Jiang, X.;Li, Z. *Chinese Sci. Bull.* **2010**, *55*, 2870–2878; (e)Sakamoto, N.;Ikeda, C.;Yamamura, M.;Nabeshima, T. *Chem. Commun.* **2012**, *48*, 4818–4820; (f)Zhong, Z.;Zhao, Y. *Org. Lett.* **2007**, *9*, 2891–2894.

6. Jo, J.;Lee, H. Y.;Liu, W.;Olasz, A.;Chen, C. H.;Lee, D. *J. Am. Chem. Soc.* **2012**, *134*, 16000–16007.
7. Nelson, J. C. *Science* **1997**, *277*, 1793–1796.
8. (a)Liu, Z.;Larock, R. C. *J. Org. Chem.* **2006**, *71*, 3198–3209; (b)Ueda, S.;Su, M.;Buchwald, S. L. *Angew. Chem., Int. Ed.* **2011**, *50*, 8944–8947.
9. Mikami, K.;Tanatani, A.;Yokoyama, A.;Yokozawa, T. *Macromolecules* **2009**, *42*, 3849–3851.
10. Reichardt, C. *Chemical Reviews* **1994**, *94*, 2319–2358.
11. Tinoco, I. *J. Am. Chem. Soc.* **1960**, *82*, 4785–4790.
12. Chen, Y.-Q.;Wang, X.-Z.;Shao, X.-B.;Hou, J.-L.;Chen, X.-Z.;Jiang, X.-K.;Li, Z.-T. *Tetrahedron* **2004**, *60*, 10253–10260.
13. Williams, A. T. R.;Winfield, S. A.;Miller, J. N. *Analyst* **1983**, *108*, 1067–1071.
14. Dolomanov, O. V.;Bourhis, L. J.;Gildea, R. J.;Howard, J. A. K.;Puschmann, H. *J. Appl. Crystallogr.* **2009**, *42*, 339–341.
15. Sheldrick, G. M. *Acta Crystallogr., Sect. A* **2015**, *71*, 3–8.
16. Sheldrick, G. M. *Acta Crystallogr., Sect. C* **2015**, *71*, 3–8.
17. Sheldrick, G. M. *Acta Crystallogr., Sect. A* **2008**, *64*, 112–122.
18. Bourhis, L. J.;Dolomanov, O. V.;Gildea, R. J.;Howard, J. A.;Puschmann, H. *Acta Crystallogr., Sect. A* **2015**, *71*, 59–75.

Fluorescent Oligomers Built with Triazole-Based Turn-Motifs: Length- and Solvent-Dependent Photophysical Properties

트리아졸 기반 형광성 올리고머의 길이와 용매에 따른 광물리적 특성 연구

국문초록

폴다머는 특정한 조건에서 가역적으로 접히고 펴지는 구조를 가지는 올리고머이다. 특히 형광성을 지니는 폴다머의 경우 분광장비를 이용하여 구조적 변화를 검출할 수 있을 것으로 기대된다. 우리는 올리고머 시리즈에 좋은 형광성을 보이는 *N*-2-아릴 그룹이 치환된 비스(트리아졸로)벤젠 모티프를 도입하였다. 해당 모티프는 굽어있는 연결 형태를 제공하여 분자가 회전을 통해서 접힐 수 있도록 한다. 이렇게 디자인된 새로운 π-컨쥬게이티드 올리고머 시리즈는 빌딩 블록 분자들과 연속적인 환원, 아조 커플링, 산화적 고리화 반응을 통해 합성되었으며, 합성된 구조는 NMR, IR, MS, 그리고 X-ray 단결정 구조분석을 통해 확인할 수 있었다. 합성된 올리고머는 아주 좋은 형광 특성을 보이는 동시에 (F_F = 81–83%), 올리고머의 길이가 증가할 수록 용매에 따른 구조적 접힘이 가능해지며 그 결과로 현저한 형광성의 변화를 수반하는 것을 확인하였다.

주요어 : 접힐 수 있는 올리고머, 트리아졸로벤젠, 형광, 아조 결합, 용매 의존성 학번: 2013–22930